UCRL-TR-204215

Probabilistic Seismic Hazard Analysis for Southern California Coastal Facilities

Jean Savy, Bill Foxall

Hazards Mitigation Center

Lawrence Livermore National Laboratory

January 2003

DISCLAIMER

Work performed under the auspices of the U.S. Department of Energy by UC, Lawrence Livermore National Laboratory under Contract W-7405-Eng-48

UCRL-TR-204215

Probabilistic Seismic Hazard Analysis for Southern California Coastal Facilities

Hazards Mitigation Center

Jean Savy, Bill Foxall

Manuscript date: March 2003

LAWRENCE LIVERMORE NATIONAL LABORATORY

University of California ● Livermore, California ● 94551

Table of Contents

List of Tables

List of Figures

Executive Summary:

The overall objective of this study was to develop probabilistic seismic hazard estimates for the coastal and offshore area of Ventura, Los Angeles and Orange counties for use as a basis for the University of Southern California (USC) to develop physical models of tsunami for the coastal regions and by the California State Lands Commission (SLC) to develop regulatory standards for seismic loading and liquefaction evaluation of marine oil terminals. The probabilistic seismic hazard analysis (PSHA) was carried out by the Lawrence Livermore National Laboratory (LLNL), in several phases over a time period of two years, following the method developed by LLNL for the estimation of seismic hazards at Department Of Energy (DOE) facilities, and for 69 locations of nuclear plants in the Eastern United States, for the Nuclear Regulatory Commission (NRC).

This method consists in making maximum use of all physical data (qualitative, and quantitative) and to characterize the uncertainties by using a set of alternate spatio-temporal models of occurrence of future earthquakes, as described in the SSHAC, PSHA Guidance Document (Budnitz et al., 1997), and implemented for the NRC (Savy et al., 2002).

In general, estimation of seismic hazard is based not only on our understanding of the regional tectonics and detailed characterization of the faults in the area but also on the analysis methods employed and the types of physical and empirical models that are deemed appropriate for the analysis.

To develop this understanding, the body of knowledge in the scientific community is sampled in a series of workshops with a group of experts representative of the entire scientific community, including geologists and seismologists from the United States Geological Survey (USGS), members of the South California Earthquake Center (SCEC), and members of academic institutions (University of California Santa-Cruz, Stanford, UC Santa Barbara, and University of Southern California), and members of consulting firms. The purpose of the workshops was to analyze and evaluate existing data and formulate

tectonic models that represent all the possible and physically valid models envisioned by the group. The basic input for the PSHA was a set of alternate earthquake source characterizations and a multi-model representation of ground motion attenuation, for adequate representation of the uncertainties. In the first phase, the physical modeling enabled rigorous analysis of uncertainty that arises from a lack of full knowledge in the characterization of both earthquake sources and ground motion. The set of ground motion prediction models included models that were updated to benefit from near field data from the most recent earthquakes (Taïwan and Turkey). The calculation were performed with LLNL computer software that is based on the Cornell, 1968 analytical model, and that propagates the knowledge uncertainties using a Monte-Carlo simulation approach (see, Bernreuter et al., 1989). Although the calculation were performed for rock-site conditions and generic soil sites, only the results for rock are given here. It is assumed that development of design parameters will include a correction of the spectral shape to reflect the site specificity. The results are for the average of the two horizontal components of the ground motion.

The PSHA was calculated for thirteen sites, including two sites offshore. These sites are: Catalina Island site 1, Catalina Island site 2, Goleta, Offshore Santa-Monica, Offshore San-Clemente, Port Dume, Palos Verde site 1, Palos Verde site 2, Port of Long Beach, Port of Los Angeles, Port Hueneme, San Pedro Escarpment, and Redondo Canyon. For these thirteen sites, the hazard curves in terms of probability of exceedence of the peak ground acceleration (PGA), was calculated. In addition for Port of Long Beach, Port of Los Angeles, Santa Monica, and a site Offshore, east of San Clemente the (5% damping) uniform hazard response spectra were calculated for five Return Periods (100, 500, 1000, 2000, 10,000 year Return Periods).

The detailed results are given in chapter 7. Emphasis has been put on the site locations of the Port of Long Beach, Port of Los Angeles, Santa Monica and a location offshore of San Clemente for the purpose of providing the input for the probabilistic estimation of seismically generated tsunamis. Tables ESX-1 gives the coordinates of the 13 locations for which the calculations where performed. Table ESX-2 gives the results for the thirteen sites, in terms of PGA values (in m/s/s), dominant magnitude (M-Dom, moment magnitude) and dominant distance (D-Dom, in km), for four return periods (500, 1000,

2000, and 10000 years) based on the mean estimates of the seismic hazard. Table ESX-3 (a and b) gives a tabulation of the mean estimates that are also shown in Figures ESX-1a and ESX-1b in which the results are plotted as a function of the logarithm of acceleration (figure a), and as a function of acceleration (figure b). Hazards curves are shown are in terms of the mean annual probability of exceedance (ordinate) as a function of the peak ground acceleration, in meters per second per second (abscissa). Figures ESX-2 to ESX-5 give the relative contributions of dominant earthquakes faults in terms of their contribution to the total seismic mean hazard.

Site Location	Longitude (West) (Decimal Degrees)	Latitude (North) (Decimal Degrees)
1. Port of Los Angeles	118.2650	33.7550
2. Port of Long Beach	118.2100	33.7480
3. Port Hueneme	119.2006	34.1464
4. Santa Monica	118.4900	34.0000
5. Offshore San Clemente	118.5800	33.0000
6. Redondo Canyon	118.4700	33.8000
7. Palos Verdes Point 1	118.4250	33.7100
8. Palos Verdes Point 2	118.2750	33.6350
9. Catalina Point 1	118.6150	33.3500
10. Catalina Point 2	118.3100	33.7235
11. Point Dume	118.8200	33.9750
12. Goleta	119.8800	34.3250
13. San Pedro Escarpment	118.1900	33.4550

Table ESX-1: Coordinates of the 13 site locations in the analysis (Decimal degrees). These locations are represented by numbers 1 to 13 in Figure 5.1a

Return Period (Years)	Port of Los Angeles			Port of Long Beach			Santa Monica		
	PGA (cm/s/s)	M-dom	D-dom (km)	PGA (cm/s/s)	M-dom	D-dom (km)	PGA (cm/s/s)	M-dom	D-dom (km)
500	435	7.13	10.8	353	7	10.8	360	7.12	11
1000	535	7.25	10.8	454	7.01	10.8	450	7.12	11
2000	647	7.38	10.8	571	7.3	10.8	564	7.12	11
10000	934	7.5	10.8	828	7.04	10.8	850	7.12	11

Return Period (Years)	Off Shore San Clemente			Redondo Canyon			Palos Verdes Point 1		
	PGA (cm/s/s)	M-dom	D-dom (km)	PGA (cm/s/s)	M-dom	D-dom (km)	PGA (cm/s/s)	M-dom	D-dom (km)
500	204	7.38	11	306	6.88	11	263	7.12	15
1000	292	7.62	11	384	6.88	11	327	7.12	15
2000	388	7.62	11	473	6.88	11	398	7.12	15
10000	656	7.62	11	706	7.12	11	585	7.12	15

Return Period (Years)	Catalina Escarpment 1			Catalina Escarpment 2			Point Dume		
	PGA (cm/s/s)	M-dom	D-dom (km)	PGA (cm/s/s)	M-dom	D-dom (km)	PGA (cm/s/s)	M-dom	D-dom (km)
500	177	7.38	15	346	6.88	11	327	7.38	11
1000	228	7.38	25	446	7.12	11	473	7.38	11
2000	302	7.38	25	552	7.12	11	536	7.38	11
10000	504	7.62	25	823	7.12	11	860	7.38	11

Return Period (Years)	San Pedro Escarpment			Port Hueneme			Palos Verdes Point 2		
	PGA (cm/s/s)	M-dom	D-dom (km)	PGA (cm/s/s)	M-dom	D-dom (km)	PGA (cm/s/s)	M-dom	D-dom (km)
500	242	7.12	15	362	7.2	14	295	7.12	11
1000	307	7.12	15	444	7.21	14	373	7.12	11
2000	377	7.12	15	530	7.25	14	461	7.12	11
10000	564	7.12	15	754	7.3	14	686	7.12	11

Return Period (Years)	Goleta		
	PGA (cm/s/s)	M-dom	D-dom (km)
500	325	7.38	11
1000	416	7.38	11
2000	517	7.38	11
10000	806	7.38	11

Table ESX-2: Summary of Peak Ground Accelerations, Dominant Magnitudes (M-dom) and Dominant Distances (D-dom) for 4 Return Periods at 13 sites.

Acceleration (m/s/s)	Port of Los Angeles	Port of Long Beach	Santa Monica	Off Shore San Clemente	Redondo Canyon	Palos Verde Point 1	Palos Verde Point 2
25	6.70E-01	3.93E-01	4.6E-01	2.25E-01	3.91E-01	3.53E-01	3.46E-01
50	2.79E-01	1.29E-01	1.6E-01	6.56E-02	1.21E-01	1.01E-01	1.04E-01
100	7.46E-02	3.29E-02	4.33E-03	1.69E-02	2.93E-02	2.20E-02	2.41E-02
200	1.62E-02	7.29E-03	9.10E-03	4.27E-03	5.74E-03	3.96E-03	4.88E-03
350	3.78E-03	2.04E-03	2.15E-03	1.46E-03	1.31E-03	7.75E-04	1.19E-03
500	1.24E-03	7.29E-04	7.32E-04	6.75E-04	4.04E-04	1.98E-04	3.70E-04
750	2.64E-04	1.54E-04	1.65E-04	2.28E-04	7.42E-05	2.69E-05	6.37E-05
1000	7.05E-05	3.85E-05	4.69E-05	8.88E-05	1.71E-05	4.87E-06	1.34E-05
1200	2.77E-05	1.42E-05	1.93E-05	4.53E-05	6.07E-06	1.47E-06	4.41E-06
1500	8.10E-06	3.76E-06	5.95E-06	1.86E-05	1.55E-06	3.08E-07	1.02E-06

Table ESX-3a: Mean hazard estimates for thirteen sites

Acceleration (m/s/s)	Catalina Escarpment 1	Catalina Escarpment 2	Point Dume	Goleta	San Pedro Escarpment	Port Huemene
25	2.21E-01	3.81E-01	4.29E-01	3.24E-01	3.04E-01	4.81E-01
50	4.98E-02	1.24E-01	1.36E-01	1.05E-01	8.65E-02	1.81E-01
100	8.37E-03	3.17E-02	3.34E-02	2.71E-02	1.78E-02	4.79E-02
200	1.30E-03	7.07E-03	6.57E-03	6.23E-03	3.11E-03	1.05E-02
350	3.20E-04	1.94E-03	1.60E-03	1.59E-03	6.34E-04	2.26E-03
500	1.02E-04	6.87E-04	6.05E-04	5.52E-04	1.66E-04	6.38E-04
750	1.88E-05	1.48E-04	1.63E-04	1.31E-04	2.30E-05	1.07E-04
1000	4.39E-06	3.85E-05	5.36E-05	3.96E-05	4.30E-06	2.38E-05
1200	1.59E-06	1.47E-05	2.45E-05	1.73E-05	1.34E-06	8.36E-06
1500	4.16E-07	4.06E-06	8.63E-06	5.84E-06	2.92E-07	2.13E-06

Table ESX-3b: Mean hazard estimates for thirteen sites (Continued)

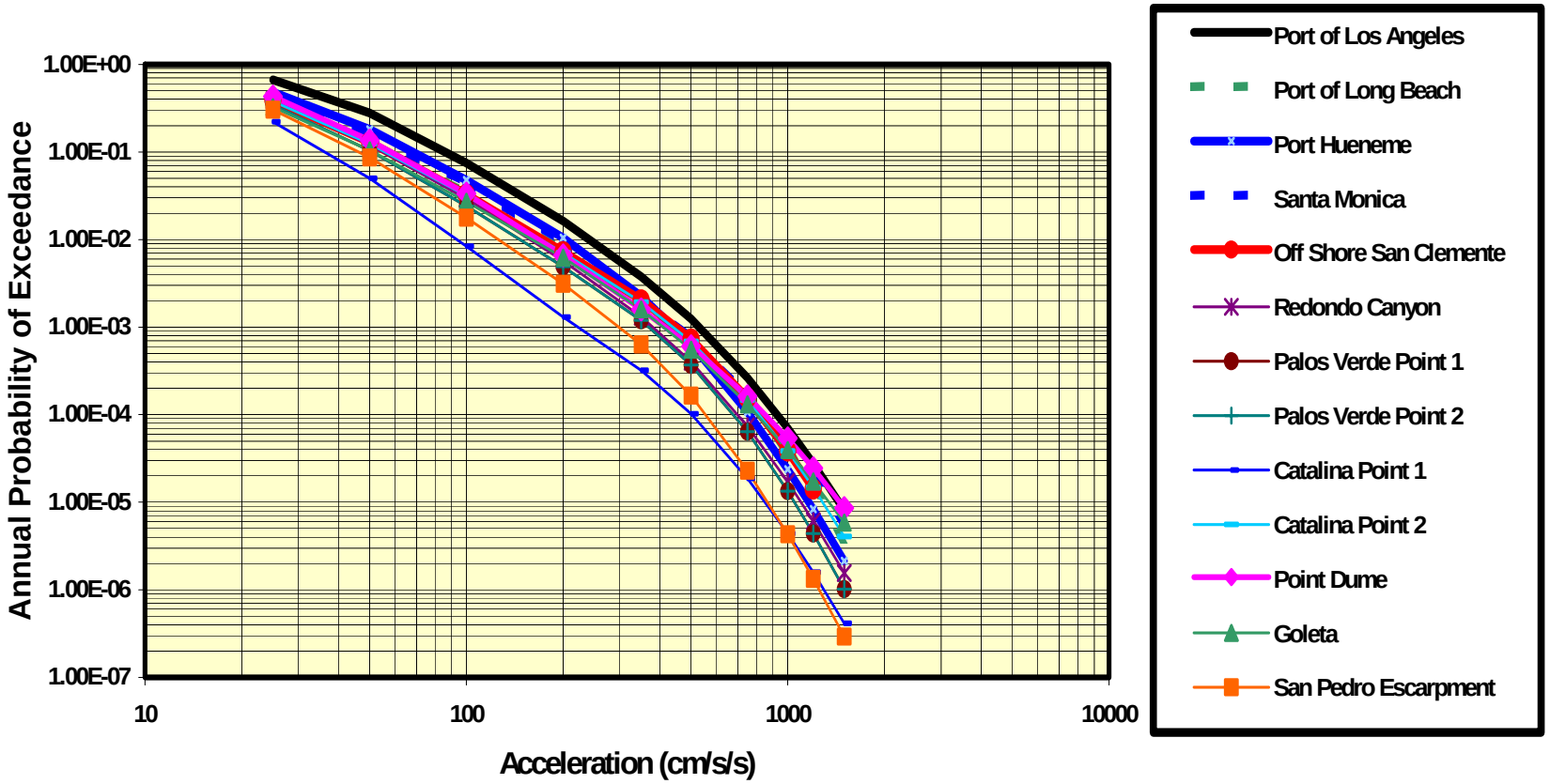

Figure EXS-1a: Peak Ground Acceleration Hazard Curves for the 13 sites for two plotting formats of the same data. The plotted horizontal axis is a logarithm in the top figure and an arithmetic value in the bottom figure.

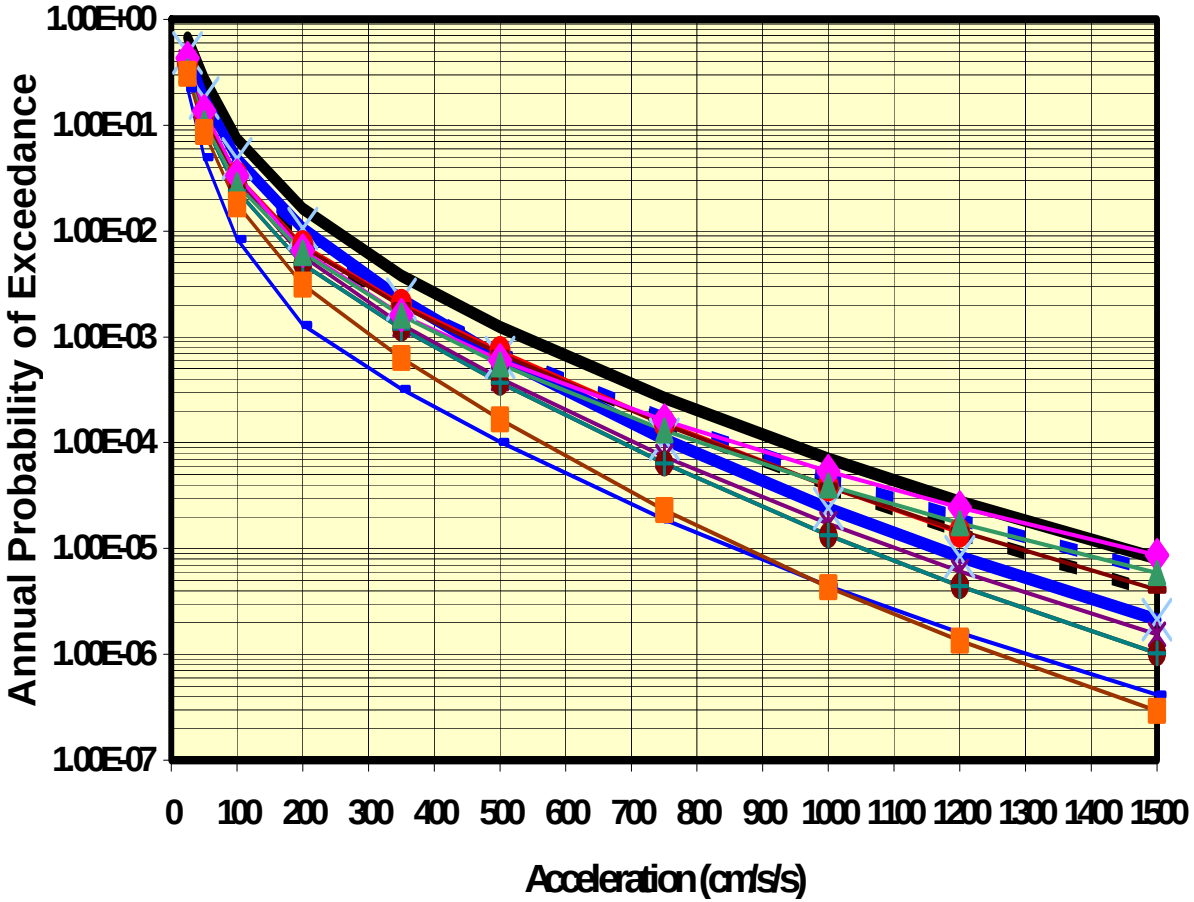

Figure EXS-1b: Peak Ground Acceleration Hazard Curves for the 13 sites for two plotting formats of the same data. The plotted horizontal axis is a logarithm in the top figure and an arithmetic value in the bottom figure.

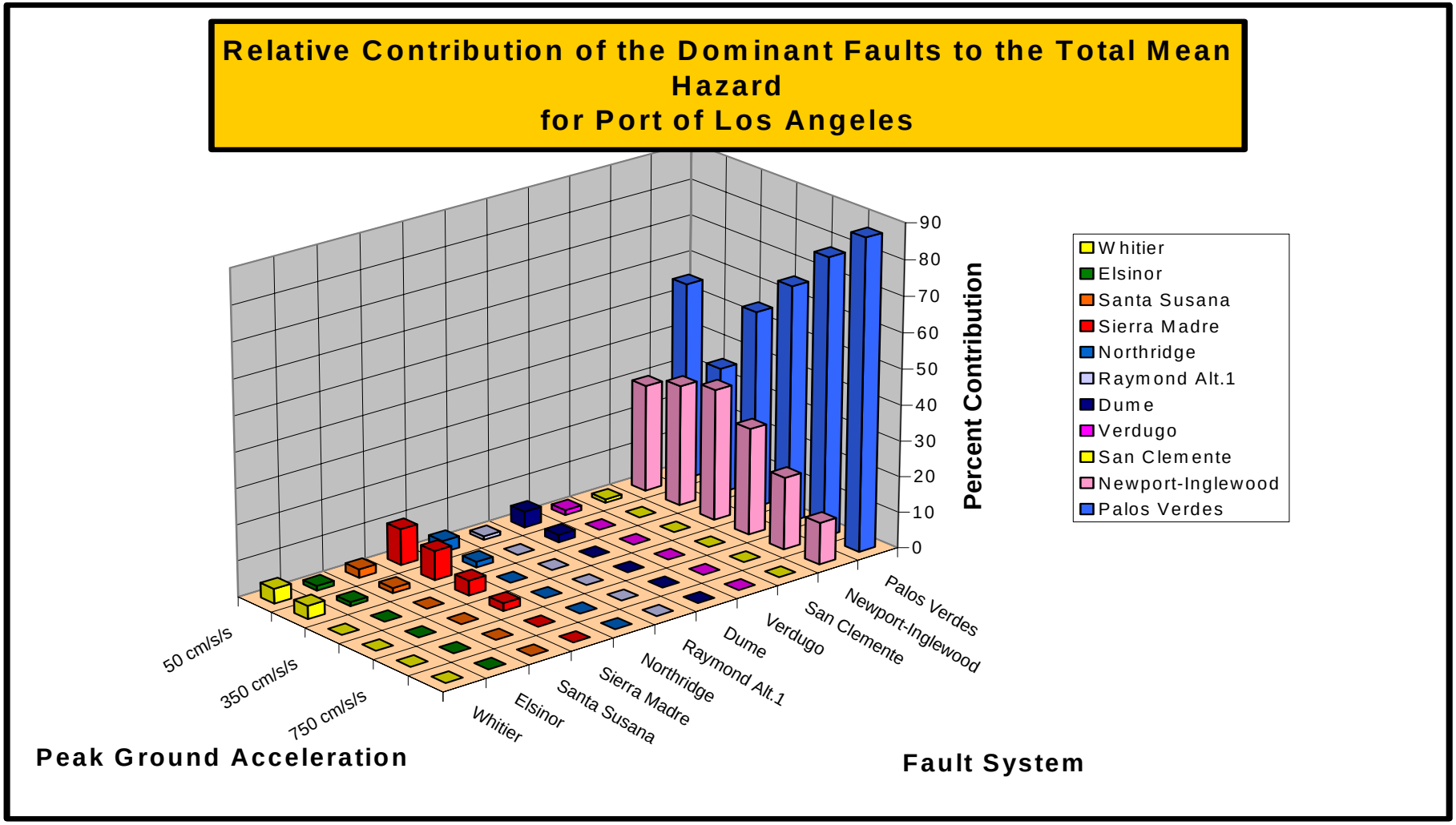

Figure ESX-2: Relative Contribution of Dominant Faults to the Total Peak Ground Acceleration Hazard for the Port of Los Angeles.

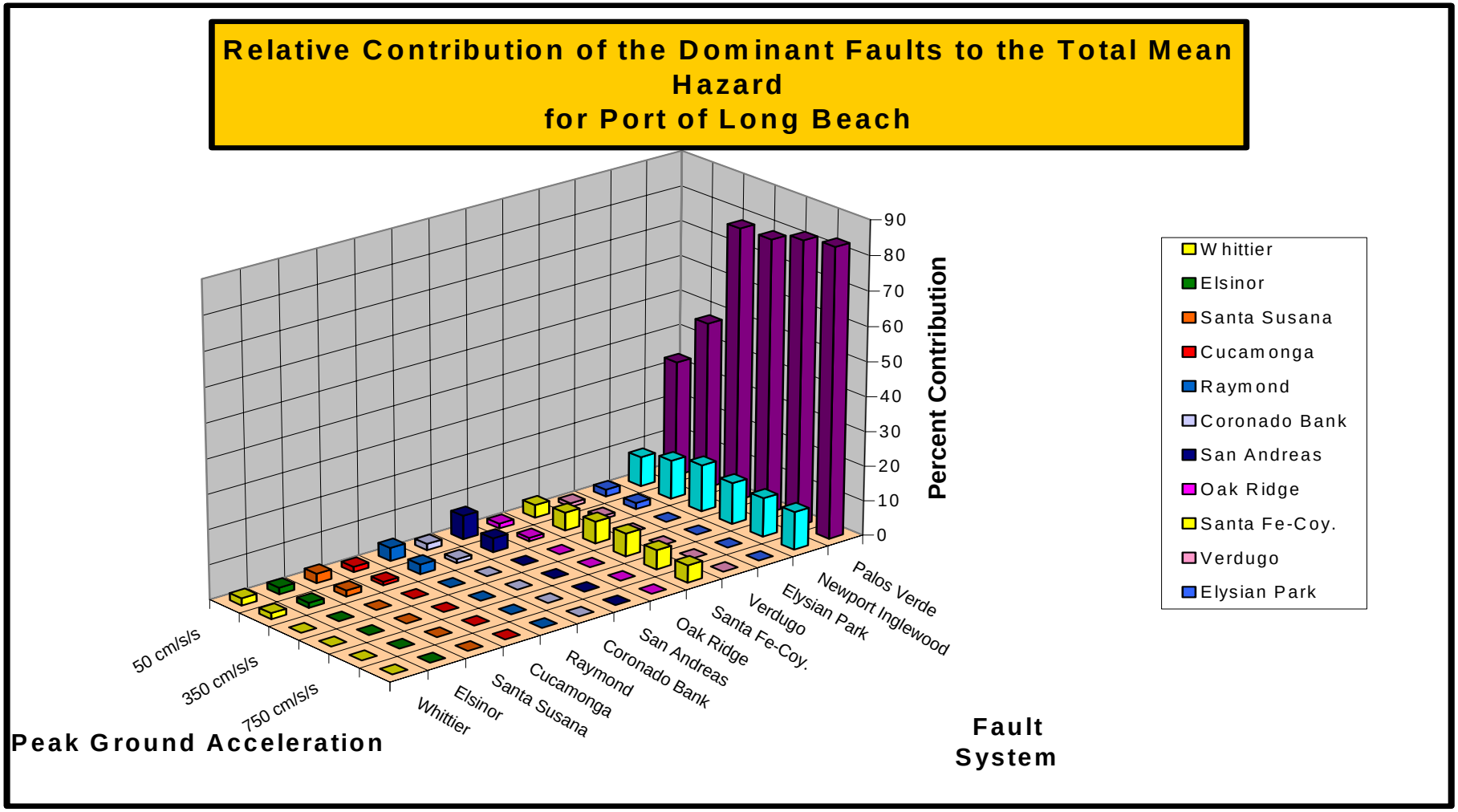

Figure ESX-3: Contribution of Dominant Faults to the Total Peak Ground Acceleration Hazard for Port of Long Beach.

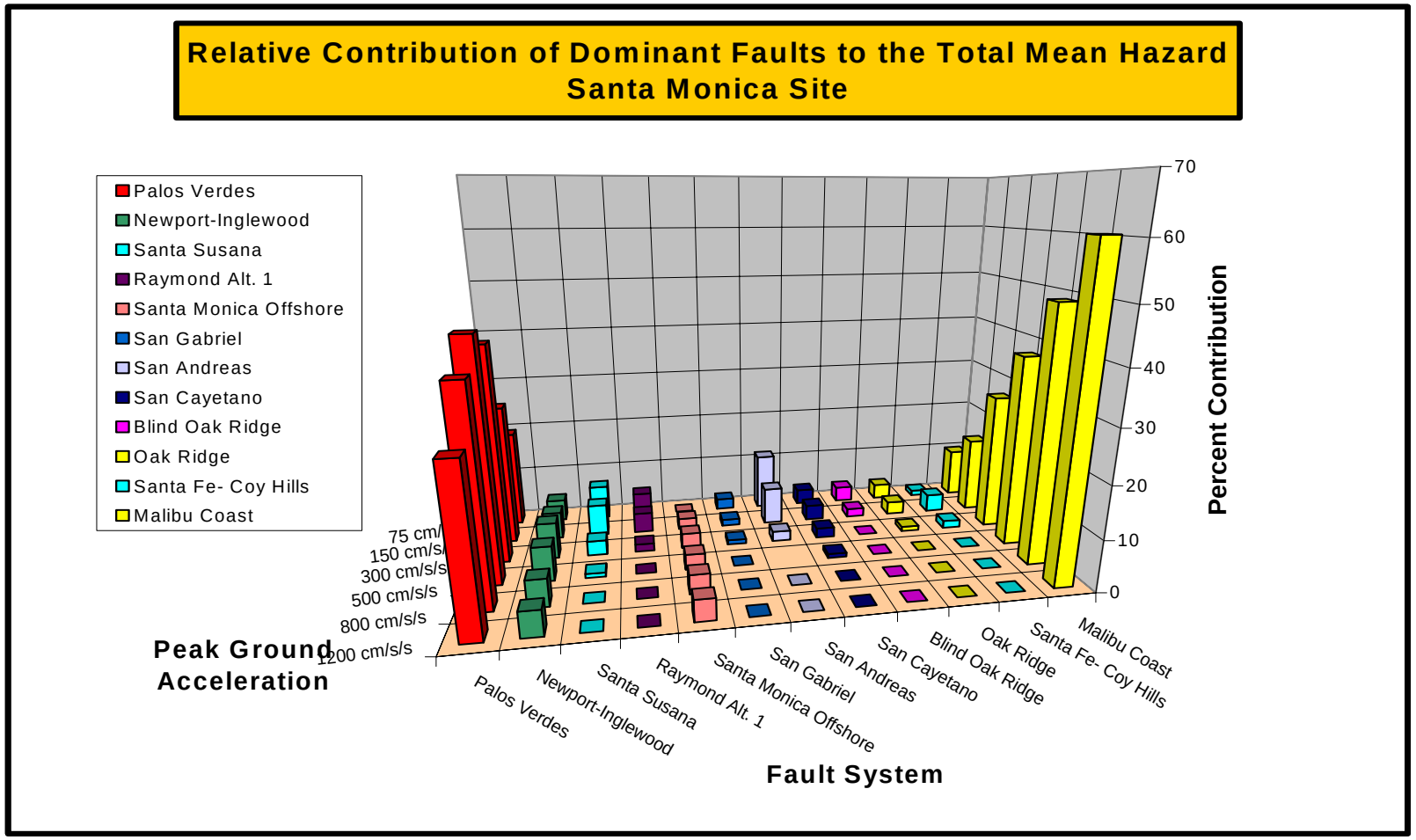

Figure ESX-4: Relative Contribution of Dominant Faults to the Total Peak Ground Acceleration Hazard for Santa Monica

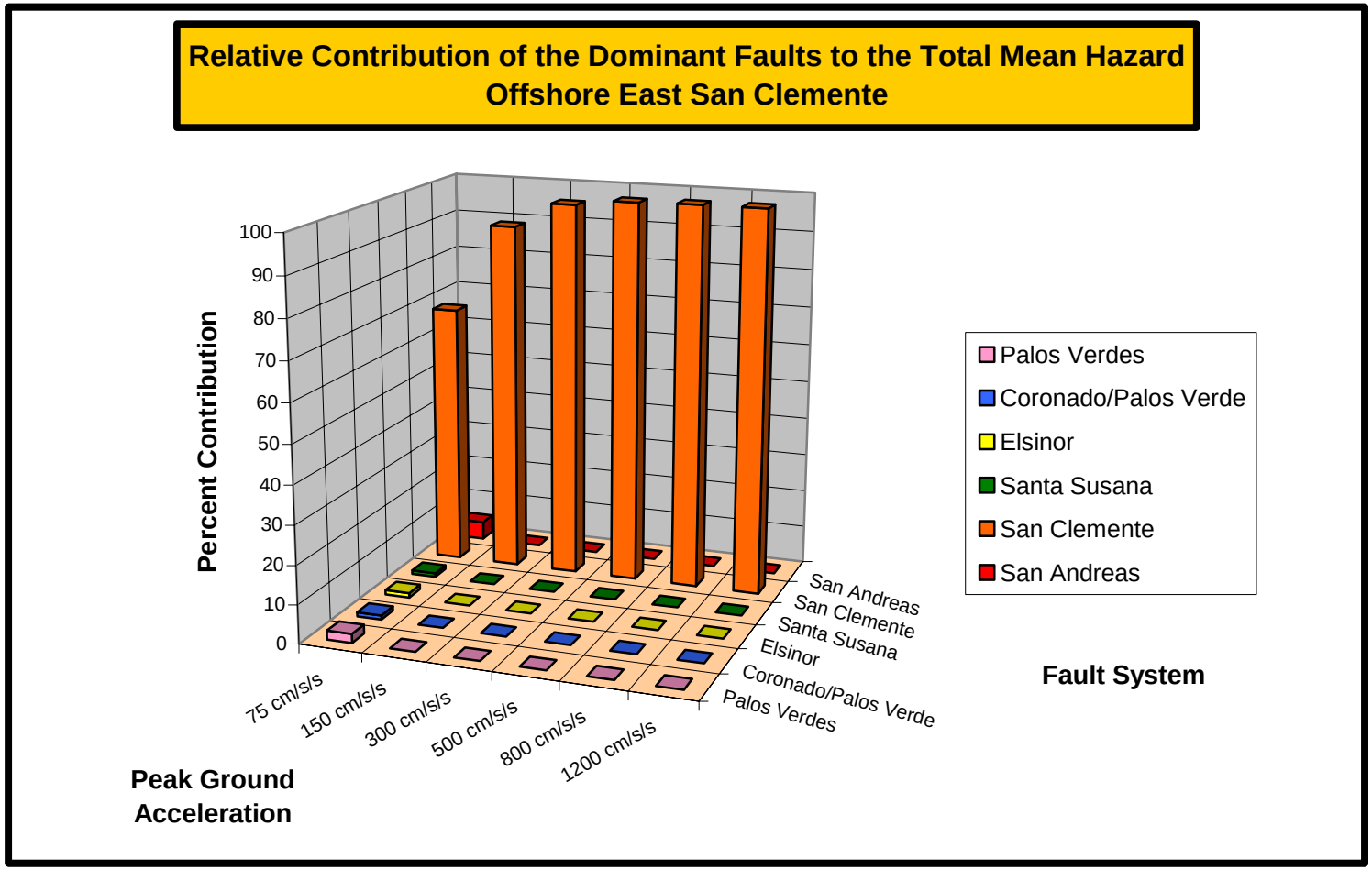

Figure ESX-5: Relative Contribution of Dominant Faults to the Total Peak Ground Acceleration Hazard for Offshore San Clemente.

1. Background

The overall objective of this study was to develop probabilistic seismic hazard estimates for the coastal and offshore area of Ventura, Los Angeles and Orange counties for use as a basis for the University Of Southern California (USC) to develop physical models of tsunami for the coastal regions and by the California State Lands Commission (SLC) to develop regulatory standards for seismic loading and liquefaction evaluation of marine oil facilities. The probabilistic seismic hazard analysis (PSHA) was carried out in five phases over a time period of two years. The basic inputs for the PSHA is a set of earthquake source characterizations and a multi-model representation of ground motion attenuation for adequate representation of the uncertainties. In Phase I the physical modeling enabled rigorous analysis of uncertainty arising from lack of full knowledge in the characterization of both earthquake sources and ground motion attenuation. This was achieved by following the state-of-the-art methodology recently developed jointly by the Nuclear Regulatory Commission (NRC), the Department Of Energy (DOE) and the Electric Power Research Institute (EPRI) (SSHAC document, Budnitz et al., 1997 and implemented for the NRC (Savy et al., 2002).

The major improvement over the previous methods of estimation is a clear and rational identification and quantification of the uncertainties, both random (aleatory) and those due to imperfect knowledge of the earthquake process (epistemic).

The PSHA was calculated for 13 sites, located on a variety of ground conditions. Since the specific conditions of the soil at most of the site were not known, we first calculated the seismic hazard for rock. A second set of calculation was also performed for the type of generic soil conditions included in the definitions of the ground motion attenuation models, but given the lack of usefulness of such results for most critical facilities, these results are not reported in this document.

A large amount of information on the sources of earthquakes in southern California has been generated by studies sponsored by the USGS, SCEC and other agencies in the last few years. The new information provided by these studies formed the basis for improved characterization of earthquake sources of significance to seismic hazard. The results are de-aggregated to show the relative contribution of each of the seismic sources considered in the hazard model.

2. Objectives and Scope

The basic purpose and objective of the present analysis is to develop reliable estimates of the mean seismic hazards for the Coastal and Offshore Area of the Orange, Los Angeles and Ventura Counties . Although all the data and experience assembled in previous studies were utilized to their fullest, the large quantity of new information and new methodologies led to the formation of a new team that includes LLNL staff and outside consultants from academia and private consulting firms.

The scope of such a PSHA depends principally of several factors, from the type of regulations that cover the facilities and their operations, to considerations of risk, and level of resources available.

A new series of standards, developed by the American Nuclear Society (ANS), and the American Society of Civil Engineers (ASCE) that are based on the DOE-STD series 1021, 1023, 1024 and 1020, is nearing completion. All these documents rely heavily on the concepts laid down by the SSHAC for the overall process of performing a PSHA.

The guidance is designed to help the analyst decide on the proper level of effort for the performance of the analysis, field investigations, and how to fulfill the requirements enunciated by SSHAC, in the spirit of providing the highest level of credibility and accuracy at the minimum level of effort. It identifies classes of analyses that are distinguishable by the level of risk exposure and performance goals associated with the existence and operation of the facility, in the present case, the review and design of marine oil terminals.

This analysis recognizes that marine oil terminals present a level of risk that is similar or greater than non-critical but important non-nuclear facilities. Thus, following the recommendations of SSHAC were followed to incorporates the following attributes:

1) **Experience Based**. The methodology takes advantage of the experience gained from recent seismic hazard analyses. Over the past decade, probabilistic methods have evolved into the generally preferred state-of-the-art for assessing vibratory ground motion at critical facilities. By incorporating recurrence information and input variability, these methods provide a more complete evaluation of hazard for risk-based design, long-term performance assessment, and regulatory review than do deterministic methods. Recent applications of probabilistic methodologies, associated lessons learned, and ongoing evaluations and integration of

seismic hazard methodologies [e.g., the Senior Seismic Hazard Analysis Committee (SSHAC) study (Budnitz et al., 1997), jointly sponsored by the DOE, the NRC, and the Electric Power Research Institute (EPRI)] provide the basis for the methodology described in this report.

2) **Data-Driven**. Development of inputs to the seismic hazard methodology and the associated input variability (uncertainty) is based on source-specific data. The methodology is capable of incorporating all relevant source-specific data available, including information on earthquake recurrence. The methodology also allows seismic hazard assessments to be easily updated as new data become available.

3) **Proper Treatment of Uncertainties** . The methodology provides an unbiased assessment of seismic hazards by incorporating and properly treating various types of input variability. These types of variability include uncertainty in data interpretations and randomness in the earthquake process. The uncertainty is directly incorporated into the calculation of hazard, rather than qualitatively contributing to selection of a deterministic value. This facilitates regulatory decision-making and risk-based design. The methodology accommodates alternative relationships describing physical processes (i.e., earthquake occurrence), alternative values of parameters associated with those relationships (e.g., fault dip, slip rates, and maximum magnitudes), and alternative seismic source characterizations based on different interpretations of the available data.

4) **Flexible**. The methodology accommodates a range of credible scientific interpretations, approaches, and data. Further, the methodology allows rational consideration of unlikely or highly uncertain scenarios. For example, the methodology accommodates the notion of seismic sources occurring in regions where faults are presently unmapped or unknown. This flexibility results from the probabilistic framework in which alternative input interpretations are explicitly incorporated.

5) **Facilitate Sensitivity Analysis**. The methodology is structured such that sensitivity analyses are facilitated. Such analyses identify important contributors to the hazard result and the relative importance of various data and interpretations. Similarly, they are used to highlight relationships or parameters for which differences in interpretation or data do not strongly influence the hazard at the site. Hence, the methodology aids in setting priorities for

additional data collection and analysis efforts, so that the most important technical issues are addressed and reductions in uncertainty have the greatest impact.

To fulfill the above requirements, the present state-of-the-art approach (as described in the SSHAC report (Budnitz et al., 1997), uses the concept of the Technical Facilitator Integrator to rationally integrate the information from a group of experts. We followed the simplified approach described by the SSHAC, in which all the criteria for performing a good PSHA are followed, albeit with a limited number of experts.

The main goals of the PSHA, regardless of its level of sophistication, is to use the best physical and empirical models for the particular project, and to quantify the uncertainty in the results. The first aspect of this goal is partly the responsibility of the peer-reviewers. The latter aspect is achieved by ensuring that most of the possibly viable interpretations of the data by the scientific community (physical models, quantification of ranges of parameters) is represented in an unbiased fashion, so that the resulting uncertainty is a fair representation of the range that exists in the community. By sampling from a homogeneous set of experts, or experts' publications, that is attempting, and are assumed, to cover the entire community, the final results include an unbiased estimate of the knowledge uncertainty.

3. Description of the process

The most important aspect of the process is to ensure that the appropriate models are used, erroneous interpretations of the data are identified, and the uncertainty is fairly represented and quantified.

The process is therefore designed (see SSHAC, Budnitz, 1997) to maximize the chance that an exhaustive set of the viable interpretations of the data be identified and properly accounted for in the analysis.

The analyst's role (LLNL Team) is to systematically uncover the interpretations, using the published literature, and with the help of the experts, to evaluate them and determine their relative weights that express the degree to which each interpretation satisfies the data.

In order to achieve these goals, the process consisted of a series of analyses and workshops with a panel of several experts from LLNL, academia, the United States Geological Survey (USGS), and researchers of consulting firms. Figure 3.1 summarizes the process, as briefly described below.

Workshop 1: Knowledge Dissemination Workshop, to review the available data and ensure that all experts contributing to the project have full knowledge and understanding of the information available. After the workshop, the analyst team formulated a range of possible interpretations that are presented in workshop 2.

Workshop 2: Formulation of interpretations, models. The interpretation of the geologic, seismologic and geophysical data into possible tectonic models and models of the geometry of possible sources of seismicity for the future, is discussed. The physically viable interpretations are retained and evaluated. The analyst team, in its role of Technical Integrator Facilitator (TFI) (see Budnitz, 1997), developed a set of alternatives and assigned weights to each.

All models that were deemed appropriate were used in the analysis with equal weights. Summaries of workshops 1 and 2 are given in sections 4.3.1 and 4.3.2. The description of the ground motion models is given in Chapter 6.

Figure 3.1 Description of the process for estimating the probabilistic seismic hazard at LLNL

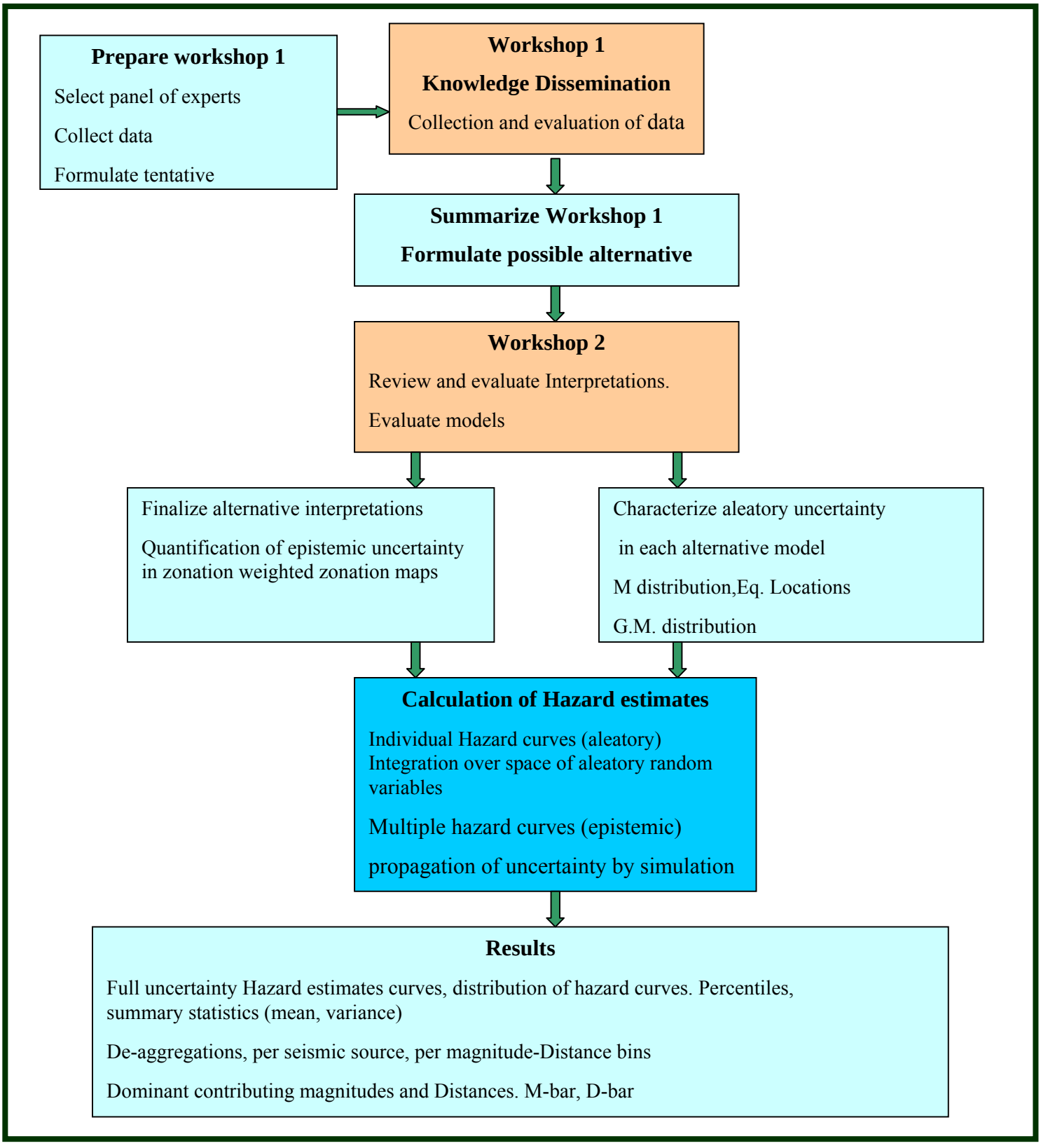

4. Overview of the PSHA Methodology

4.1 Seismic Hazard Characterization Model

4.1.1 Systematic Process

Five steps are involved in deriving the distribution of seismic hazard.

Step 1: Evaluation of Seismic Sources.

Determine the geometries and spatial distribution of potential sources of future seismic activity in the region around the site. Characterize the uncertainty in the spatial description of each source.

Step 2: Assessment of Earthquake Recurrence and Maximum Magnitude.

For each seismic source, describe the distribution of the rates of occurrence of future earthquakes as a function of magnitude. Estimate the maximum magnitude for each source. Characterize the uncertainty in recurrence relations and in maximum magnitude.

Step 3: Ground Motion Attenuation.

For the site region, evaluate or determine relations that express how the amplitudes of selected ground motion parameters vary with earthquake magnitude and source-to-site distance. Characterize the uncertainty in these ground motion/attenuation relations.

Step 4: Mathematical Model to Calculate Seismic Hazard.

Integrate over each combination of inputs determined in steps 1 through 3 to calculate a seismic hazard and plot a curve expressing the annual probability that a given value of ground motion will be exceeded. Carry out the integration for all combinations of inputs to incorporate the variability of input estimates.

Step 5: Presentation of the Hazard Results.

Express the results of step 4 as a distribution of seismic hazard curves that can be represented by a mean curve and curves representing particular percentiles of the distribution.

Each of these steps is discussed below and shown schematically in Figure 4.1.

4.1.2 Evaluation of Seismic Sources

A seismic source represents a portion of the earth's crust having the potential to generate future earthquakes. The assumption is made that the geological regime is stationary over the period ranging from the time of the earliest available historical data to some date in the near (geological) future, so that the probability of earthquake occurrence as a function of magnitude and the maximum magnitude associated with a given source can be considered invariant. Seismic sources include mapped or modeled faults and volumetric zones within which future earthquakes may occur but for which specific faults are not identified. Since the dimensions of a fault govern the maximum magnitude of the earthquakes it can generate, the size of the features that need to be considered in the source characterization increases with increasing distance from the site. For a given distance from the site, there is a size of feature below which its effect on the site can be neglected and generally, the geometries of distant sources can be defined in less detail than those of more local sources. Definition of zone sources is based upon regional seismicity and tectonic characteristics. Characterization of fault sources is based upon evaluation of available geological, seismological, geophysical and geodetic data. The characterization of each source contains the following elements:

- **Segmentation model**: Earthquakes often rupture only segments of their source faults and are therefore of lower magnitude than would be generated by a rupture of the entire fault. These events are often arrested by recognizable structural or other barriers to rupture propagation. Therefore, mapped features such as prominent fault bends and offsets or other structural characteristics or behavioral changes (e.g. seismicity or slip rate) are used to define segmentation points in building fault segmentation models. Successive earthquakes may behave differently, some being arrested by a given barrier and others breaking through it. This variability in behavior leads to alternative rupture scenarios for each multi-segment fault; for example, a two-segment fault (one segmentation point) can produce earthquakes that rupture either the individual segments or both segments together. The relative rates of these scenarios is governed by assigning a probability of failure to each segmentation point, based on the available data.

- **Source Geometry**: The locations and geometries of fault segments are defined in three dimensions by the map coordinates of the upper fault tip (i.e. the fault trace in the case of surface faults), fault dip, δ, and the upper and lower depth limits of seismogenic rupture, D_1 and D_2, respectively. Volumetric source zones are defined by the vertices of polygons on the Earth's surface and by the upper and lower limits of seismogenic rupture.

- **Fault slip rate**: Slip rates assigned to fault segment sources are derived from paleoseismic observations, where these are available. These provide estimates of geological slip rates averaged over a few to many earthquake cycles, which are generally appropriate for characterizing long-term mean earthquake recurrence rates as described below. In active tectonic regions, such as the western US, the assigned slip rates are constrained by the regional strain budget imposed by geodetic observations and global plate tectonic models. Slip rates for faults for which paleoseismic data are not available can sometimes be estimated from kinematic modeling within the same geodetic and tectonic constraints.

- **Probability of activity**: The overall probability that a fault is active is assigned based primarily on historic observations of past earthquakes and paleoseismic evidence for late Quaternary, and particularly Holocene, events.

In general, seismic source characterization is subject to significant epistemic uncertainty, stemming typically from the sparseness of the available data. The objective of the source characterization approach is to capture the full ranges of parameter values and viable interpretations that are consistent with the data. The uncertainty distribution contains contributions from: (1) The ranges of parameter values (fault length, width, dip, slip rate, segmentation point probabilities, etc.) that are permitted by the data; and (2) fundamentally different tectonic interpretations, which result not only in definition of alternative sets of sources (each with a different set of probabilities of existence) but also in different geometrical dependencies among the faults. Uncertainties in the parameters are described by assigning a simple weighted distribution to each parameter, and the full range of parameter combinations is sampled and propagated to model the uncertainty in the hazard estimates within the overall Monte Carlo routine used in the PSHA, as described later. Alternative tectonic interpretations and dependencies among the sources are described by branches of a logic tree that are input to

the hazard calculation explicitly. Each branch is weighted according to the ability of that interpretation to explain the available data.

4.1.3 Assessment of Earthquake Recurrence and Maximum Magnitude

Each seismic source is characterized by a maximum magnitude, an earthquake recurrence model, and the uncertainties in the parameters of the model. The maximum magnitude, m^u, for each fault source is calculated from the fault area using a weighted distribution of alternative empirically based magnitude-area relationships. A recurrence relationship expresses the expected number of earthquakes per year having magnitudes greater than some minimum, m° (M5 in this study) and less than m^u. Recurrence relationships for fault sources are developed from the slip rates and segmentation point failure probabilities discussed earlier. For source zones, historical and instrumental seismicity form the primary data for characterization of maximum magnitudes and recurrence.

4.1.4 Ground Motion Attenuation

A ground motion attenuation function for use in PSHA is a probability density function whose parameters depend on the earthquakes and site characteristics. The standard version is a function of the earthquake magnitude of the earthquake and site-source distance from the site of interest (i.e., distance from the earthquake source to the terminal sites). The probability of exceeding a certain value of the ground motion caused by an earthquake of magnitude M and located at a distance R from the site is calculated by means of the ground motion attenuation functions.

For both, the peak ground acceleration, and for the spectral values, we selected a set of four models, whose general form is described in the Seismological Research Letters (SRL), 1997 with updates from the Taiwan and Turkey data (Abrahamson, 2000). These models are the following:

- Abrahamson and Silva, (Seismological Research Letters. pp94-127)
- Boore, Joyner and Fumal, (Seismological Research Letters. pp128-153)
- Campbell, (Seismological Research Letters. pp154-179)

- Sadigh, Chang, Egan, Makdisi, and Youngs, (Seismological Research Letters. pp180-189)

For each of the models, spectra are defined at 9 frequencies: 33.3, 20.0, 10.0, 6.67, 5.0, 3.33, 2.0, 1.0, and 0.5 Hz. For those models that did not provide all these frequencies, we interpolated between the closest frequency values. These attenuation models are described in 6.2.1 to 6.2.4.

4.1.5 Mathematical Model to Calculate Seismic Hazard

As developed by Cornell (1968), the probabilistic hazard methodology aims to calculate the annual probabilities that various levels of ground motion (characterized as, e.g., peak horizontal ground acceleration, peak ground velocity, or peak spectral values) will be exceeded at a site. Procedures to accomplish this assessment are described by Cornell and form the basis for recent state-of-the-practice methodologies recommended for DOE facilities.

The probabilistic hazard curve represents the integration, over all earthquake sources and magnitudes, of the probability of occurrence of all possible future earthquakes, and for each earthquake, the probability that a particular value of ground motion is exceeded at the site. Although more sophisticated time dependent models exixt, the current state-of-the-practice followed in this study is to represent the temporal occurrence of earthquakes as a memoryless Poisson process. The probability of earthquake occurrence as a function of magnitude is generally represented by an exponential distribution (Gutember-Richter). In the western United States, the characteristic earthquake concept (Schwartz and Coppersmith, 1984) is also often applied to individual faults for which there are sufficient data to describe their behavior (see Sections 4.2 and 5. The occurrence model we have developed combines both exponential and characteristic earthquake behavior for single and multi-segment rupture scenarios, and is implemented using Monte Carlo simulation to derive a frequency of occurrence versus magnitude relationship for each single segment and multi-segment source.

The Poisson probability that, at a given site, a ground motion parameter, Z, will exceed a specified value, z, during a specified time period, T, is given by the expression:

$$P(Z > z) = 1.0 - e^{-\nu(z)\cdot T} \quad (1)$$

Where *v(z)* is the average frequency during time period *T* when the level of ground motion parameter *Z* exceeds *z* at the site resulting from earthquakes from all sources in the region

The frequency of exceedance, *v(z),* incorporates the variability (aleatory and epistemic) in the time, size, and location of future earthquakes and variability in the level of ground motions they produce at the site. It is computed by the expression:

$$\nu(z) = \sum_{n=1}^{N} a_n(m^\circ) \int_{m=m^\circ}^{m^u} \int_{r=0}^{\infty} f_n(m)\ f_n(r|m)\ P(Z > z|m,r)\, dr\ dm \quad (2)$$

where

$a_n(m^\circ)$ is the frequency of earthquakes on seismic source *n* above a minimum magnitude of engineering significance, m°;

$f_n(m)$ is the probability density function of event size on source *n* between m° and a maximum earthquake size for the source, m^u;

$f_n(r \mid m)$ is the probability density function for distance to earthquake rupture on source *n*, which may be conditional on the earthquake size; and

P(Z>z|m,r) is the probability that, given a magnitude *m* earthquake at a distance *r* from the site, the ground motion exceeds a value *z*.

In practice, the double integral in Equation 2 is replaced by a double summation with the density function $f_n(m)$ and $f_n(r \mid m)$ replaced by discrete representations of their corresponding cumulative functions. As shown in Figure 4.2 (Step 4), the result is a hazard curve expressing the annual probability that various levels of the ground motion parameter will be exceeded.

4.1.6 Presentation of the Hazard Results

The basic calculation described above results in a seismic hazard estimate for a single characterization of a set of seismic sources, including recurrence and maximum magnitude values, and a single ground motion attenuation relation. Thus, the result of this calculation is a single hazard curve (Figure 4.2, Step 4) that represents the randomness, or aleatory uncertainty,

inherent in the location and magnitude of future earthquakes, and in the generation and seismic wave propagation.

There is also uncertainty in the characterizations of seismic sources and ground motion/attenuation. This uncertainty, called epistemic uncertainty, arises from incomplete knowledge of earthquake processes, limited data, and permissible alternative interpretations of the available data. The methodology explicitly incorporates these uncertainties into the analyses to quantify the uncertainty in the final hazard results.

The Monte Carlo approach to uncertainty propagation, used in this study, makes use of multiple subjective probability distributions for the various parameters of the hazard input model parameters. The Monte Carlo simulation technique samples from these distributions and a large number of hazard curves are calculated to create an artificial data set from which statistics are performed to derive the mean and percentiles of the distribution of the hazard.

In this approach, uncertainty in seismic source zonation is represented by weighted alternative maps (in which each map represents a possible, yet weighted, realistic physical model of future seismicity); uncertainty in recurrence is characterized by subjective probability distributions on the recurrence parameters; and uncertainty in ground motion evaluations is characterized by a set of alternative ground motion relationships and their associated weights.

4.2 Summary of Workshops

4.2.1 Workshop 1: Knowledge Dissemination

The first workshop was a two-day meeting that was held at the University of Southern California on January 30, and 31 2001. The attendance list is given in appendix, in Table A.1.

The format of the workshop was tailored to follow the guidance of the SSHAC, in which a Technical Facilitator Integrator (TFI), (Bill Foxall, LLNL), facilitates the discussions. The agenda is given in Table 3.2.

The purpose of the workshop was to review and evaluate the existing data and start formulating alternative tectonic and fault models of the region. The participants presented interpretations of

the data for all the major faults, and explored the diversity of opinions. This diversity was captured in the formulation of the alternative models that are described in section 5.

During the period between the first and second workshop, the alternative models were refined, and a new working set of models were presented and discussed at the second workshop.

4.2.2 Workshop 2: Evaluation of Interpretations

This workshop took place at the University of Southern California, Los Angeles, on October 19-th, 2001. Attendance list and agenda are given in appendix in appendix, in Table A.1 to A.4.

The purpose of the meeting was to present the status of the models so far developed by LLNL with input from various experts at the previous workshop, the work of SCEC, USGS, LLNL and the literature.

An emphasis was made on discussing the methods of representation of the uncertainties. The elements of the meeting were as follows:

1. Review the models developed by LLNL for the characterization of the seismogenic faults. This included the possible models and their alternatives that express the various types of uncertainties in the geometries and in the occurrence properties (aleatory and epistemic uncertainties.)
2. Review the selection of existing models of ground motion attenuation that are used in the PSHA, and the selection of weights that express the epistemic uncertainty in ground motion prediction.
3. Review the preliminary LLNL hazards calculation for selected sites and the results of another independent study performed by Earth Mechanics, Inc., for the port of LA.
4. Review a method presented by Homa Lee (USGS) for analyzing underwater landslides, with an emphasis on (a) predicting the probability of failure, given a slope geometry and a ground motion input, and then (b) characterizing the tsunami initial conditions, given a sliding scenario.
5. Develop a consensus on the final models, or on the way to finalize them, and agree on final steps to complete the project.
6. Review the existing ground motion attenuation models, and discuss the selection of appropriate models for this study, including a set of weights for each selected model.

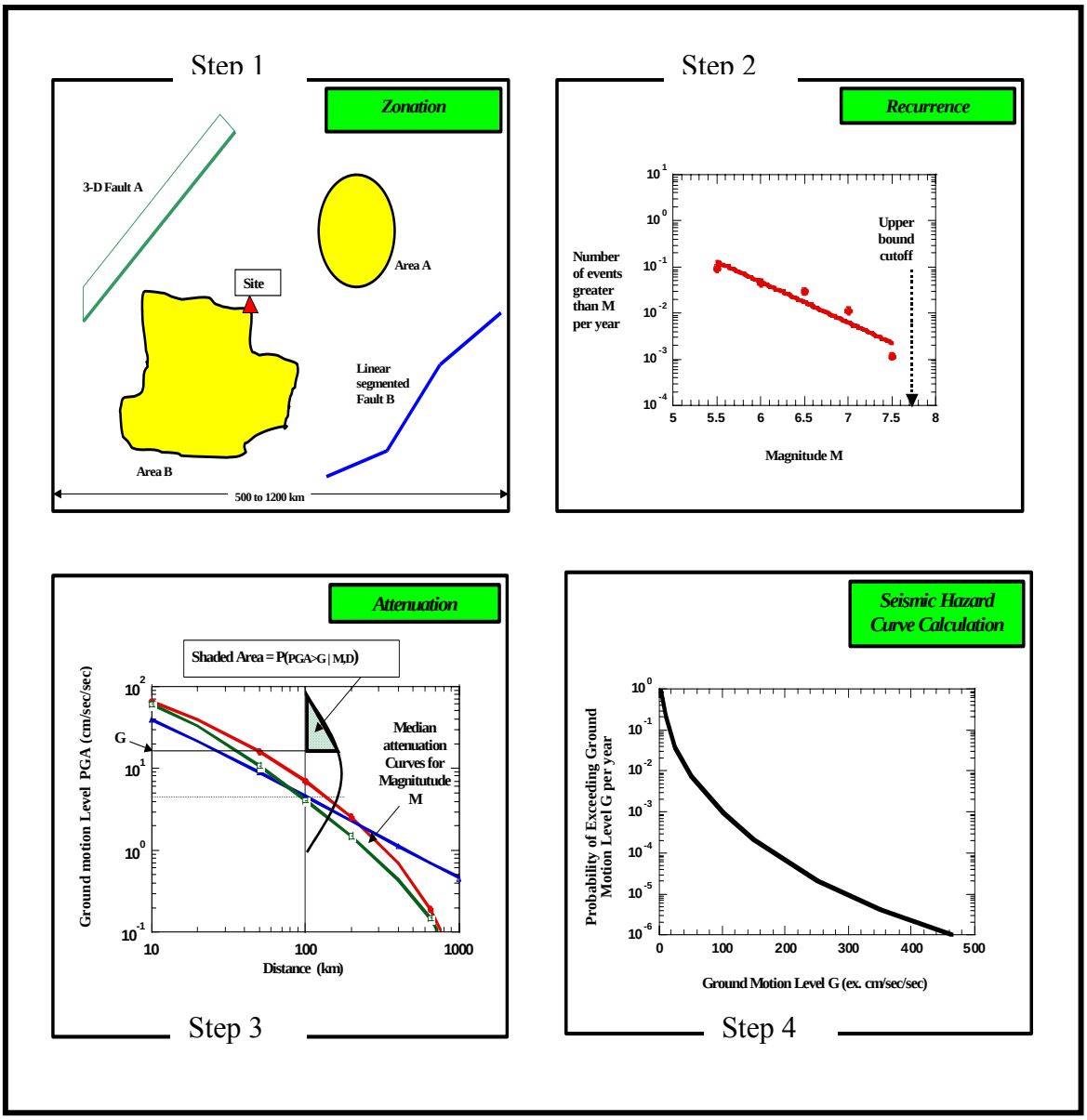

Figure 4.1: The Four Steps in the calculation of the PSHA

5. Seismic Source Characterization

5.1 Introduction

The earthquake source characterization described here synthesizes current understanding of the tectonics and faults of the Los Angeles Basin and surrounding region (including the inner continental borderland) and quantifies uncertainties in the characterizations. This work has focused on capturing epistemic uncertainty; i.e. uncertainty stemming from ignorance of the true characteristics – in some cases, the existence – of the active faults in the region and of the tectonic forces that drive them. In the present context, epistemic uncertainty has two components: First, the uncertainty in source geometrical and occurrence rate parameters deduced from the limited geological, geophysical and geodetic observations available; and second, uncertainties that result from fundamentally different interpretations of regional tectonic deformation and faulting. We pay particular attention, in Section 5.3, to the alternative source models that result from uncertainties of the second type.

5.2 Approach

Characterization of the large number of active and potentially active faults that need to be included in source characterization for the Los Angeles region requires synthesis and evaluation of large amounts of data and numerous interpretations. This was accomplished primarily through a series of carefully facilitated workshops, smaller meetings involving key researchers on given topics, and email groups. The workshops and meetings were facilitated in part by integrating the present project with a parallel source characterization study for the Southern California Earthquake Center (SCEC). The workshops proved to be extremely effective forums for the exchange and critical debate of data and interpretations that are essential in constructing fully representative source models (e.g. Senior Seismic Hazard Analysis Committee , 1997). Furthermore, SCEC's programmatic approach enabled the source characterization to evolve over time by focusing research efforts and day-to-day discussion on some of the key geological and tectonic issues that came to light during the process.

The source model represents known and postulated active faults as rectangular fault sections. These are assembled into fault segments, each of which is the smallest fault unit that is considered to be capable of rupturing independently, generating earthquakes of a characteristic size. Contiguous segments of a given fault can also combine to fail in multi-segment ruptures ("cascades") (e.g. Jackson et al., 1995).

The final (2001) SCEC Group C report - http://www.scec.org/research/special/SCEC001activefaultsLA.pdf – summarizes the large amounts of currently published and unpublished geological data and interpretations used to characterize the geometries and slip rates of faults in and surrounding the Los Angeles Basin. Data and interpretations for faults that make a particularly significant contribution to the seismic hazard and its uncertainty are discussed in some detail in Section 5.3 below. Figure 5.1 shows the base earthquake source characterization model. Rectangles show surface projections of fault planes dipping less than 75°; dip direction is indicated by teeth on the surface trace (or buried upper fault tip). Faults shown in red are predominantly strike-slip and those in purple oblique slip. Surface reverse faults are colored cyan and blind reverse faults and thrusts green. Major blind thrusts are shown in yellow. The fault plane and trace shown on Figure 5.1 represent the best estimate of the geometry of each fault. Fault parameters of given in Table 5.1, which shows estimates of both parametric and model uncertainty. Alternative interpretations of the geometries of the Santa Monica Mountains and Compton-Los Alamitos thrusts and the northern segment of the Oceanside thrust are summarized in Table 5.1 and described in more detail in Section 5.3 and in Figures 5.3, 5.5 and 5.7. Filled black circles on Figure 5.1 are fault segmentation points, red diamonds are locations at which hazard was calculated, and red stars show the ports of Los Angeles and Long Beach.

5.3 Alternative Source Characterizations

Alternative characterizations for a given fault system are required when viable interpretations of the data support distinctly different geometries, faulting styles, or slip rates. In the Los Angles region the main (but not only) tectonic issue that leads to

alternative characterizations remains the postulated existence of active regional-scale, blind, shallow-dipping thrusts and detachments that can accommodate part of the N-NE directed shortening observed geodetically across the region. Postulated blind faults underlie mapped active, steeply dipping surface faults, and, in certain cases, the shallow- and steeply-dipping fault systems must intersect and interact kinematically within the seismogenic crust. Therefore, the blind faults are not only potentially significant earthquake sources themselves, but also imply geometric and kinematic dependencies that have a major influence on the characterization of some surface faults. The blind faults are seldom imaged directly, other than perhaps in the top few kilometers of the crust, so their geometries and kinematics are most often constrained only by structural modeling of surface folding. Generally, such modeling is highly non-unique, which leads to wide ranges of plausible alternative configurations for the blind faults, and hence for the fault systems they interact with.

This section describes the development of alternative characterizations for three cases that make significant contributions to uncertainty. The two parts of the source model that cover these cases are shown in Fig. 5.2. The alternative characterizations for inter-dependent fault systems are developed using logic trees like the one shown in Fig. 5.4. The branch tips on the right of each tree (or sub-tree) correspond to mutually exclusive alternative sets of earthquake sources. For clarity, only the longest multi-segment source for each fault system is shown in the logic trees, but single- or shorter multi-segment ruptures are of course also permitted. In using the trees as input to the PSHA each branch at each decision point is assigned a weight expressing the relative likelihood that it represents the true description of the system. Summaries of the arguments upon which the trees are based and references to the original data sources are given below.

Malibu-Northern Los Angeles Basin Left-oblique System and Santa Monica Mountains Thrust

The left-lateral/left-reverse faults bounding the Los Angeles Basin and Santa Monica Bay on the north (Fig. 5.2a) are characterized under the assumption that they form a system

that can break in multi-segment ruptures and that is continuous with the Santa Cruz Island-Santa Rosa Island system to the west. Alternative characterizations of this system also include the possible existence of an active Santa Monica Mountains thrust, as shown in cross-sections BB' and CC' (Fig. 5.3). The logic tree shown in Fig. 5.4 is developed from left to right (Columns 1-9), following the reasoning summarized below:

1. Left-lateral slip on the Santa Cruz Island fault could be transferred eastward to the onshore Santa Monica fault via either the Malibu Coast fault or the Dume and offshore Santa Monica faults (Dolan et al., 2000), or be partitioned between these systems (Cols. 1-2). The eastern end of the Santa Cruz Island fault appears to be continuous with the Malibu Coast fault, but it is also possible that slip could be transferred to the western end of the Dume fault across a zone of complex faulting (C. Sorlien, personal communication). The Malibu Coast fault appears to have a very low slip rate (<0.5 mm/yr), and may be inactive. There is increasing evidence, however, that the Dume fault W of Pt. Dume may accommodate significant left-lateral slip (Dolan et al., 2000; Sorlien et al., 2001). Sorlien and Kammerling (C. Sorlien, written communication) have seismic evidence that the Dume fault continues E of Pt. Dume, striking ENE, and propose that left-lateral slip on the offshore Santa Monica fault of Dolan et al. (2000) is transferred to the Dume fault across a ≈2 km left step (Fig. 5.2). They propose, therefore, that the WNW-striking fault W of Pt. Dume is a restraining segment that experiences left-reverse slip. There is evidence that slip on the onshore Santa Monica fault is left-reverse (Dolan et al., 2000), but the left-lateral rate is not constrained.

2. Based on Dolan et al. (2000) the Santa Monica fault is estimated to dip 65°N (Col. 3) and to root into the 20°N-dipping blind Santa Monica Mountains thrust at a depth of about 14 km (Fig. 5.2b), as proposed by Davis and Namson (1994). Alternatively, Tsutsumi et al. (2001) propose that the Santa Monica fault dips 45° at depth and is the upward continuation of an active Santa Monica Mountains thrust that dips >45°N (Fig.5. 3b). In this scenario the eastern part of the Malibu Coast fault is truncated at shallow

depth by the Santa Monica fault, and is therefore not considered a significant earthquake source.

3. Gravity and air-photo lineations suggest that the Raymond fault may be continuous with the Hollywood fault, but this has not been confirmed by mapping (Weaver and Dolan, 2000) (Col. 5).

4. Recent analyses (e.g. Meigs et al., 1999) indicate that the Santa Monica Mountains thrust is slipping at a rate ~0.1 mm/yr, much slower than the rate proposed by Davis and Namson (1994), and even that the thrust may not be active (Col. 7). The dip-slip rate in the model of Tsutsumi et al. (2001) is <1.3 mm/yr. Based on seismicity, Seeber and Sorlien (unpublished) suggest that the thrust may extend under and south of the Dume fault up to a depth of about 8 km (Col. 8) (see also Dolan et al., 2000).

Compton-Los Alamitos Thrust, Palls Verdes and Newport-Inglewood Faults

Shaw and Suppe (1996) (referred to as SS96) modeled the Compton-Los Alamitos (CL) thrust as a ramp dipping 20°-25°NE with an average dip-slip rate of 1.4±0.4 mm/yr since ≈2.5Ma. SS96 proposed two alternative models (their Fig. 5.7). In the first the ramp flattens to horizontal decollements at its lower and upper edges, generating the CL and Torrence-Wilmington-Belmont (TWB) fault-bend fold trends, respectively. In the second, the CL trend is generated above a wedge-fault geometry, in which the CL ramp is a backthrust above a lower horizontal decollement and SW-dipping ramp. Ongoing analysis of seismic reflection lines further SW suggests that the TWB trend is a fault-propagation fold above the blind tip of a NE-dipping blind fault, the Wilmington thrust, imaged at about 4 km depth, which may splay off the CL system (J. Shaw, written communication).

J. Shaw (written communication) also interprets offset reflections under San Pedro Bay as a blind fault dipping about 45°SW from a depth of about 4 km, which he suggests may be the deeper plane of the near-vertical surface Palos Verdes fault (PV). Oblique slip on this plane would be partitioned into right-lateral and reverse components in the near surface. Ward and Valensise (1994) (referred to as WV) had previously proposed an oblique-slip plane dipping 65°SW under the Palos Verdes peninsular between 6 and 12 km depth, the base of the seismicity. WV attribute this oblique slip PV plane to the restraining geometry of the onshore segment of the fault (Fig. 5.1). Shaw's interpretation can be viewed as an alternative geometry for an oblique slip deeper PV plane, although his seismic line passes several km SE of the restraining bend. Alternatively, either plane could be interpreted as a fault separate from a PV that dips near vertically to the base of the seismogenic zone.

Fig. 5.1 shows the CL ramp of the original SS96 ramp-flat model. The non-uniqueness inherent in the SS96 modeling and interaction of an active CL system with both the active Newport-Inglewood and Palos Verdes faults result in the rather complicated set of alternative characterizations shown in Fig. 5.4. The cross-sections depict the Wilmington thrust with a nominal dip of 45° and the Shaw and WV SW-dipping oblique planes as mutually exclusive alternatives. The logic tree shown in Fig.5.5 is developed as follows:

Recent work by K. Meuller and T. Rockwell (Mueller, 1997; K. Mueller, written communication) including trenching, cone penetrometer profiles and structure contours on dated aquifers strongly suggests that the either the slip rate on the CL system since ≈330Ka is much slower (about 0.3 mm/yr) than the average Pliocene-Quaternary rate derived in SS96, or that the system is now inactive (Col. 1). None of the work reported to date can discriminate between the (modified) ramp-flat and wedge models (Col. 2).

One possibility is that the CL terminates as the Wilmington thrust (Col. 3). However, the seismic across the TWB shows only gently folding at the base of the Quaternary, strongly suggesting that Quaternary slip on the CL bypassed the Wilmington thrust, which is

probably now inactive (J. Shaw, written communication). Note that the original SS96 interpretation of the CL flattening under the TWB is not supported by the Shaw's more recent interpretation of the folding. The CL ramp can either stop short and refold the upper part of the PV (Fig. 5.4a), or it can extend into San Pedro Bay (Figs. 5.4b-d) (Col. 4), perhaps as the source of the San Pedro Bay escarpment. (Characterization of the CL-PV interaction is deferred until Cols. 7-9, discussed in (5) below.)

SS96 modeling does not constrain the depth of the CL thrust or Central Basin decollement (Col. 5). The minimum depth of the lower fault bend (or the wedge tip) is constrained to 8.5 km by interpretation of well and seismic data, but the maximum depth could be the base of the seismogenic crust, estimated as 17 km in this location (Fig. 5.4).

Any scenario that involves an active CL ramp-flat geometry in which the Central Basin decollement is significantly shallower than the base of the seismogenic zone implies that the Newport-Inglewood fault (NI) is offset by the CL, so that the NI is split into segments in the hanging and foot walls of the thrust. Alternative CL, NI and Wilmington thrust source combination scenarios are shown in Col. 6. The hypocentral location of the 1933 Long Beach earthquake suggests that the hanging wall segment of the NI extends to a depth of at least 12 km. The resulting width of the footwall segment would then be ≤ 5 km so that this segment would not be considered a significant earthquake source. However, the possibility of an earthquake nucleating at the base of the seismogenic crust on the foot wall segment and propagating across the offset – presumably involving rupture of that section of the CL – on to the hanging wall segment is also considered. The feasibility of this scenario depends on the offset distance. Assuming that slip on the NI and CL system initiated at approximately the same time (3-2.5 Ma: SS96), the offset is equal to the total slip on the CL, estimated as 4 km by SS96. This seems like a substantial rupture barrier. This offset could exist even if the CL became inactive ≈330 ka or later. The opposite alternative (no offset) is that the NI extended downwards to form a single, near vertical plane to the base of the seismogenic zone once the CL

became inactive. Only the latter alternative is implemented in the logic tree branch (Col. 1) for an inactive CL.

If the CL extends into San Pedro Bay (Col. 4), then it must interact with the PV. The several alternative possibilities for the interaction, shown as sub-trees (A)-(E), depend on the choice of the ramp-flat or wedge model (Col. 2) and depth to the ramp or wedge (Col. 5). The resulting PV source combination scenarios in Col. 9 are combined with the NI-CL-W scenarios in Col. 5.

(**A**) corresponds to Fig.5.4e where the depth to the upper decollement of a wedge is 12 km – coinciding with the estimated base of the seismogenic zone - or greater, and to all cases in which the CL stops short of the PV (e.g. Fig. 4a). In these cases the CL does not interact with the PV within the seismogenic crust. The sub-vertical PV in the shallow subsurface can be either continuous with a SW-dipping plane at depth or can extend vertically through the seismogenic crust (Col. 7). In the latter case the SW-dipping plane is considered to be a separate blind fault. The Shaw or WV SW-dipping geometry is selected in Col. 8. If the Shaw plane is treated as the downward extension of the PV in Col. 7, then it slip on it is oblique. Treated as a separate fault, it can be either reverse or oblique. Slip on the WV plane is oblique in both cases, in accord with their modeling result.

(**B**) corresponds to Fig. 5.4b in which the CL ramp cuts the PVF at a depth about 4 km. This is the minimum depth for the CL/PV intersection, since the PV is imaged seismically as deep as this (J. Shaw, personal communication). The PV is offset by the CL ramp. Since the location of the SW-dipping plane defined by either Shaw or WV is fixed by observations or modeling, neither can be the continuation of the surface PV, and either is considered only as a separate source in Col. 8. Lacking any other constraint, the PV is considered to be vertical in both the hanging and footwalls of the CL. The range of

offset alternatives considered for the NI also applies to the PV, although the offset models for the two faults are not necessarily correlated. It is unlikely that the narrow hanging wall segment of the PV in this scenario is a viable independent source. Therefore, the relatively high slip rate at the surface (≈3 mm/yr) would require events that nucleate on the wider foot wall segment and propagate on to the hanging wall segment. Here again, the feasibility of this depends on the width of the PV offset.

(**C**) covers the case where either the CL ramp (Fig. 5.4c) or wedge upper decollement (Fig. 5.4f) cut the PV near the upper edge of the WV oblique plane. This scenario is similar to (B), except that Shaw's SW-dipping plane is confined to the CL hanging wall, and is not considered a viable source.

(**D**) covers the case of a ramp-flat model with the Central Basin decollement near the base of the seismogenic crust (Fig. 5.4d). This scenario is analogous to (A), except that the PV/SW-dipping plane root into the CL ramp above the base of the seismogenic crust.

(**E**) applies to wedge model cases intermediate between (A) and (C), where the upper decollement cuts the PV between 6 and 12 km depth. The SW dipping planes are treated the same as in (A), except that they root into the upper decollement and the WV plane is considered too narrow to be a viable independent source. The offset vertical PV is treated the same as in (C). The viability of the hanging wall PV segment as an independent source increases as the decollement becomes deeper.

Oceanside and San Joaquin Thrusts, and Newport-Inglewood and Rose Canyon Faults

Seismic reflection profiles clearly image an ENE-dipping Miocene low-angle normal detachment underlying the continental shelf between Dana Pt. and Oceanside (Crouch and Suppe , 1993; Bohannon and Geist, 1998). Rivero et al. (2000) (referred to as R00)

mapped the detachment from Laguna Beach to the US-Mexican border (Fig. 5.1b), and proposed that the entire structure has been reactivated since the Late Pliocene as the Oceanside blind thrust (OT), capable of generating large earthquakes having return periods $\sim 10^3$ years. This proposal was based on interpretation of growth strata in the east-vergent San Mateo fold and thrust belt (Fischer and Mills, 1991; Crouch and Suppe, 1993) in the hanging wall of the detachment, associated young seafloor scarps along the continental slope, and uplifted marine terraces along the coast. R00 and Mueller et al. (1998) further proposed that the fold crest beneath the shelf slope break is the offshore extension of the San Joaquin Hills (SJH), which they propose are being actively uplifted above a bend in a SW-dipping blind backthrust off the OT, interpreted on offshore seismic profiles to the SE. R00 estimate that the dip of the thrust as about 15° in the north, increasing to about 25° offshore San Diego. The geometry shown in Fig. 5.1b is based on the R00 mapping, but divides the thrust into north and south segments. This is based on the distinct bend in the trend of the breakout zone at about 33°N shown in R00, the change in dip across this bend, and the greater intensity and extent of contractional deformation above the northern segment (C. Rivero and J. Shaw, personal communication).

The fold crest along the shelf break interpreted by R00 is coincident with the offshore NI zone interpreted from the seismic data by, among others, Fischer and Mills (1991) and Crouch and Suppe (1993). Several authors have identified this zone as a continuous, active right-lateral transpressive system that connects the onshore NI and Rose Canyon faults. Although in some locations the high-angle faults appear to disrupt the Oceanside detachment, the nature of the interaction is generally unclear. Fischer and Mills suggest that the active, inner compressional complex of the San Mateo system along the mid slope is part of the positive flower structure that they interpret in the vicinity of the shelf break along the length of the NI zone. The OT of R00 appears to correspond to the main thrust of the outer San Mateo complex (in the vicinity of the slope base), which Fischer and Mills suggest is truncated at a shallow depth by the westernmost fault of the inner complex. Alternatively, Crouch and Suppe suggest that east-dipping thrusts of the San Mateo system root into the detachment, which they propose has been reactivated locally

under NE-SW regional contraction. They propose that the contractional deformation belt uplifts the NI zone, but that contraction is decoupled from dextral shear. Fischer and Mills divide the offshore NI into Dana Point and Oceanside segments (Fig. 5.1b), both having a preferred right-lateral slip rate of 1 mm/yr.

None of the above interpretations establishes unequivocally whether either the right-lateral system or the thrust is a continuous source capable of generating large earthquakes, or how the two systems might coexist. R00 did not address high-angle faulting along the shelf break as an alternative (or addition) to their seismic interpretation, but did discuss alternative models of interaction between the OT and an assumed active offshore NI. This interaction must take place at depths of approximately 5 km or less, and further south the OT must also interact with the SE segment of the Coronado Bank fault. The cross-sections in Fig. 5.6 show alternative modes of interaction, based on the four alternative models proposed by R00. The logic tree is shown in Fig. 5.7 and discussed below.

Direct evidence for reverse separation on the OT is not observed, and lack of control on sediment ages renders evidence for activity based on disruption of the seafloor less than definitive (R00) (Col. 1). R00 used indirect methods to estimate slip rate bounds. A minimum slip rate of 0.3-0.4 mm/yr is estimated from the uplift rate of the SJH, and R00 show that this estimate is consistent with marine terrace uplift rates to the south. However, the backthrust (wedge) model for the SJH is open to question [see (6) below], and regional coastal uplift could be attributed other causes (e.g. Kier et al., 2002); if slip on the thrust were responsible for coastal uplift, then the uplift rate would be expected to decrease from north to south as the thrust diverges from the coast and its dip increases. Instead, coastal uplift is essentially constant. Also, tilting that might be expected from slip on the thrust is not observed, and the onset of coastal uplift may post-date the Pliocene initiation of thrusting estimated by R00 (T. Rockwell, personal communication). R00 based a maximum rate of 2.2 mm/yr on a geodetic estimate of convergence between the coast and Santa Catalina Island by Kier and Mueller (1999), but recent analyses

indicate that convergence is below the noise level (≈1 mm/yr) (Y. Bock, personal communication).

Fischer and Mills (1991) strongly assert that the NI is continuous with the Rose Canyon fault and is Quaternary active in the offshore (Col. 2). However, they state that only the 12 km-long segment offshore San Onofre displays convincing evidence for late Holocene displacement, while apparent Holocene slip decreases from Newport Bay to zero off San Mateo point. In general, Holocene activity is inferred by thinning or absence of sediments interpreted on high-resolution seismic, but these do not appear to have been reliably dated. Therefore, while fault splays within the zone cut the sea floor locally, evidence for Holocene through-going slip is not definitive.

If both the OT and the offshore NI are active, then one alternative (Col. 3) is that they represent local slip partitioning (Lettis and Hanson, 1991) and merge at depth into a single oblique-slip plane (Figs. 5.6c,d). The detachment is not imaged at depths greater than about 5 km, so that its dip east of the NI is not constrained. In their oblique slip scenario, R00 assumed that the dip of the oblique-slip plane is the same as the shallow OT. However, in an empirical study of 173 earthquakes Wells and Coppersmith (1991) found no events having rake less than 50° that occurred on faults dipping less than 45°. Therefore, the oblique-slip plane is shown schematically with a dip of 45° in Fig. 5.6. North of Dana Pt. slip on the oblique plane can propagate on to both the shallow thrust and the NI (Fig. 5.6c). South of Dana Pt. the situation is more complex [Fig. 5.6d; see (5) below)] and the oblique slip model appears less plausible.

Other models for the coexistence of the OT and offshore NI involve regional partitioning of dextral and reverse slip (Lettis and Hanson, 1991). In the first of these models the offshore NI truncates the OT (Fig. 5.6a), such that only the shallow OT imaged in the seismic is active (Col. 4). In this case the OT is not considered a significant earthquake

source. The alternative is that the OT offsets the NI (Fig. 5.6b). North of Dana Pt. the tip of the wedge of R00 is east of the NI, and the offset model is generally similar to that for the PV-CL (i.e. narrow hanging wall strike-slip segment) (Fig. 5.6b). However, south of Dana Pt. the NI and fault-bend fold - as they are presently interpreted - are coincident, so that the NI is offset by both the OT and the backthrust. This results in the rather complex situation shown in Fig. 5.6d, in which it seems improbable that a rupture of the foot wall segment of the NI would propagate to the surface.

If the OT is inactive, then active strike slip faults are assumed to extend to the base of the seismogenic crust. As for the NI-CL interaction discussed above, the strike-slip faults conceivably could still be offset as a result of previous slip on the thrust, but this possibility is not considered in the logic tree.

The back thrust is an integral part of the R00 model, and has two consequences. First, it structurally links the OT to the SJH (Col. 5), requiring that the northern segment of the OT extend to the northwestern end of the San Joaquin fold (OT-long). Otherwise the OT could terminate south of Dana Pt (OT-short). The NI Dana Pt. segment is divided into sub-segments north and south of Dana Pt. to accommodate these two alternatives in both the oblique and offset models ; OT-long interacts with both the north and south sub-segments , OT-short only with the south sub-segment. Secondly, the SW-dipping blind fault (SJ) in the backthrust interpretation is confined to the hanging wall (e.g. Figs. 5.6b,d) and is not, in itself, considered a significant earthquake source. Alternatively, the preferred model of Grant et al. (1999) locally partitions slip across the NI zone, reverse slip being accommodated on the SJ. The SJ dip is not constrained, but this model permits a steeply dipping fault that extends to seismogenic depth (Col. 6), either as an independent source or as a splay off the NI (e.g. Fig. 5.6a). One observation that argues against the backthrust model is that the SJH fold and the offshore fold as mapped by Mueller et al. (1998, Fig. 5.1) plunge to the south and NNW, respectively, and do not trend towards each other as might be expected if the two structures were directly linked.

Given the distance from the upper edge of the southern OT segment to the Rose Canyon fault and an estimated dip of ≈25°, the OT and Rose Canyon fault intersect at a depth of about 14-15 km. Since this is close to the base of the seismogenic zone, alternative interaction models are not needed. However, the SE segment of the potentially active Coronado Bank fault intersects the OT at a depth of about 6 km. Since this is similar to the OT-NI intersection, arguments analogous to (3)- (5) above are used to construct the sub-trees in Fig 5.7b, Cols. 7-9, under the assumptions that the slip styles on the NI and Coronado Bank faults are correlated (e.g. oblique slip on one implies oblique slip on the other), and that one active OT segment implies the other segment is also active.

Table 5.1: Fault Parameters

Fault segment	L (km)	D_1 (km)	D_2 (km)	Dip (deg)	V (mm/yr)
Whittier	23 +14/-8	0 +2/0	18 +2/-1	70 ±10	2.5 +0.5/-1.5
Chino	31 ±6	0 +2/0	15 +2/-1	90 ±10	1.0 +1.6/-0.6
Clamshell-Sawpit	14 ±3	0 +2/0	16 +2/-3	50 +10/-5	0.5 +1/-0.1
San Jose	15 ±4	1 +2/-1	14 +2/-1	75 +5/-10	1.0 ±0.5
Elsinor: Glen Ivy	36 ±4	0 +2/0	15 +2/-1	90 ±10	5.6 +0.4/-0.6
Temecula	47 ±4	0 +2/0	15 +2/-1	90 ±10	5.6 +0.4/-0.6
Julian	76 ±6	0 +2/0	15 +2/-1	90 ±10	5.6 +0.4/-0.6
Coyote Mtn.	43 ±4	0 +2/0	15 +2/-1	90 ±10	4 ±2
Laguna Salada	67 ±7	0 +2/0	15 +2/-1	90 ±10	3.5 ±1.5
San Andreas:					
Cholame-Carrizo	234 ±4	0 +2/0	11 +2/-1	90 0/-15	34 ±3
Mojave	100 ±10	0 +2/0	11 +2/-1	90 0/-15	23 ±7
S. Bernadino- Coachella	213 ±11	0 +2/0	11 +2/-1	90 0/-15	24 ±6
San Jacinto: S. Bernadino	36 ±4	0 +2/0	18 ±2	90 0/-15	12 ±6
S. Jacinto Valley	43 ±4	0 +2/0	18 ±2	90 0/-15	12 ±6
Anza	91.5 ±4.5	0 +2/0	16 ±2	90 0/-15	12 ±6
Coyote Creek	41 ±4	0 +2/0	13 +2/-1	90 0/-15	4 ±2
Borrego Mtn.	29 ±3	0 +2/0	12 ±2	90 0/-15	4 ±2
Superstition Mtn.	24 ±2	0 +2/0	12 ±2	90 0/-15	5 ±3
SuperstitionHills	23 ±2	0 +2/0	12 ±2	90 0/-15	4 ±2
Imperial	62 ±6	0 +2/0	12 ±2	90 0/-15	20 ±5
Santa Susana	28 ±3	0 +2/0	14 +2/-1	35 +15/-5	5.5 +4.5/-3.5
Sierra Madre: San Fernando	25 ±4	0 +2/0	14 +2/-1	40 ±5	1.0 +1/-0.4
W.	31 ±5	0 +2/0	14 +2/-1	50 +10/-15	1.0 +1/-0.4
E.	29 ±5	0 +2/0	14 +2/-1	50 +10/-15	1.0 +1/-0.4

Cucamonga	25 ±4	0 +2/0	14 +2/-1	40 ±10	4 +1/-2
San Cayetano: W.	20 ±3	4 0/-3	20 ±2	50 ±10	4.0 +1.8/-3.1
E.	17 ±3	0 + 2/0	20 ±2	50 ±10	7.4 ±3
Northridge (blind)	27 +7/-4	3 ±1	18 +2/-1	40 ±5	1.7 ±1
Verdugo	33 +2/-4	0 +2/0	14 +2/-4	60 +10/-15	1.0 +1/-0.5
Raymond	27 ±2	0 +2/0	16 +2/-1	70 ±10	4.0 +1/-0.5
San Gabriel: Central	34 ±10	0 +2/0	9 +7/-2	75 +10/-15	1.0 +1.5/-0.5
Vasquez Creek	25 +5/-7	0 +2/0	8 +8/-2	75 +10/-15	1.0 +1.5/-0.5
Holser	14 +6/-2	0 +2/0	14 ±2	75 +10/-15	0.5 ±0.5
Los Angeles	15 +1/-2	2 ±1	16 +2/-1	60 +10/-5	0.1 +0.1/0.05
Elysian Park	17 0/-2	4 ±1	16 +2/-1	50 ±10	1.5 ±0.7
Santa Fe-Coyote:					
Santa Fe Springs	14 ±2	2.0 ±0.5	15 +2/-1	25 ±5	1.0 +1/-0.5
Coyote Hills	8 ±2	2 ±1	15 +2/-1	25 ±5	1.2 +1.4/-0.5
Red Mtn. W.	28	2 +3/-2	20 ±2	50 ±10	0.5 +0.6/-0.4
Central	19	2 +3/-2	20 ±2	50 ±10	0.5 +6.0/-0.4
E.	7	2 +3/-2	20 ±2	50 ±10	3.5 +3.5/-3.1
Oak Ridge W.	11 ±3	2 +5/-2	20 ±2	50 +15/-5	5.1 +0.5/-0.3
E.	19 ±3	2 +5/-2	20 ±2	50 +15/-5	4.5 +0.5/-0.1
Ojai blind thrust W.	13	6 +1/-2	20 ±2	30 +20/-10	6.1 ±0.1
E.	15	8 +1/-2	20 ±2	30 +20/-10	2.6 ±0.1
Blind Oak Ridge W.	13	7 +1/-2	20 ±2	30 +20/-10	5.0 +2.5/-1
Central	31	7 +1/-2	20 ±2	30 +20/-10	5.0 +2.5/-1
E.	23	7 +1/-2	20 ±2	30 +20/-10	5.0 +2.5/-1
North Channel	51	2 +3/-2	20 ±2	50 ±10	0.5 +6.0/-0.4
Pitas Point	47	2 +3/-2	8 ±2	65 +10/-15	1.0 +0.5/-0.2
Santa Ynez					
S. Branch + L. Cachuma	58	1 +2/-1	12 ±2	70 ±15	1.0 0/-0.95

Central	53	1 +2/-1	17 ±2	70 ±15	1.0 +5.7/-0.95
E.	34	1 +2/-1	11 ±3	70 ±15	1.0 0/-0.95
Arroyo Parida	59	1 +2/-1	11 ±3	70 ±15	0.4 0/-0.1
Santa Rosa Is. [1]	62	1 +2/-1	18 +3/-2	85 +15/-10	0.8 ±0.7
Santa Cruz Is. W. [1]	62	1 +2/-1	18 +3/-2	85 +15/-10	0.5 +0.5/-0.4
Santa Cruz Is. E. [1]	62	1 +2/-1	18 +3/-2	85 +15/-10	0.8 ±0.7
Channel Is. Thrust	79 +25/-20	8 ±2	17 ±2	15 +10/-5	1.3 +0.2/-1.2
Malibu Coast [2,3]	72 +7/-6	0 +2/0	13.5 ±1.5	70 ±10	0.5 +0.25/-0.45
Dume [2,4,5,6]	33 +9/-4	2 ±1	18.5 ±1.5	60 ±10	0.5 +0.25/-0.45
Santa Monica offshore [2,4,5,6]	26 +5/-3	0 +2/0	18.5 ±1.5	65 +5/-10	0.5 +0.25/-0.45
Santa Monica onshore [5,6]	11 ±2	0 +2/0	18.5 ±1.5	65 +5/-10	1.0 +0.5/-0.9
Hollywood	15 ±2	0 +2/0	16 +2/-1	70 ±10	1.0 +0.5/-0.9
Sta Monica Mtns. Thrust [7]	91 ±10	10.5 ±1.5	18.5 ±1.5	20 ±5	0.4 +0.6/-0.3
Newport-Inglewood					
Baldwin Hills [8]	26 +15/-10	0 +2/0	16 +3/-2	90 +15/-10	1.0 +0.5/-0.7
1933 segment [8]	36 +12/-13	1 +2/-1	16 +3/-2	100 ±10	1.0 +0.5/-0.7
Dana Point [9]	56 ±10	1 +2/-1	16 +3/-2	100 ±10	1.0 +0.5/-0.7
Oceanside [10]	51.5 ±10.5	1 +2/-1	15 ±2	100 ±10	1.0 +0.5/-0.7
Rose Canyon Del Mar [11]	26.5 +11.5/-10.5	1 +2/-1	15 ±2	100 ±10	1.0 +0.5/-0.7
San Diego [11]	16 +11/-8	1 +2/-1	15 ±2	100 ±10	1.0 +0.5/-0.7
P**alos Verdes**					
Santa Monica Bay [12]	20 +3/-14	1 +2/-1	12 +3/-2	100 +10/-20	1.0 +2/-0.5
Palos Verdes Hills [12]	23.5 +1.5/-10	0 +3/0	11 +2/-1	100 +10/-20	3.0 +1/-0.5
San Pedro Bay [12]	43.5 +9.5/-13.5	1 +2/-1	12 +3/-2	90 ±15	3.0 +1/-2.5
Coronado Bank (seg.)	30 +16/-4	1 +2/-1	12 +3/-2	90 ±15	3.0 +1/-2.5
Coronado Bank NW	63 +13/-10	1 +2/-1	12 +3/-2	90 ±15	3.0 +1/-2.5
SE [13]	127 +13/-10	1 +2/-1	12 +3/-2	90 ±15	3.0 +1/-2.5

San Diego Trough NW [14]	59 ±10	1 ±1	12 +3/-2	90 +10/-15	1.0 +1/-0.5
Los Coronados	78 ±10	1 ±1	12 +3/-2	90 +10/-15	1.0 +1/-0.5
SE	73 ±10	1 ±1	12 +3/-2	90 +10/-15	1.0 +1/-0.5
San Clemente NW + Santa Barbara	89 ±9	1 ±1	12 +3/-2	90 +10/-15	2.0 +2/-1.5
San Clemente Is.	62 +10/-13	1 ±1	12 +3/-2	90 +10/-15	2.0 +2/-1.5
SE	75 +10/-13	1 ±1	12 +3/-2	90 +10/-15	2.0 +2/-1.5
Compton-Los Alamitos Baldwin Hills	23 ±5	9.5 +2/-3	15 +2/-3	24 +6/-4	0.2 +0.3/-0.15
Central	46 ±2	9.5+2/-3	15 +2/-3	24 +6/-4	0.2 +0.3/-0.15
Santa Ana	30 ±3	9.5+2/-3	15 +2/-3	24 +6/-4	0.2 +0.3/-0.15
Oceanside thrust N **[15,16]**	86 +5/-6	2.5 ±1	15 ±2	14 ±2	0.4 +0.6/-0.3
S	53 +8/-9	1.5 ±1	13.5 ±2	24 ±2	0.3 +0.7/-0.2
Thirty Mile Bank thrust [17]	87.5 +15.5/-9.5	2 ±1	13 +3/-2	25 ±5	0.3 +0.7/-0.2

Notes:

(1) D_2 = 8±2 km for thin-skinned interpretation above Channel Is. Thrust (See Fig. 5.1 a and b)

(2) Left-lateral slip partitioned between Dume+Santa Monica offshore and Malibu Coast faults (Fig. 3, col. 1).

(3) For left-lateral slip continuity along Malibu Coast – Santa Monica onshore faults only ; (i.e. no slip partitioning) slip rate is 1.0 +0.5/-0.9 mm/yr.

(4) For left-lateral slip continuity along Dume-Santa Monica onshore+offshore only slip rate is 1.0 +0.5/-0.9 mm/yr.

(5) D_2 = 13.5±1.5 km for thin-skinned interpretation above Santa Monica Mtns. Thrust (Fig.3, col. 7).

(6) Alternative dip = 50° 0/-5 for Santa Monica and Dume faults (Fig. 3, col. 3).

(7) Alternative D1 = 8 +3/-3.5 km (Fig. 3, col. 8).

(8) D_2 = 15 +3/-2 km for thin-skinned interpretation above Compton-Los Alamitos thrust (Fig. 5, col. 1).

(9) D2 = 5 +2/-1 km for thin-skinned interpretation above Oceanside thrust (Fig. 7a, cols. 1, 2).

(10) D2 = 7 +2/-1 km for thin-skinned interpretation above Oceanside thrust

(11) D2 = 13.5 +1.5/-1 km for thin-skinned interpretation above Oceanside thrust.

(12) D_2 = 9.5 +2/-3 km for thin-skinned interpretation above Compton-Los Alamitos thrust (Fig. 5, col. 1).

(13) Not considered in thin-skinned interpretation above Thirty Mile Bank thrust (Fig.7b).

(14) D2 = 8 ±1 km for thin-skinned interpretation above Thirty Mile Bank thrust.

(15) Length = 54 +5/-6 km for short interpretation (Fig. 7a, col. 5).

(16) D_2 = 7±1 km for surface segment above oblique slip fault (Fig. 7a, col. 3). Deep oblique slip fault has D_1 = 7±1 km, dip = 50°±10.

(17) D_2 = 8±2 km for surface segment above oblique slip fault (Fig. 7b, col. 9). Deep oblique slip fault has D_1 = 8±2 km, dip = 50°±10.

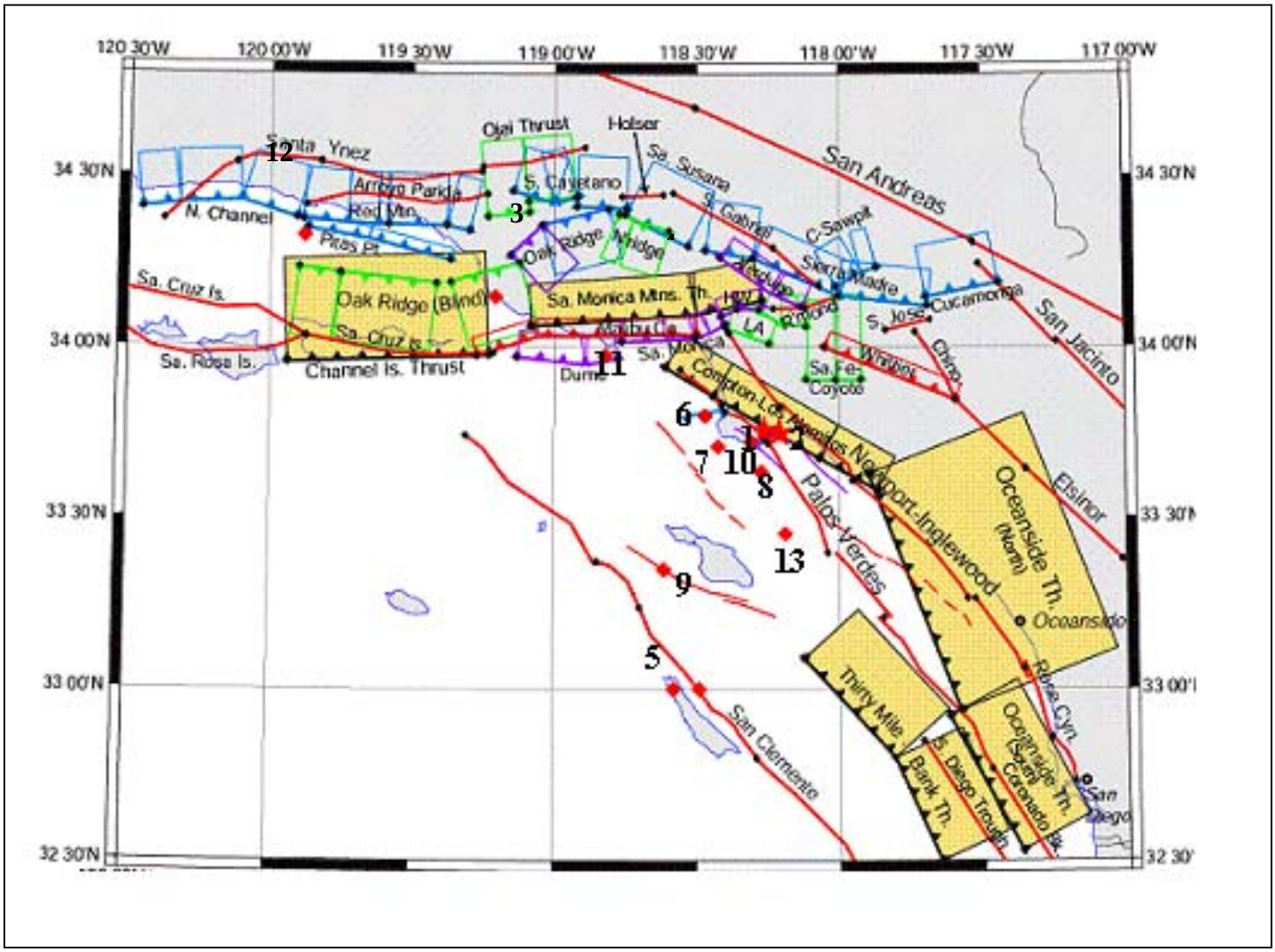

Figure 5.1a: Base earthquake source characterization model. The bold numbers show the sites given in Table ESX-1.

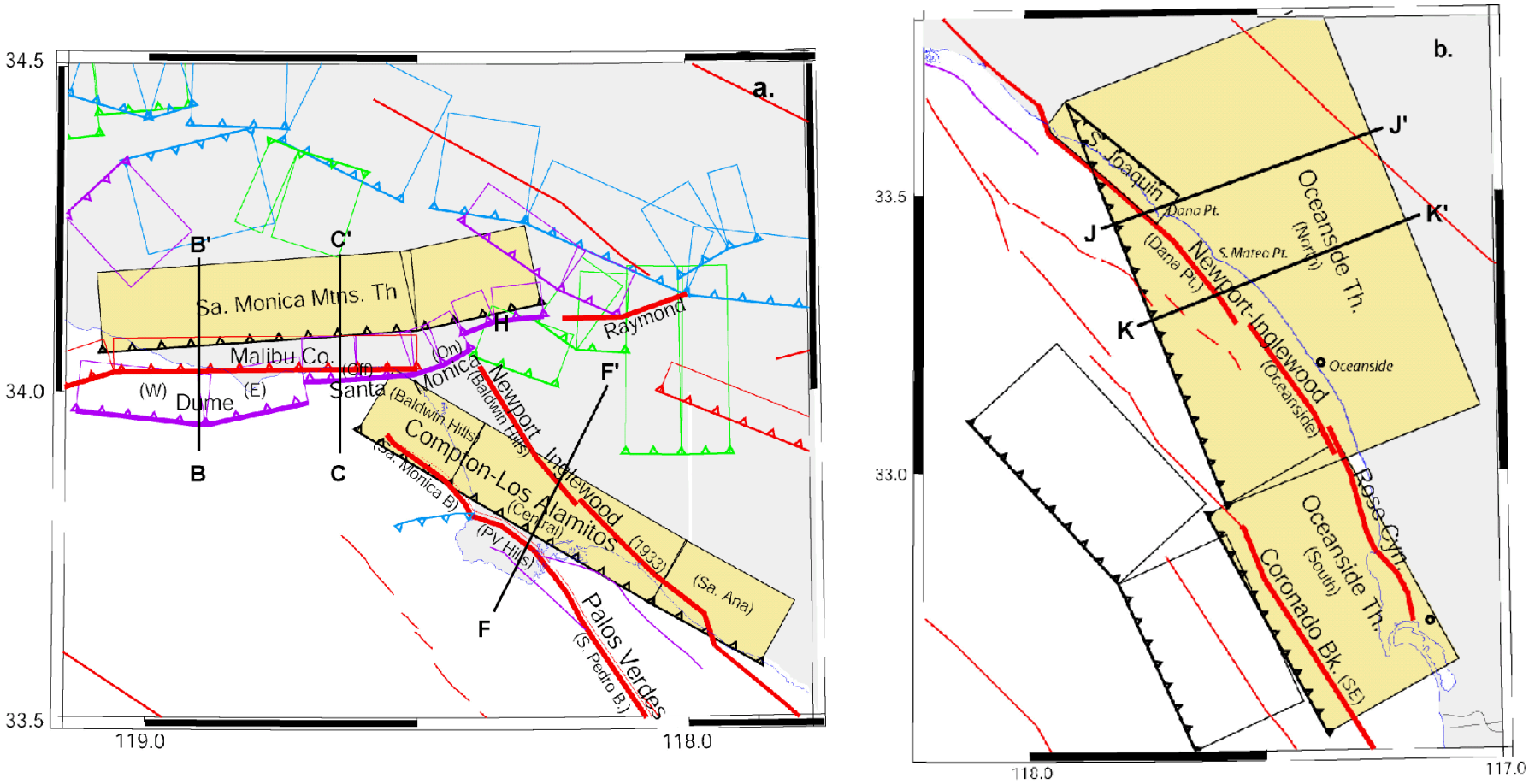

Figure 5.1b: Maps of two sections of the earthquake source model. Rectangles show surface projections of dipping faults. Blind thrust/reverse faults discussed in text shown in yellow, barbs on upper edge. Hollywood fault denoted H in a. Fault

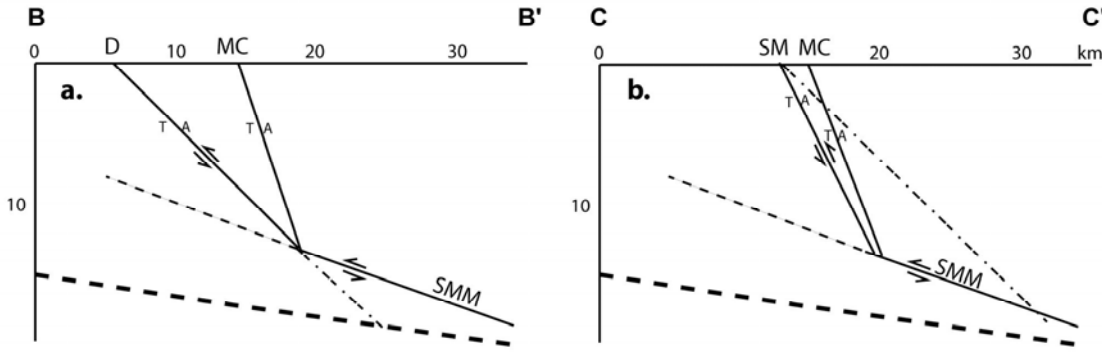

Cross-sections showing Dume (D), Malibu Coast (MC), Santa Monica (SM), and Santa Monica Mtn thrust (SMM) geometries (see Fig. 1 for cross-section locations). Dash-dot lines show alternative geometries of Dume and Sa. Monica faults according to Tsutsumi et al. (2001) interpretation of SM fault/SMM thrust. Alternative (shallow) geometry of SMM thrust shown as light dashed line. Heavy dashed line shows approximate base of seismicity (Magistrale and Zhou, 1996).

Figure 5.2: Cross-sections showing Dume, Malibu Coast, Santa Monica and Santa Monica MountainThrust.

Figure 5.3: Logic Tree for Dume/Malibu Coast – Santa Monica – Hollywood – Raymond Fault system and Santa Monica Mountain Thrust

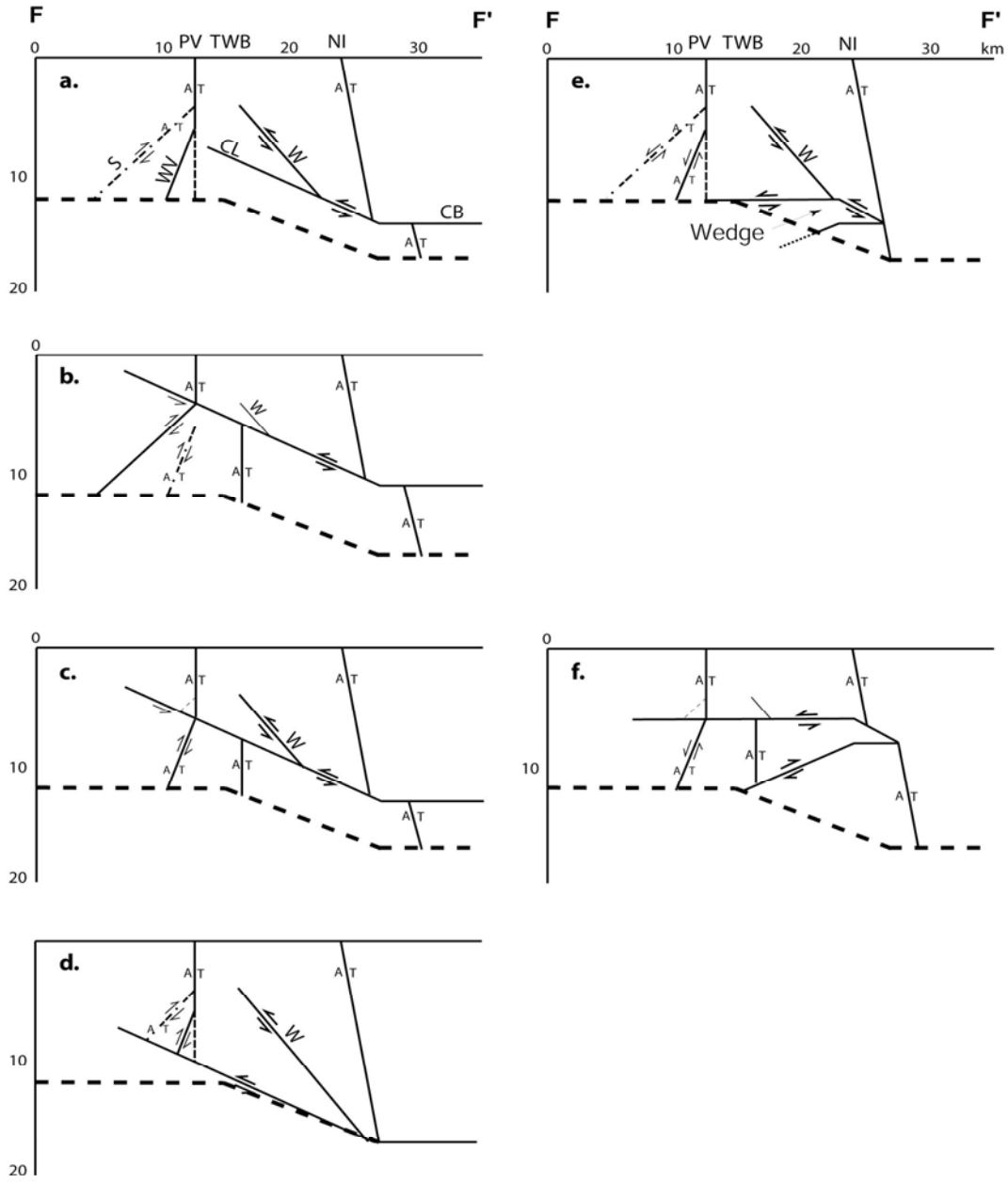

Figure 5.4: Cross-sections showing Alternative Compton-Los Alamitos ramp-flat (CL,CD) and Wedge geometries and possible relationships to Newport-Inglewood (NI) and Palos Verde (PV) faults, Wilmington thrust (W), and oblique-slip fault plane of Shaw (S) and Ward and Valensise (1996) (WV).S and WV are mutually exclusive alternatives (solid dash and dash-dot) in a, b, d, e. Vertical alternative to SW-dipping deep PV plane shown dashed in a, d, e. Heavy dashed line shows approximate base of seismicity

Segments

NIB: Newport-Inglewood, Baldwin Hills
NI33: Newport-Inglewood, 1933
CLB: Compton-Los Alamitos ramp, Baldwin Hills
CLC: Compton-Los Alamitos ramp, Central
CLS: Compton-Los Alamitos ramp, Sa. Ana
CD: Central Basin decollement
W: Wilmington thrust

PVM: Palos Verdes, Sa. Monica Bay
PVH: Palos Verdes, PV Hills
PVP: Palos Verdes, S. Pedro Bay
WV: Ward and Valensise SW-dipping plane
S: Shaw SW-dipping plane

Multi-segment Sources

NI: [NIB + NI33]
CL: [CLB + CLC + CLS]
PV: [PVM + PVH + PVP]
We: Tectonic wedge(7)

-hf [hanging- + foot-wall](6)
-su Surface PV fault

NOTES:

(1) Cols. 6 & 9 show longest multi-segment sources, enclosed in brackets. Each fault system can also break in single-segment or smaller multi-segment ruptures.
(2) Sources in Col. 9 are added to those in Col. 6.
(3) Oblique or reverse
(4) Reverse
(5) CL plane above 12 km depth
(6) Rupture of PV or NI offset foot- and hanging-walls as multi-segment source may involve the intervening part of the CL plane.
(7) Wedge includes lower (SW-dipping) & upper (NE-dipping) ramps and lower and upper flats (Figs. 4b,e).

Figure 5: Logic tree for Compton-Los Alamitos thrust - Newport-Inglewood fault - Palos Verdes fault interactions

Figure 5.5: Logic Tree for Compton-Los Alamitos Thrust – Newport Inglewood – Palos Verde Fault Interactions

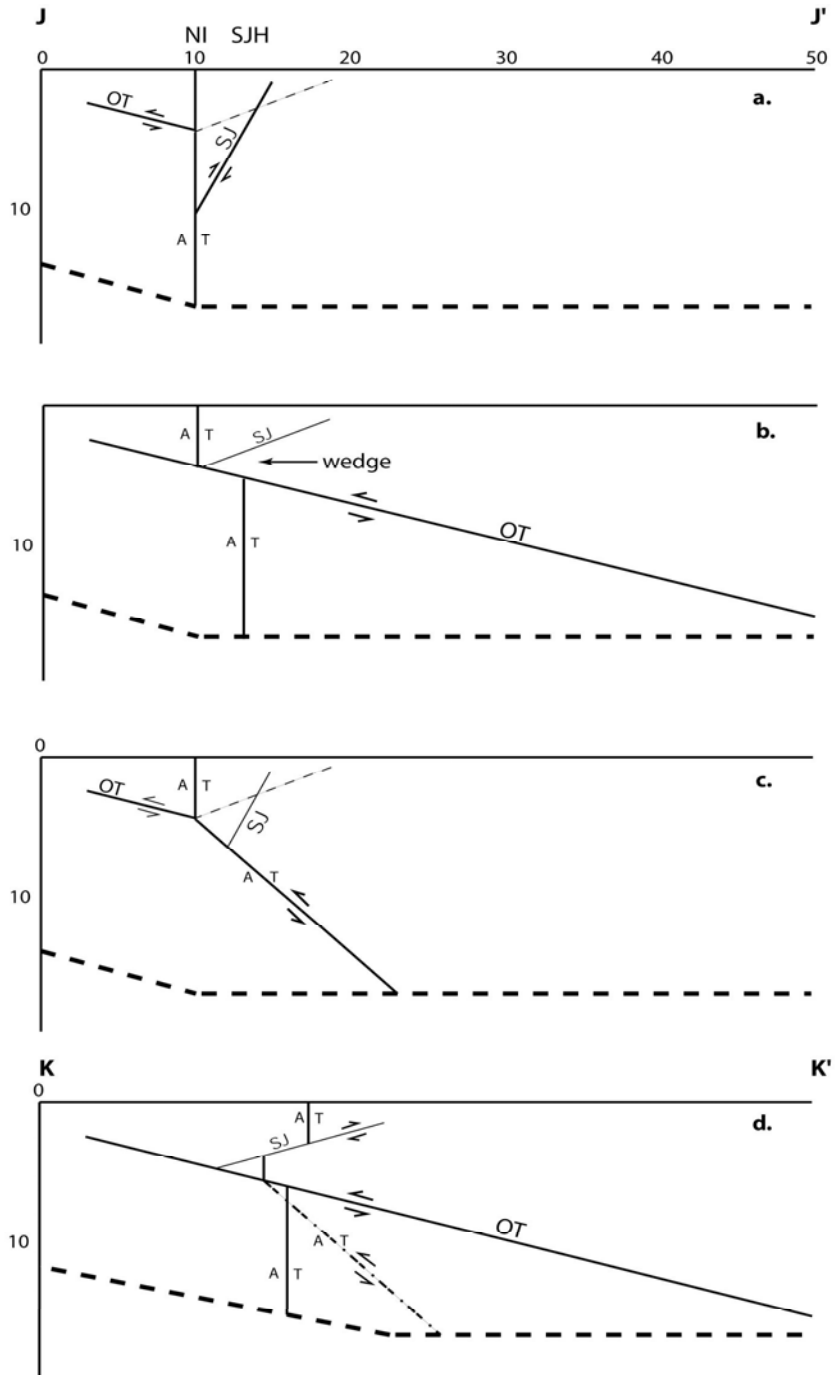

Figure 5.6: Cross-sections Showing Alternative Relationships among Northern Thrust (OT),Offshore Newport-Inglewood and Blind Fault under San Joaquin Hills. Steep-and-shallow-dipping alternative geometries for SJ shown as solid and dashed, respectively. Oblique portion slip alternative shown as dashed-dot in section KK' (d). Heavy dashed line shown approximate base of seismicity.

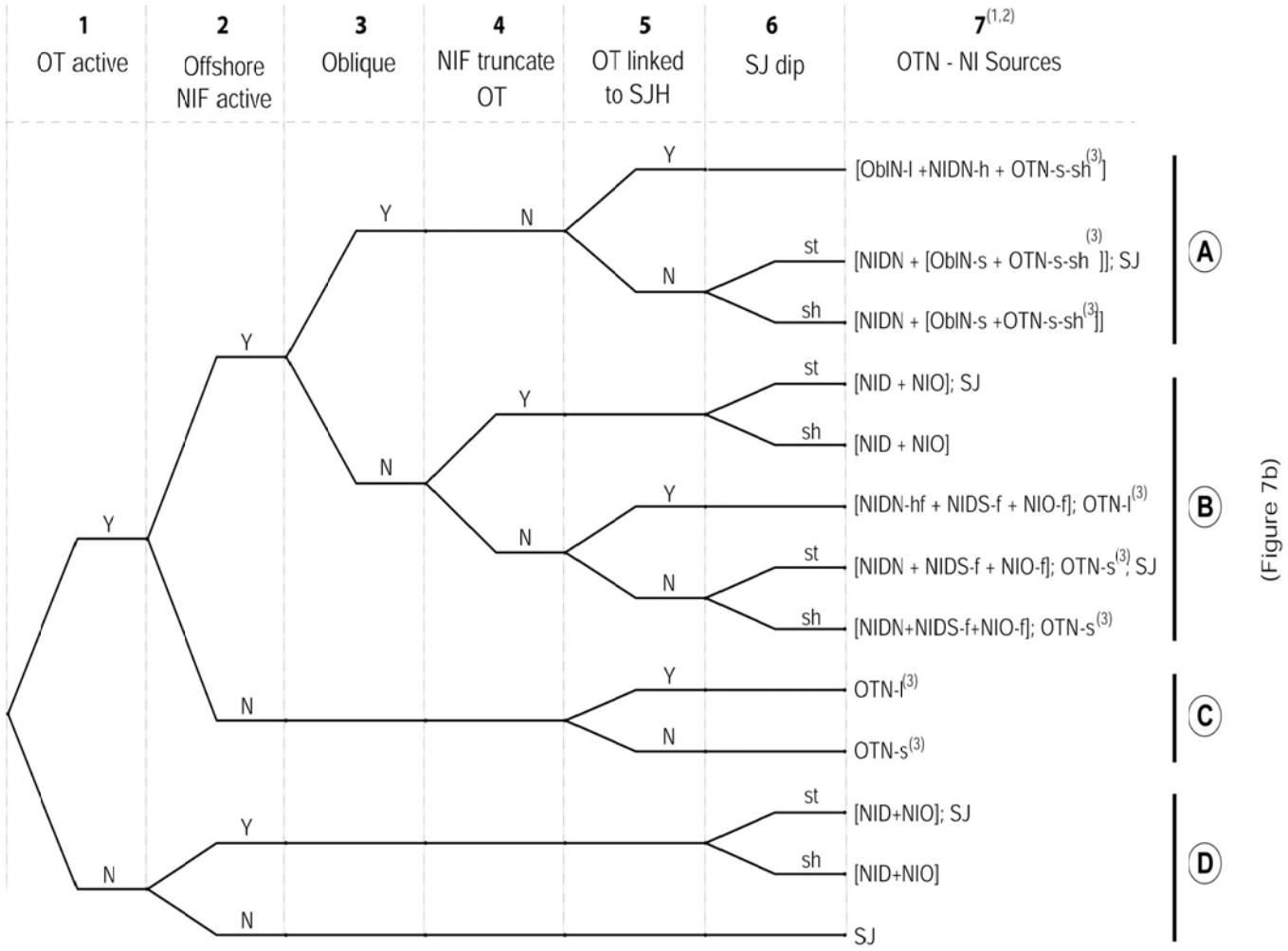

Segments

SJ:	San Joaquin Hills thrust
NID (N, S):	Newport-Inglewood, Dana Pt. (N, S sub-segments)
NIO:	Newport-Inglewood, Oceanside
OTN (-I, -s):	Oceanside thrust N (long, short)
OTS:	Oceanside thrust S
Obl (N, S)(-I, -s):	Oblique slip NIF/OT plane (N, S segments) (long, short)
-h,- f,-hf	Hanging-, foot-wall, [hanging- + foot-wall](4)
-sh	Shallow OT fault plane (depth < 5 km)

Multi-segment Rupture Sources

NID: [NIDN + NIDS]

NOTES:

(1) Col. 7 shows longest multi-segment sources, enclosed in brackets. Each fault system can also break in single-segment or shorter multi-segment ruptures.
(2) Sources in Fig. 7b, Col. 11 are added to those in Col. 7.
(3) OTN and ObIN combine with OTS and ObIS in Fig. 7b, Col. 11 to generate mulri-segment OT events.
(4) Rupture of PV or NI offset foot- and hanging-walls as multi-segment source may involve the intervening part of the CL plane.

Figure 7a: Logic Tree for N. Oceanside Thrust - Newport-Inglewood Fault - San Joaquin Hills Fault Interactions

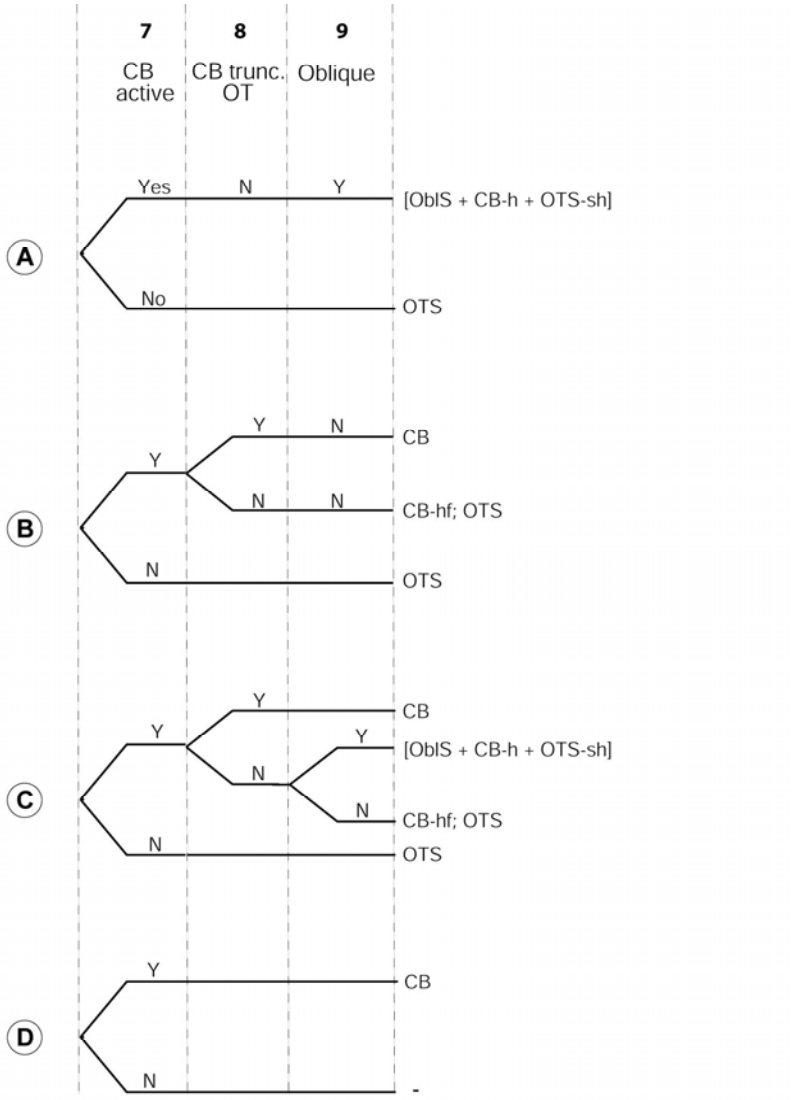

Figure 5.7b: Logic tree for S. Oceanside Thrust – Coronado Bank Fault Interactio

6. Ground Motion Attenuation Models

6.1 Ground Motion Modeling and Uncertainty

The choice of ground motion attenuation models for use in PSHA should reflect our best understanding of the local geology and regional wave propagation properties and the characterization of the earthquake sources. Ideally, a combination of physical models and observed strong motion data would produce the necessary models. Rarely is there a sufficient number of ground-motion recordings near a site to allow a direct empirical estimation of the motions expected for a particular set of conditions (Magnitude, Distance, fault geometry, source parameters). It is therefore necessary to develop relationships, expressed in the form of equations or look-up tables, for estimating ground motions in terms of magnitude, distance, site conditions, and other variables from the body of strong-motion data from a large region or a particular tectonic setting.

There has been a large number of earthquakes in the last decade that produced strong motion data. In addition, new modeling techniques have also led to a variety of new functional forms, some based on principles of seismology (e.g. Joyner and Boore, 1993), and others based more on statistical considerations (e.g. Campbell, 1997). Some models are also based largely on ensembles of numerically simulated data.

Recently, the Chi-Chi earthquake, in Taiwan (1999), and the Izmit, Turkey earthquake (1999) provided a wealth of new data in the near field and for relatively large magnitudes. This led to a general updating of a number of existing models. It also provided the opportunity to introduce new independent parameters such as the source mechanism, directivity and basin effects.

This has enabled modeling of the aleatory uncertainty to be refined. The standard error “sigma” that expresses the aleatory uncertainty in an attenuation model can now be expressed in terms of magnitude, distance from the site, and/or ground motion (acceleration) level.

The epistemic uncertainty, stemming from the differences in formulation of models by individual experts in the last decade, has not changed substantially, however.

In this study, we considered the latest published models and used the correction factors that are provided for different styles of faulting (strike-slip, normal, or reverse), and the relative position of the site with respect to the fault (foot-wall, hanging-wall). The estimates of the seismic hazard are based on the average of the two horizontal components of the ground motion, for a free field instrument at a hypothetical California rock site (V_s around 600m/sec) and for a generic western soil site (V_s around 310m/sec).

The epistemic uncertainty in the ground motion modeling was quantified by sampling through the community of ground motion models experts. We used a set of models from a selected group of experts who represent the knowledge of the scientific community for the region, and we assigned weights to each of them, according to the degree to which we believed they explained the data.

For each model selected, we used the characterization of the aleatory uncertainty "sigma", as stipulated by the developer of the model, who presumably would have fitted that uncertainty to the data.

6.2 Description of the Ground Motion Attenuation Models

For both, the peak ground acceleration, and for the spectral values, we selected a set of four models, whose general form is described in the Seismological Research Letters (SRL), 1997 with updates from the Taiwan and Turkey data (Abrahamson, 2000). These models are the following:

- Abrahamson and Silva, (Seismological Research Letters. pp94-127)
- Boore, Joyner and Fumal, (Seismological Research Letters. pp128-153)
- Campbell, (Seismological Research Letters. pp154-179)

- Sadigh, Chang, Egan, Makdisi, and Youngs, (Seismological Research Letters. pp180-189)

For each of the models, spectra are defined at 9 frequencies: 33.3, 20.0, 10.0, 6.67, 5.0, 3.33, 2.0, 1.0, and 0.5 Hz. For those models that did not provide all these frequencies, we interpolated between the closest frequency values. These attenuation models are described in 6.2.1 to 6.2.4.

6.2.1 Abrahamson and Silva

6.2.1.1 General Description and Comments

Using a database of 655 worldwide recordings from 58 earthquakes, a prediction models for the average component of ground motion in active tectonic regions was developed. All events greater than 4.5 magnitude, up to the 1994 Northridge earthquake, excluding subduction events. The sites were put into five distinct classes, as follows:

Class A	Rock for V_S >600m/s
	Or very thin soil (<5m) over rock
Class B	Shallow Soil
	Soil 5-20 m thick over rock
Class C	Deep Soil in Narrow Canyon
	Soil > 20 m thick
	Canyon < 2 km wide
Class D	Deep Soil in Broad Canyon
	Soil > 20 m thick
	Canyon > 2 km wide
Class E	Soft Soil for V_S <150 m/s

This model introduces new factors to account for effects of hanging wall and footwall of dipping faults. The total standard error is estimated as the square root of the sum of the squares of the intra-event and intra-event contributions.

6.2.1.2 Functional Form and Parameter Values

The general functional form of the spectral acceleration Sa is given by equation 6.1:

$$\ln Sa = f_1(M, r_{rup}) + F f_3(M) + HW f_4(M, r_{rup}) + S f_5(pga_{rock}) \quad (6.1)$$

where: M is moment magnitude, r_{rup} is the closest distance to the rupture plane in km, F is the faults type (1 for reverse, 0.5 for reverse/oblique, and 0 otherwise), HW is a dummy variable for hanging wall sites (1for sites over the hanging wall, 0 otherwise), and S is a dummy variable for the site class (0 for rock or shallow soil, 1 for deep soil).

The function $f_1(M, r_{rup})$ is the basic functional form of the attenuation for strike-slip events (SS) recorded at rock sites.

For $M \le c_1$:

$$f_1(M, r_{rup}) = a_1 + a_2(M - c_1) + a_{12}(8.5 - M)^n + \left[a_3 + a_{13}(M - c_1)\right] \ln R$$

For $M > c_1$: (6.2)

$$f_1(M, r_{rup}) = a_1 + a_4(M - c_1) + a_{12}(8.5 - M)^n + \left[a_3 + a_{13}(M - c_1)\right] \ln R$$

where $R = \sqrt{r_{rup}^2 + c_4^2}$

The style of faulting is defined by the following equation:

$$f_3(M) = \begin{cases} a_5 & \text{for } M \le 5.8 \\ a_5 + \dfrac{a_6 - a_5}{c_1 - 5.8} M & \text{for } 5.8 < M < c_1 \\ a_6 & \text{for } M \ge c_1 \end{cases} \quad (6.3)$$

and the hanging wall effect is given by $f_4(M, r_{rup}) = f_{HW}(M) f_{HW}(r_{rup})$ (6.4)

where:

$$f_{HW}(M) = \begin{cases} 0 & \text{for } M \le 5.5 \\ M - 5.5 & \text{for } 5.5 < M < 6.5 \\ 1 & \text{for } M \ge 6.5 \end{cases} \tag{6.5}$$

and

$$f_{HW}(M) = \begin{cases} 0 & \text{for } r_{rup} < 4 \\ a_9 \dfrac{r_{rup} - 4}{4} & \text{for } 4 < r_{rup} < 8 \\ a_9 & \text{for } 8 < r_{rup} < 18 \\ a_9 \left(1 - \dfrac{r_{rup} - 18}{7} \right) & \text{for } 18 < r_{rup} < 24 \\ 0 & \text{for } r_{rup} > 25 \end{cases} \tag{6.6}$$

The inter-event and intra-event variability are only dependent on magnitude M and are combined into the total standard error $\sigma_{total}(M)$:

$$\sigma_{total}(M) = \begin{cases} b_5 & \text{for } M \le 5.0 \\ b_5 - b_6(M - 5) & \text{for } 5.0 < M < 7.0 \\ b_5 - 2b_6 & \text{for } M \ge 7.0 \end{cases} \tag{6.7}$$

The values of the constants a_i, b_j, and c_k are given in table 6.1.

6.2.2 Boore, Joyner, and Fumal

6.2.2.1 General Description and Comments

This model of ground motion attenuation was developed for estimating horizontal response spectra and peak accelerations from western north America data. The equations give ground motion in terms of moment magnitude, distance and site conditions for strike-slip, reverse-slip or unspecified faulting mechanisms. Site conditions have not been used in this study, as the ground motion was estimated for rock.

The data set used to determine the parameters of the equations is based on the data set of Joyner and Boore of 1982 (Boore et al, 1982), augmented by data from the 199 earthquakes Petrolia and 1992 Landers, collected for the most part by the California Division of Mines and Geology (CDMG, 1992). The data was restricted to shallow earthquakes (less than 20 km deep) in western north America with moment magnitudes greater than 5.0.

The measure of distance (r_{jb}) is equal to the closest horizontal distance from the station to the point on the earth's surface that lies directly above the rupture. In the classification of the data, the strike-slip events are defined as those with a rake angle within 30 degrees of horizontal and reverse slip earthquakes are those with positive rake angles and their absolute value for left-lateral slip is less than 90 degrees.

6.2.2.2 Functional Form and Parameter Values

The complete form of the empirical relationship of the median logarithm of the acceleration is given by:

$$\ln Y = b_1 + b_2(M-6) + b_3(M-6)^2 + b_5 \ln r + b_V \ln \frac{V_S}{V_A} \tag{6.8}$$

where $r = \sqrt{r_{jb}^2 + h^2}$ (6.9)

and

$$b_1 = \begin{cases} b_{1SS} & \text{for strike-slip earthquakes} \\ b_{1RS} & \text{for reverse-slip earthquakes} \\ b_{1ALL} & \text{if mechanism is not specified} \end{cases} \tag{6.10}$$

The total uncertainty, including earthquake-to-earthquake variability, and the contribution from the random direction of the ground motion components, is characterized by $\sigma_{\ln Y}$.
The b, h, V, and $\sigma_{\ln Y}$ parameters are given in Table 6.2 for Y expressed in units of gravity (g), the distance in km, average shear wave velocity to 30m, in m/s, and h is a fictitious parameter determined by regression. The value of V_S, for rock, is taken equal to 620 m/s, in accordance with the recommendation made by the developers of the model.

6.2.3 Campbell

6.2.3.1 General Description and Comments

The attenuation relationships developed by this author represent a compendium and synthesis of near-source attenuation relationships previously developed by the same person. (see Campbell, 1981, 1987, 1989, 1990, 1992, and Campbell and Bozorgnia, 1994). The functional form of the final empirical model includes independent parameters that identify specific characteristics of the events, such as the depth to basement, the style of faulting, and local site conditions. The source-to-site distance (R_{SEIS}) is defined as the shorthest distance between the recording site and the presumed zone of seismogenic rupture on the fault. Following the observation that the top 2 to 4km of a fault is not seismogenic (Marone and Sholz, 1988), it follows that R_{SEIS} cannot be less than the depth to the top of the seismogenic part of the earth's crust.
Moment magnitude is the parameter that defines the size of events. The data set was restricted to near-source distances to minimize the influence of regional differences

In crustal attenuation and to avoid the complex propagation effects that have been observed at longer distances during, for example the 1987 (M=6.1) Whittier Narrows, the 1989 (M=6.9) Loma Prieta, and the 1992 (M=7.3) Landers, California earthquakes (Campbell 1988,1991c, Campbell and Bozorgnia, 1994b). Records that were influenced by the presence of heavy structures were not included in the analysis to avaoid soil-structure interactions effects.

6.2.3.2 Functional Form and Parameter Values

Case of the PGA:
The mean of the logarithm of the two horizontal components of peak ground acceleration (in units of g) is denoted A_H, and is given by the expression:

$$\ln(A_H) = -3.512 + 0.904M - 1.328\ln\sqrt{R_{SEIS}{}^2 + \left[0.149e^{(0.647M)}\right]^2} + \left[1.125 - 0.112\ln(R_{SEIS}) - 0.0957M\right]F + \left[0.440 - 0.171\ln(R_{SEIS})\right]S_{SR} + \left[0.405 - 0.222\ln(R_{SEIS})\right]S_{HR} \quad (6.11)$$

where the site condition parameters are $S_{SR} = 1$, and $S_{HR} = 0$ for rock.

F is the style of faulting parameter that is equal to 0 for strike-slip, and 1 for reverse, thrust , reverse-oblique and thrust-oblique. Reverse faulting being distinguished from thrust by the value of the dip angle of the fault plane. A dip angle greater than $\pi/2$ defines a reverse faults. A strike-slip fault has a rake angle less than $\pi/4$. A zero rake represents left-lateral strike-slip, π represents right-lateral, $\pi/2$ represents thrust, and -$\pi/2$ is for normal faulting.

The uncertainty in prediction of the acceleration is modeled by a nomal distribution centered on the mean defined by equation 6.11, and with standard deviation σ dependent on the value of the mean A_H, and defined by equation 6.12:

$$\left.\begin{array}{ll} \sigma = 0.55 & \text{for } A_H < 0.068g \\ \sigma = 0.173 - 0.140\ln(A_H) & \text{for } 0.068g \le A_H \le 0.21g \\ \sigma = 0.39 & \text{for } A_H > 0.21g \end{array}\right\} \quad (6.12)$$

Case of the spectral accelerations:

The mean of the logarithm of the geometric average of the two horizontal components of the spectral acceleration is given by equation 6.13:

$$\ln S_{AH} = \ln A_H + c_1 + c_2\tanh\left[c_3(M - 4.7)\right] + (c_4 + c_5M)\,R_{SEIS} + 0.5c_6S_{SR} + c_6S_{HR} + c_7\tanh(c_8D)(1 - S_{HR}) + f_{SA}(D) \quad (6.13)$$

In this equation, S_{AH} has units of g. It is given by equation 6.11, above. D, that represents the depth to basement rock is 0 for rock sites, and f_{SA} is given by equation 6.14:

$$f_{SA} = c_6(1 - S_{HR}) + 0.5c_6S_{SR} \quad (6.14)$$

The values of the parameters in equations 6.11 to 6.14 are given in table 6.3.

The uncertainty in the prediction of the spectral accelerations is represented by the standard deviation, σ_H, of the normal distribution centered on the mean values of calculated with equation 6.13.

$$\sigma_H = \sqrt{\sigma^2 + 0.27^2} \quad (6.15)$$

where σ is the standard error of estimate of $\ln S_{AH}$ from equation 6.11 and 6.12.

6.2.4 Sadigh, Chang, Egan, Makdisi, and Youngs

6.2.4.1 General Description and Comments

The authors present attenuation relationships for peak acceleration and 5% damping response spectral accelerations from shallow, crustal earthquakes, based on ground motion data primarily from California earthquakes. The relationships are developed for strike-slip and reverse-faulting earthquakes, rock and deep firm soils deposits, and earthquakes of moment magnitude M 4 to 8, and distances up to 100 km.

The present models represent a snapshot in the evolving development of relationships that started with the work of Sadigh et al. (1986, 1989, 1993), that included data from the 1989 M 7 Loma Prieta and 1992 M 7.2 Landers, and M 6.4 Big Bear earthquakes. More recently, the relationships were updated with the use of new data from the M 6.7 1994 Northridge earthquake.

6.2.4.2 Functional Form and Parameter Values

The logarithm of the ground motion Y, in units of g, is defined by its mean (Equation 6.16) and standard error $\sigma_{\ln Y}$ (Equation 6.17). The distance, in km, is the distance from the site to the surface projection of the closest point to the rupture.

$$\ln Y = C_1 + C_2M + C_3(8.5 - M)^{2.5} + C_4\ln(r_{rup} + C_{13}e^{C_5+C_6M}) + C_5\ln(r_{rup} + 2) \quad (6.16)$$

$$\sigma_{\ln Y} = (C_8 + C_9M)(1 - H(C_{10}) + C_{11}H(C_{10}) \quad (6.17)$$

where: $H(M) = 1$ for $M \geq C_{10}$

0 otherwise

Parameters C's are given in Table 6.4 for rock sites, and in Table 6.5 for soil sites.

6.2.5 Comparison of the Ground Motion Models

The four different types of models considered in the analysis are compared, first on the basis of their median values for the PGA on rock, and second on the basis of the median values for the PGV on rock, for several frequencies, and several styles of faulting, when available.

Figures 6.1 to 6.4 show all the median models for rock and PGA, including the three different faulting styles, namely strike slip (SS), reverse (Rev.) and those qualified as "others", for magnitudes 5.0, 6.5, 7.0, and 7.5.

The epistemic uncertainty is not only measured by the variability in the median models, but should also include the variability in standard deviations. Thus for a given magnitude and distance, based on an analysis of the median values and assuming that the variation in the standard deviations is smaller than that of the medians, we can observe that the epistemic uncertainty varies with magnitude and distance.

The dispersion in the estimates is lowest where the data is the most abundant, thereby showing the very good agreement between all the models between 15 km and 20 km for magnitude 5.0, 20 km and 40 km for magnitude 6.0, and between 25 km and 45 km for magnitudes 7.0 and above.

In the distances less than 10 km, the SS models have a range of prediction within a factor of 4 from the lowest to the highest value, for magnitude 5.0. This range decreases with magnitude, to reach a factor of 2 for magnitude 7.5.

The models start diverging for larger distances, to reach a factor of 3 at 100 km, between lowest and highest predicted values, for magnitude 5.0, and decreasing to a factor of 2 for magnitude 7.5. Including models for the other styles of faulting in the comparisons only increases the variability.

Similar observations can be made with the median estimation models of the spectral accelerations for a given frequency and magnitude. This is shown in Figures 6.5 to 6.16 for the actual median spectra used in the analysis for all the style of faulting models and for magnitudes 5.0, 6.5, and 7.0, for distances covering the close range, distances similar to that of the Greenville fault, and greater distances similar to that of the Hayward and San Andreas faults.

Period (sec)	a_1	a_3	a_5	a_6	a_9	a_{12}	b_5	b_6	c_4
2.00	-0.150	-0.7250	0.400	-0.094	0.160	-0.1400	0.85	0.105	3.50
1.00	0.828	-0.8383	0.490	0.013	0.281	-0.1020	0.83	0.118	3.70
0.50	1.615	-0.9515	0.581	0.119	0.370	-0.0635	0.80	0.130	4.30
0.30	2.114	-1.0350	0.610	0.198	0.370	-0.0360	0.78	0.135	4.80
0.20	2.406	-1.1150	0.610	0.260	0.370	-0.0138	0.77	0.135	5.10
0.15	2.407	-1.1450	0.610	0.260	0.370	0.0050	0.75	0.135	5.27
0.10	2.160	-1.1450	0.610	0.260	0.370	0.0280	0.74	0.135	5.50
0.05	1.870	-1.1450	0.610	0.260	0.370	0.0280	0.71	0.135	5.60
0.03	1.690	-1.1450	0.610	0.260	0.370	0.0143	0.70	0.135	5.60
0.01	1.640	-1.1450	0.610	0.260	0.370	0.0000	0.70	0.135	5.60
a_2 = **0.512,** a_4 = **-0.144,** a_{13} = **0.17,** c_1 = **6.4, and** n = **2, for all periods.**									

Table 6.1: Coefficients for the Average Horizontal Component Response Spectral Accelerations (5% Damping) for Abrahamson-Silva, 1997 model, rock sites.

Period (sec)	b_{1SS}	b_{1RV}	b_{1ALL}	b_2	b_3	b_5	b_V	V_A	h	c_{lnY}
2.00	-1.699	-1.801	-1.743	1.085	-0.085	-0.812	-0.655	1795.	5.85	0.672
1.00	-1.133	-1.009	-1.080	1.036	-0.032	-0.798	-0.698	1406.	2.90	0.613
0.50	-0.122	0.087	-0.025	0.884	-0.090	-0.846	-0.553	1782.	4.13	0.556
0.30	0.598	0.803	0.700	0.769	-0.161	-0.893	-0.401	2133.	5.94	0.552
0.20	0.999	1.170	1.089	0.711	-0.207	-0.924	-0.292	2118.	7.02	0.502
0.15	1.128	1.264	1.204	0.702	-0.228	-0.937	-0.238	1820.	7.23	0.492
0.10	1.006	1.087	1.059	0.753	-0.226	-0.934	-0.212	1112.	6.27	0.479
PGA	-0.313	-0.117	-0.242	0.527	0.000	-0.778	-0.371	1396.	5.57	0.520
V_S = 620 m/s for rock.										

Table 6.2 Coefficients for the Average Horizontal Component of Response Spectral Accelerations (5% Damping) for Boore, Joyner and Fumal 1997 model, rock sites.

Period (sec)	c_1	c_2	c_3	c_4	c_5	c_6	c_7	c_8
2.00	-0.328	2.23	0.66	.01	-.001	-0.36	0.83	0.62
1.00	-1.79	1.59	0.66	.0085	-.001	-0.38	0.57	0.62
0.50	-028	0.74	0.66	.0068	-.001	-0.42	0.25	0.62
0.30	0.77	0	0	.0035	-.00072	-0.40	0	0
0.20	0.79	0	0	.0011	-.00053	-0.18	0	0
0.15	0.72	0	0	-.001	-.00027	-0.02	0	0
0.10	0.48	0	0	-.0024	$7.0\ 10^{-6}$	0.14	0	0
0.05	0.05	0	0	-.0011	$5.5\ 10^{-5}$	0.20	0	0

Table 6.3: Coefficients for the Average Horizontal Component Response Spectral Accelerations (5% Damping) for Campbell, 1997 model, rock sites.

Period (sec)	c_1	c_3	c_4	c_7	c_8	c_{11}	$c_{12}=0, c_{13}=1$ **for rock**
2.00	-2.945	-0.070	-1.670	0	1.53	0.52	
1.00	-1.705	-0.055	-1.800	0	1.53	0.52	
0.50	-0.588	-0.40	-1.945	0	1.50	0.49	
0.40	-0.298	-0.028	-1.990	0	1.48	0.47	
0.30	-0.057	-0.017	-2.028	0	1.45	0.44	$M \leq 6.5$
0.20	0.153	-0.004	-2.080	0	1.43	0.42	
0.10	0.275	0.006	-2.148	-0.041	1.41	0.40	
PGA	-0.624	0	-2.100	0	1.39	0.38	
$C_2 = 1.0, C_5 = 1.29649, C_6 = 0.250, C_9 = -0.14, C_{10} = 7.21$							
2.00	-3.595	-0.070	-1.670	0	1.53	0.52	
1.00	-2.355	-.0.055	-1.800	0	1.53	0.52	
0.50	-1.238	-0.040	-1.945	0	1.50	0.49	
0.40	-0.948	-0.028	-1.990	0	1.48	0.47	
0.30	-0.707	-0.017	-2.028	0	1.45	0.44	$M > 6.5$
0.20	-0.497	-0.004	-2.080	0	1.43	0.42	
0.10	-0.375	0.006	-2.148	-0.041	1.41	0.40	
PGA	-1.274	0	-2.100	0	1.39	0.38	
$C_2 = 1.1, C_5 = -0.48451, C_6 = 0.524, C_9 = -0.14, C_{10} = 7.21$							

Table 6.4: Coefficients for the Average Horizontal Component of Response Spectral Accelerations (5% Damping) for Sadigh et al., 1997 model, rock sites.

Period (sec)	c_3	c_8	c_{10}	c_{12} **Strike-Slip**	c_{12} **Reverse**
2.00	-0.108	1.70	10.0	0.1001	-0.0526
1.00	-0.065	1.66	10.0	0.5665	0.5075
0.50	-0.33	1.61	10.0	0.8494	0.8285
0.40	-0.024	1.595	10.0	0.9251	0.9005
0.30	-0.014	1.58	10.0	0.9547	0.9547
0.20	-0.004	1.565	10.0	0.9187	0.9187
0.10	0.005	1.54	10.0	0.6395	036395
PGA	0	1.52	10.0	0	0

C_1=-2.17 for strike-slip, -1.92 for reverse and thrust earthquakes

C_2=1.0, C_4=1.70

C_5=0,C_6=0.32,C_{13}=2.1863 for $M \leq 6.5$

C_5=0,C_6=0.5882,C_{13}=0.3825 for $M > 6.5$

C_7=0

C_9=-0.16,C_{11}=0

Table 6.5: Coefficients for the Average Horizontal Components of Response Spectral Acceleration (5% Damping) for Sadigh et al., 1997 model, soil sites.

7. Results

7.1 Hazards Results

The results are presented for the rock site conditions only, in the form of hazard curves, for the 15-th, 50-th (median), 85-th percentile and mean estimates of the average of the two horizontal components of the ground motion. The hazard curves are presented for the 13 sites described in Table 1. The corresponding plots for PGA are shown in Figures 7.1 to 7.13.

Calculations were also performed for generic soil conditions, as provided in the models of ground motion attenuation (Section 6.). However, this type of information has a limited usefulness, since the exact site conditions at each of the sites was unknown at the time of the analysis. Therefore, these are not presented herein, but are available if necessary.

Mean Uniform hazards Spectra (UHS) are constructed as locï of 5% damping spectral values with the same probability of exceedance at each of the 9 frequencies (33.3 , 20.0, 10.0, 6.7, 5.0, 3.3, 2.0, 1.0, and 0.5 Hz). The UHS were calculated for 4 of the 13 sites whose coordinates are given in Table 1, namely for: Port of Los Angeles, Port of Long Beach, Port Hueneme, and Santa Monica. Figures 7. 14 to 7.17 show the mean UHS for 5 Return Periods (100, 500, 1000, 2000, and 10,000 year Return Periods), Figure 7.18 to 7.21 show the uncertainty (15-th, 50-th, 85-th percentiles and mean hazard curves) for 500 year Return Period, and Figures 7.22 to 7.25 show these uncertainties for 1000 year Return Period.

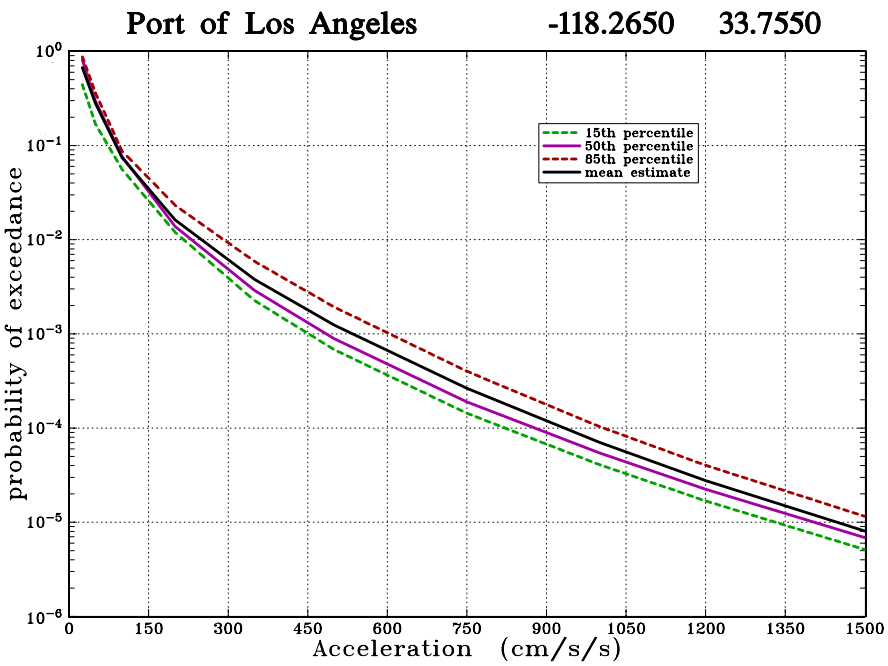

Figure 7.1 Peak Ground Accelerations (cm/s/s) Hazard Curves for Port of Los Angeles

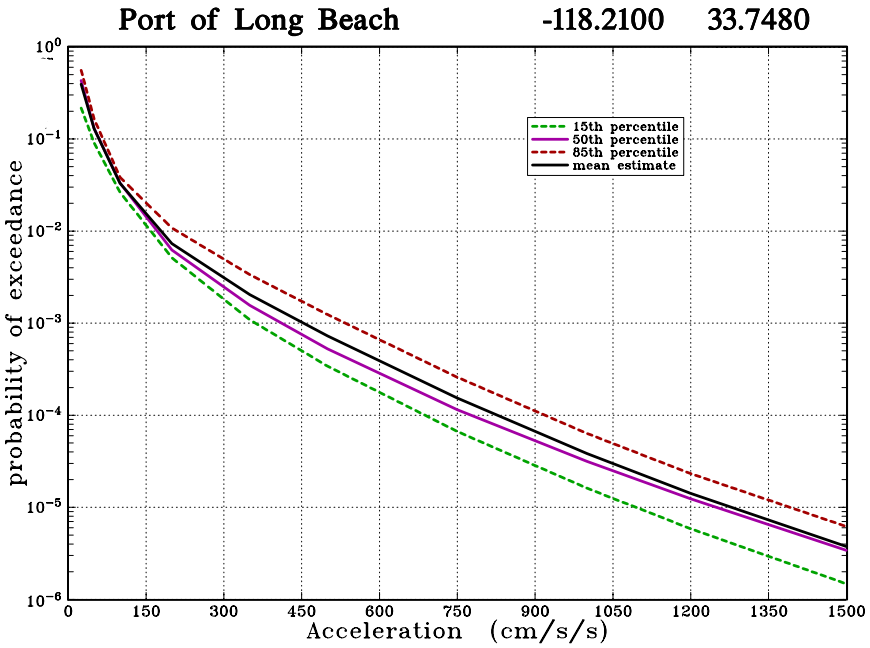

Figure 7.2: Peak Ground Accelerations (cm/s/s) Hazard Curves for Port of Long Beach

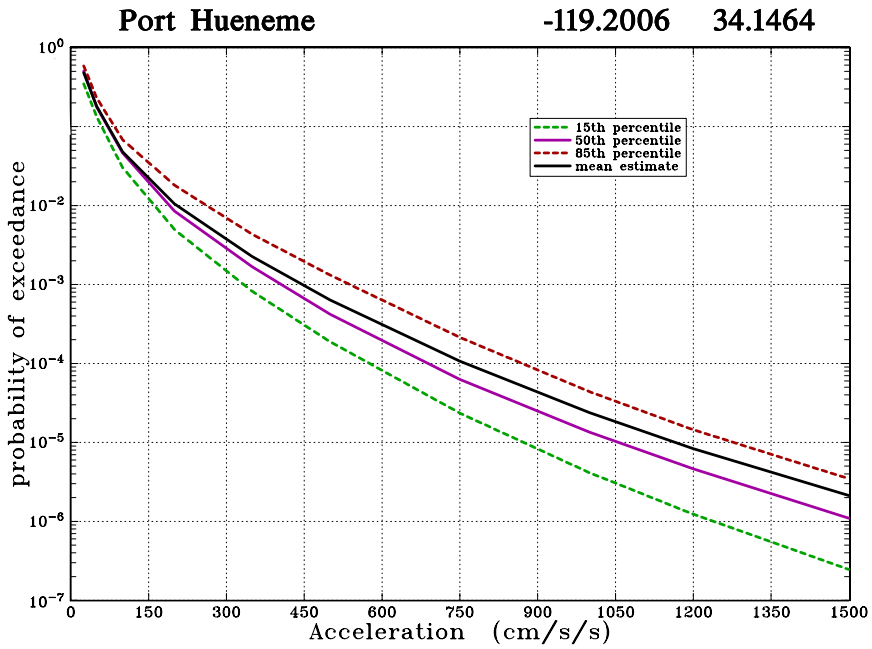

Figure 7.3: Peak Ground Accelerations (cm/s/s) Hazard Curves for Port Hueneme

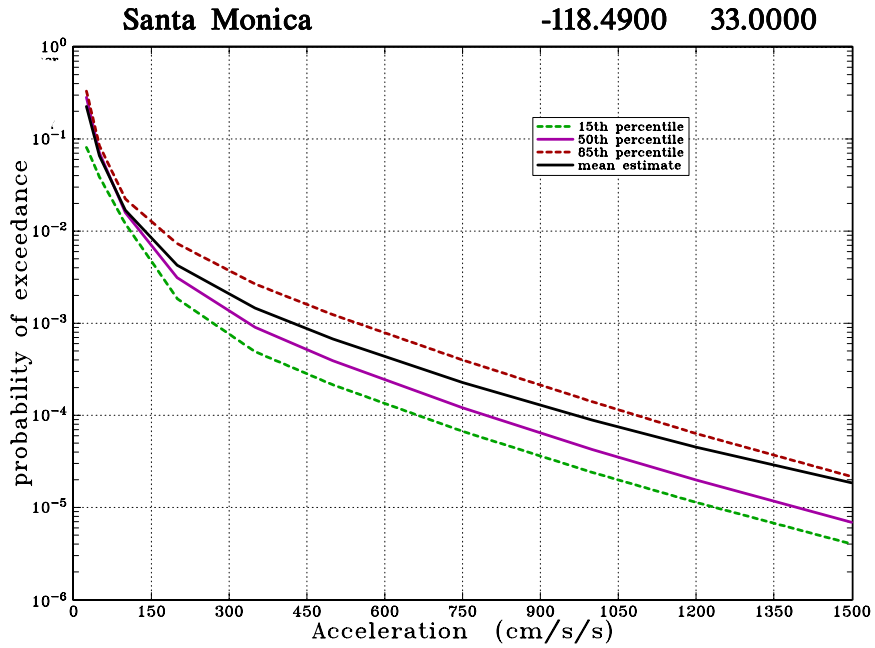

Figure 7.4: Peak Ground Accelerations (cm/s/s) Hazard Curves for Santa Monica

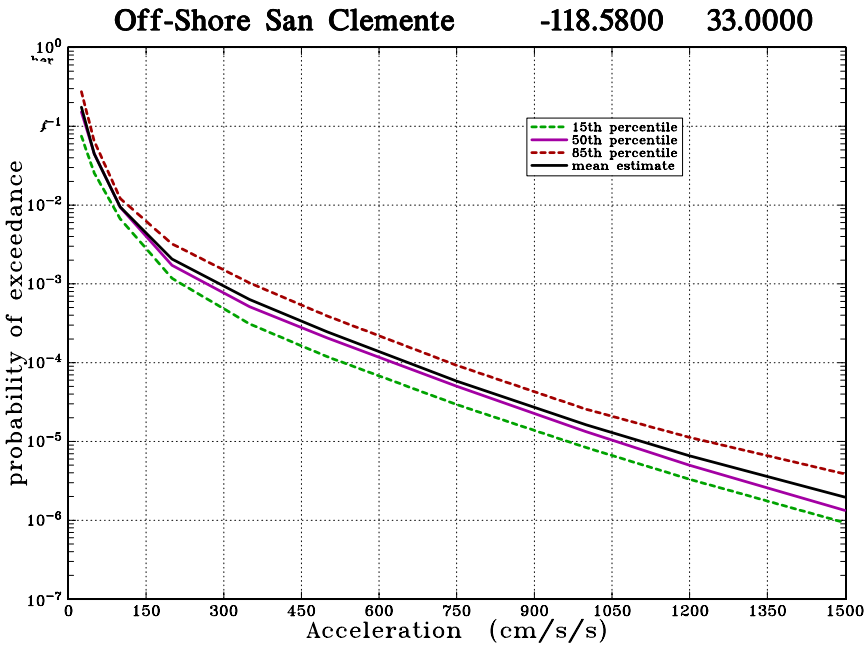

Figure 7.5: Peak Ground Accelerations (cm/s/s) Hazard Curves for Offshore San Clemente

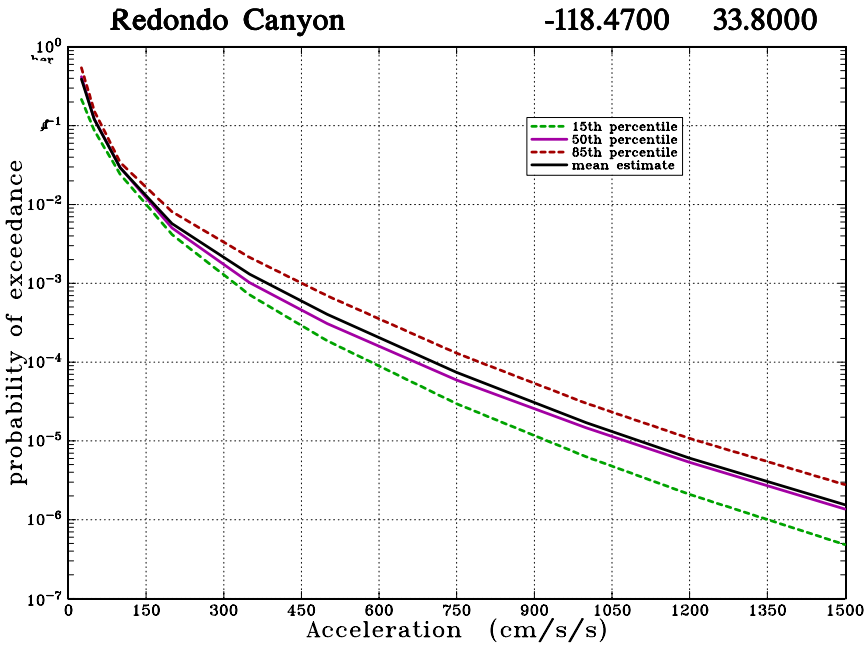

Figure 7.6: Peak Ground Acceleration (cm/s/s) Hazard Curves for Redondo Canyon

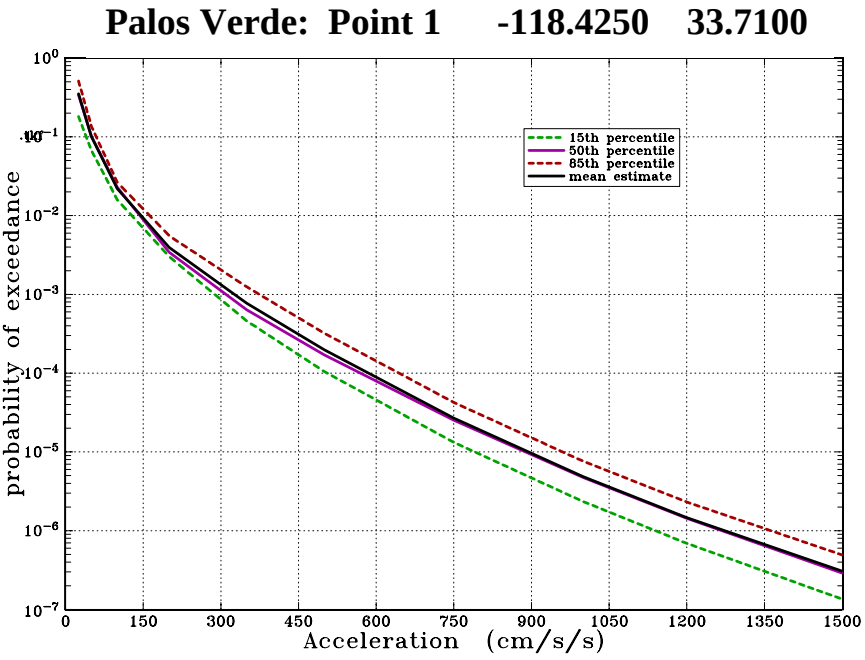

Figure 7.7: Peak Ground Accelerations (cm/s/s) Hazard Curves for Palos Verde Point 1

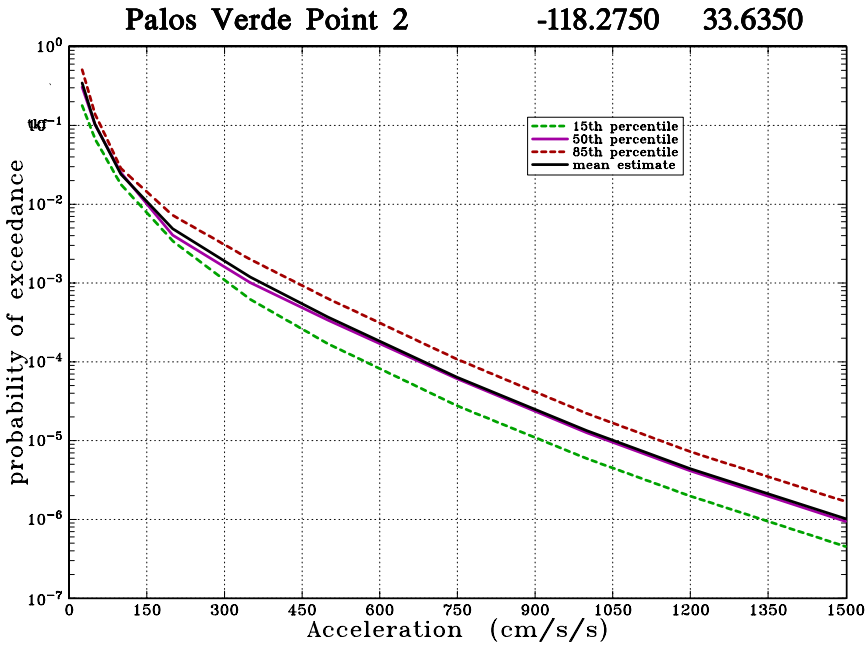

Figure 7.8: Peak Ground Accelerations (cm/s/s) Hazard Curves for Palos Verde Point 2

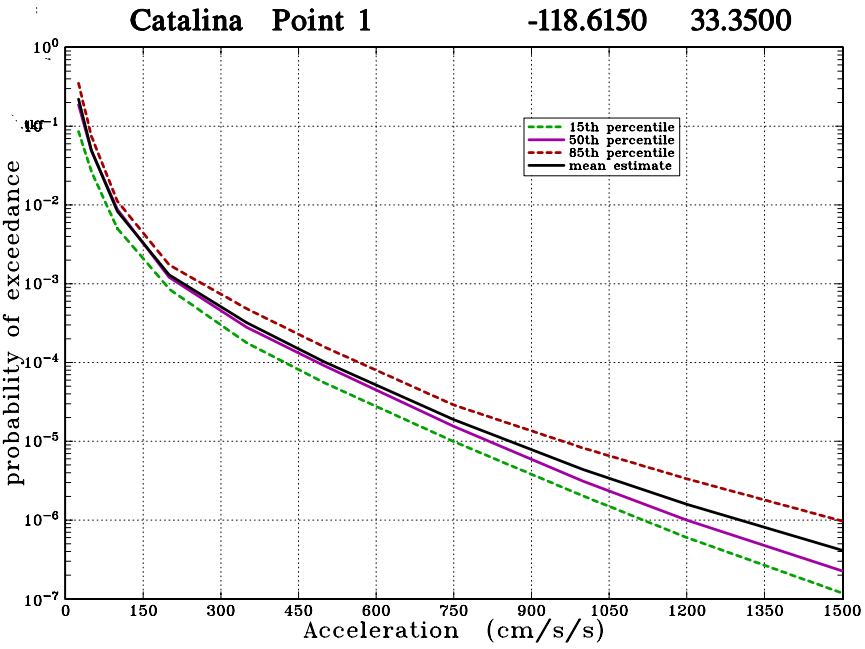

Figure 7.9: Peak Ground Accelerations (cm/s/s) Hazard Curves for Catalina Point 1

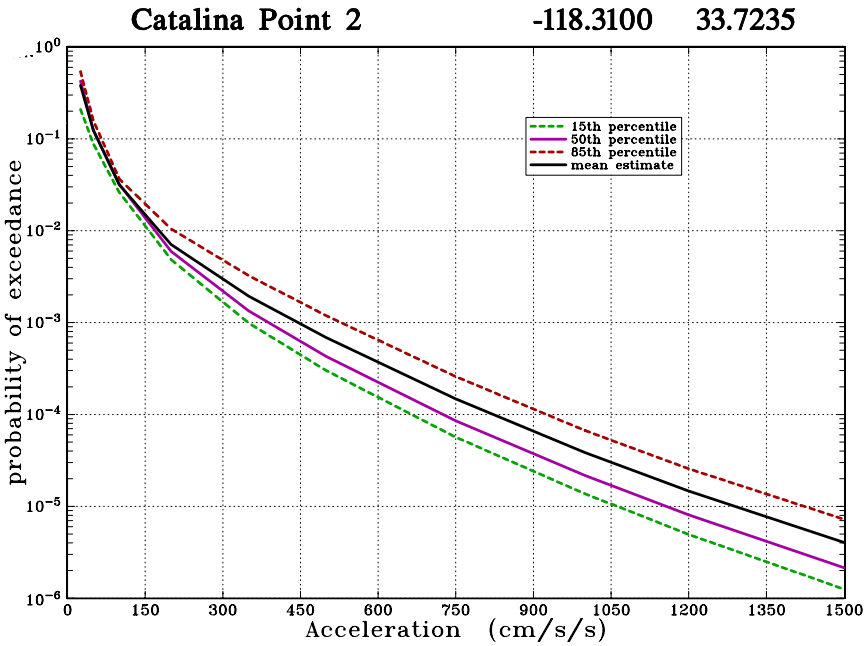

Figure 7.10: Peak Ground Accelerations (cm/s/s) Hazard Curves for Catalina Point 2

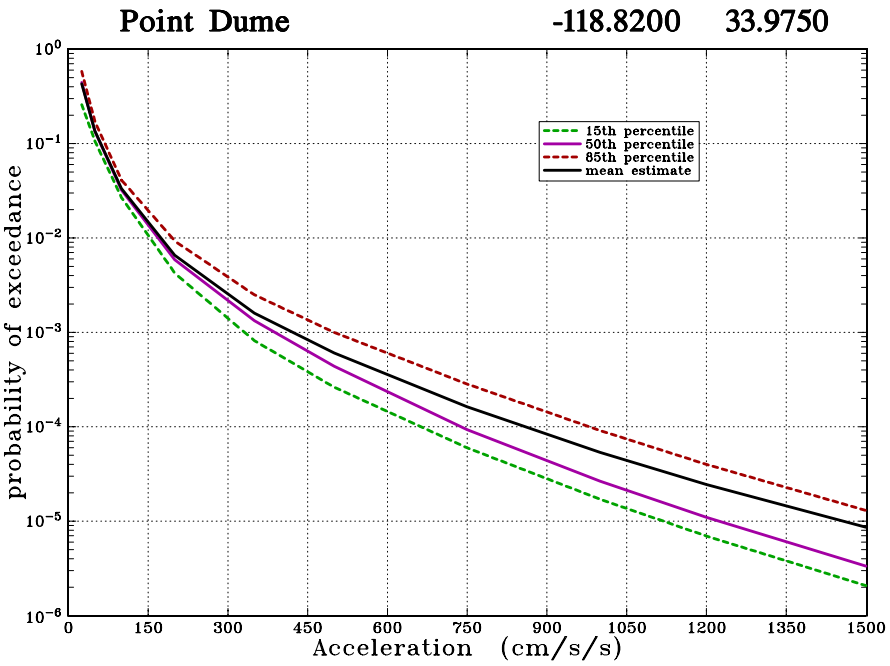

Figure 7.11: Peak Ground Accelerations (cm/s/s) Hazard Curves for Point Dume

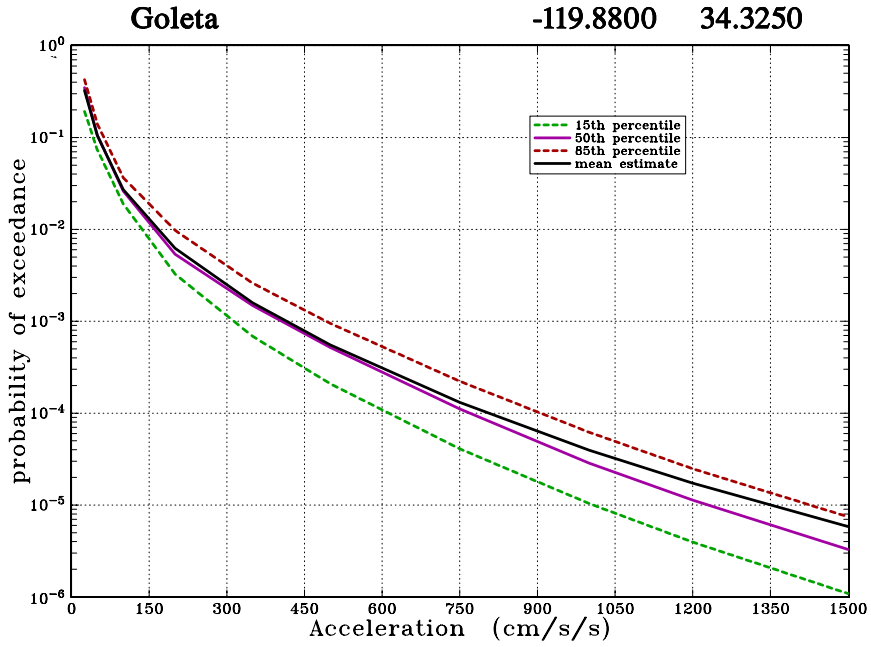

Figure 7.12: Peak Ground Accelerations (cm/s/s) Hazard Curves for Goleta

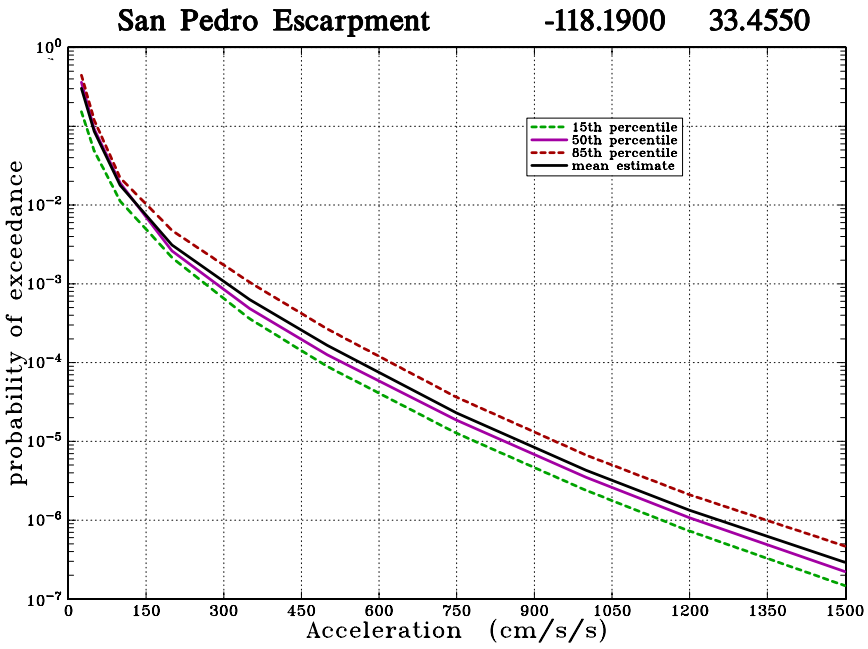

Figure 7.13: Peak Ground Accelerations (cm/s/s) Hazard Curves for San Pedro Escarpment

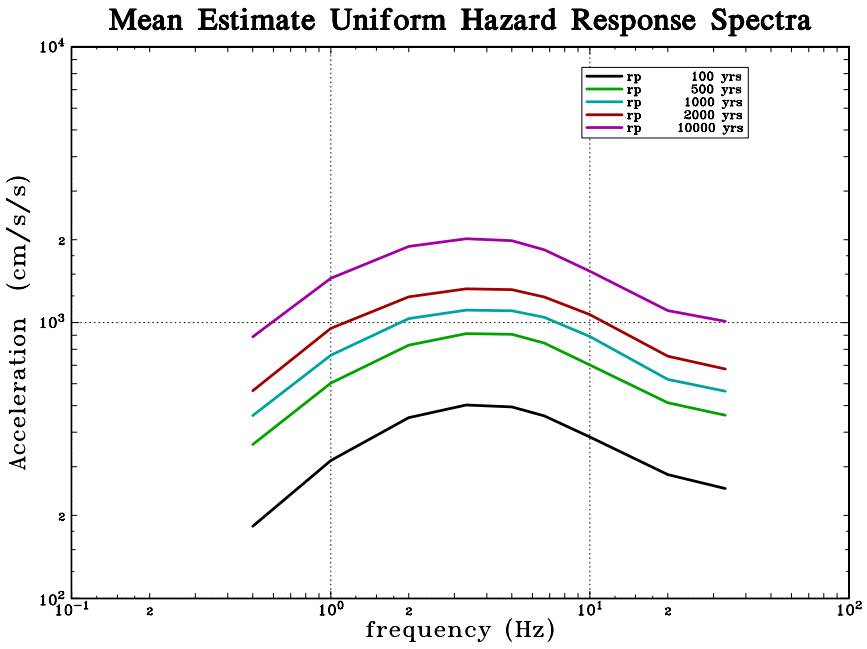

Figure 7.14: Mean Uniform Hazard Spectra for Port of Los Angeles (5% Damping)

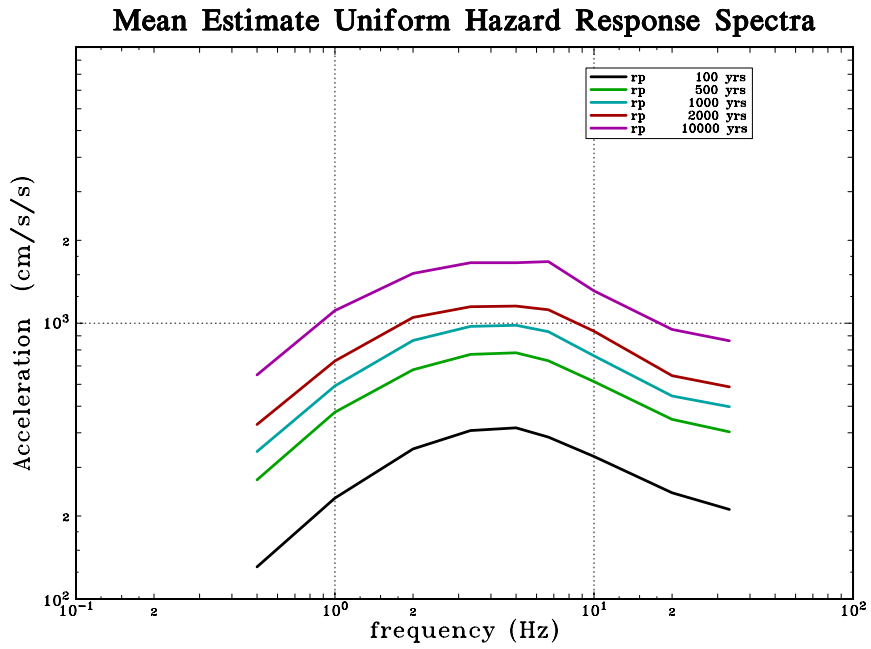

Figure 7.15: Mean Uniform Hazard Spectra for Port of Long Beach (5% Damping)

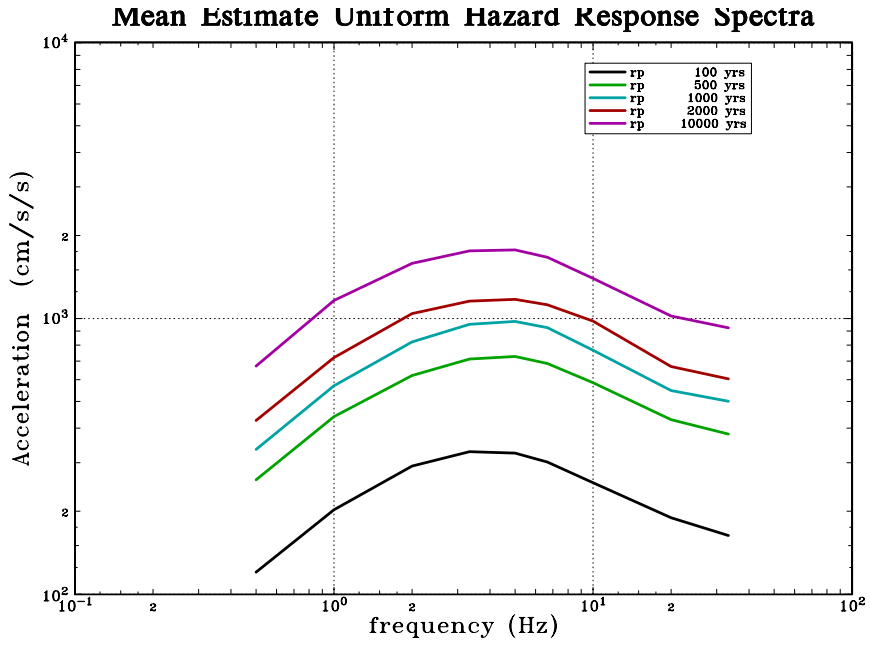

Figure 7.16: Mean Uniform Hazard Spectra for Port Hueneme (5% Damping)

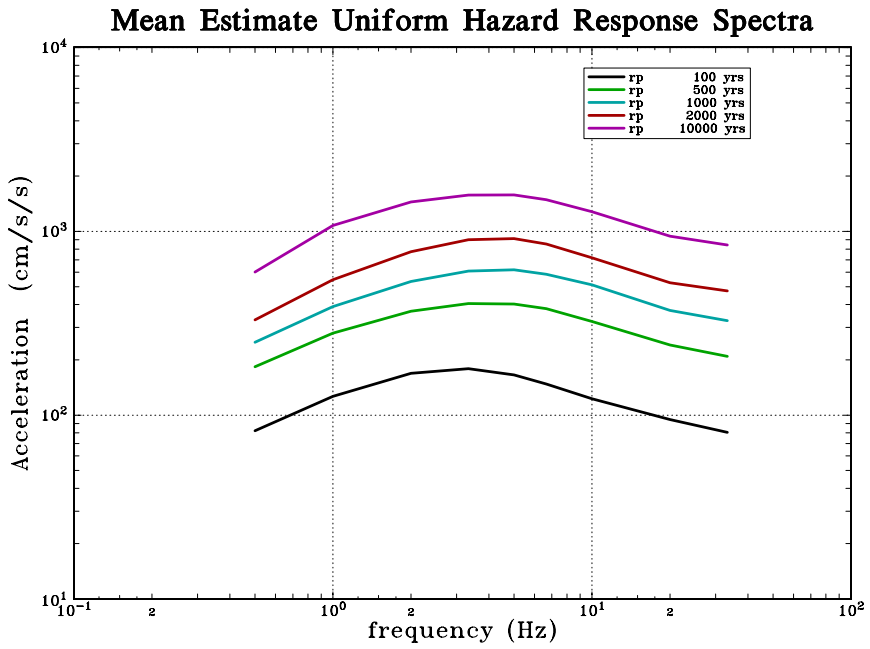

Figure 7.17: Mean Uniform Hazard Spectra for Offshore Santa Monica (5% Damping)

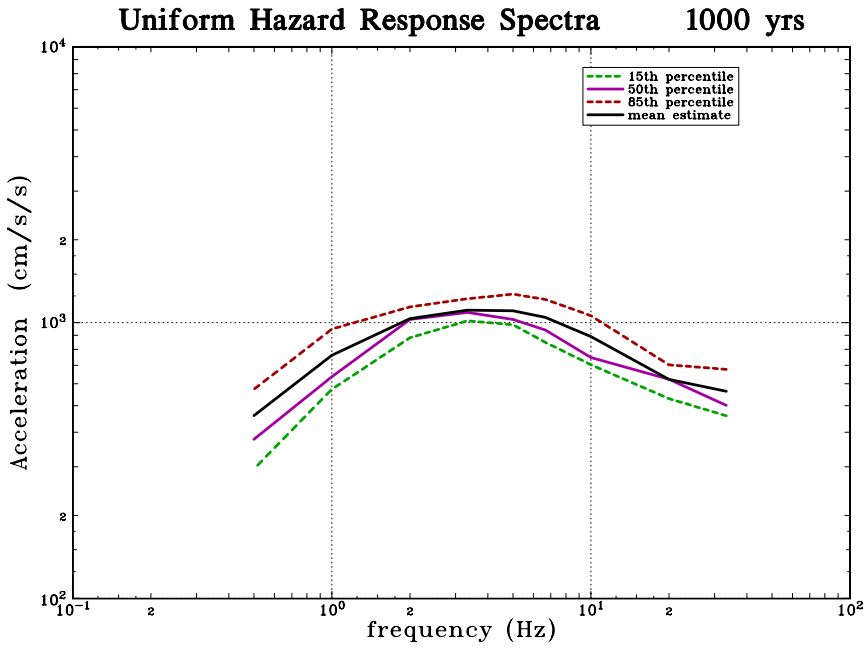

Figure 7.18: 15-th. 50-th and 85-th Percentile Uniform Hazard Response Spectra for Port of Los Angeles (5% Damping) for 1000 year Return Period

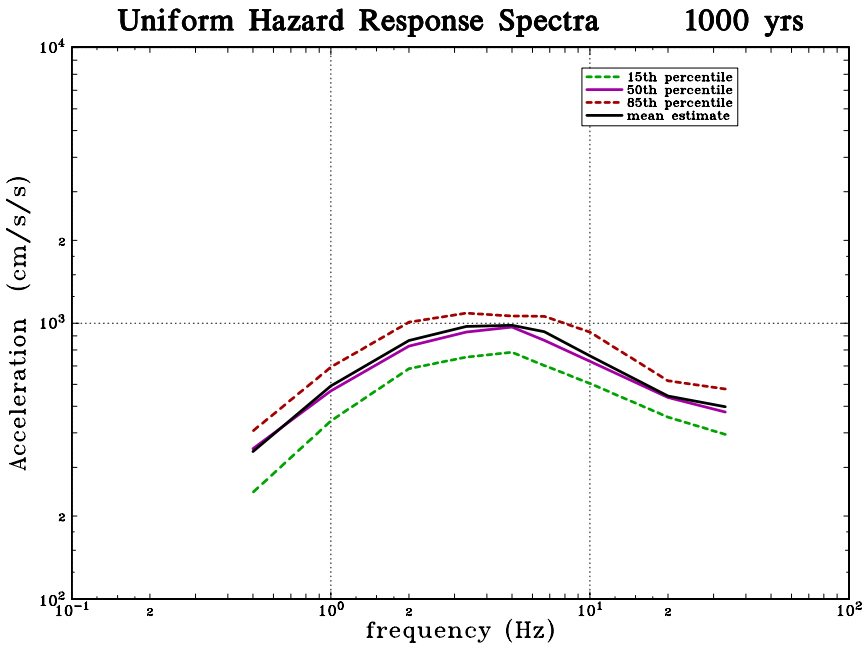

Figure 7.19: 15-th. 50-th and 85-th Percentile Uniform Hazard Response Spectra for Port of Long Beach (5% Damping) for 1000 year Return Period

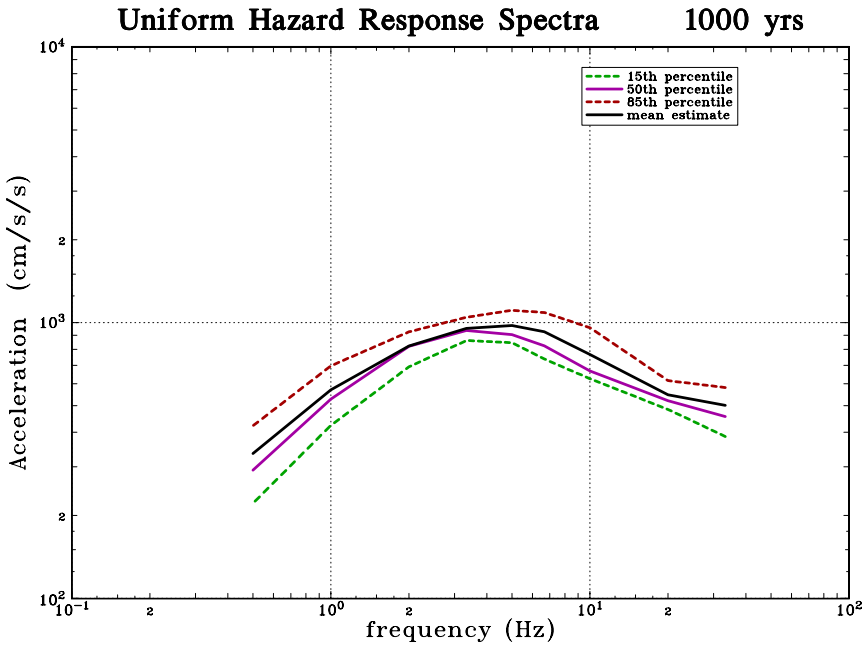

Figure 7.20: 15-th. 50-th and 85-th Percentile Uniform Hazard Response Spectra for Port Hueneme (5% Damping) for 1000 year Return Period

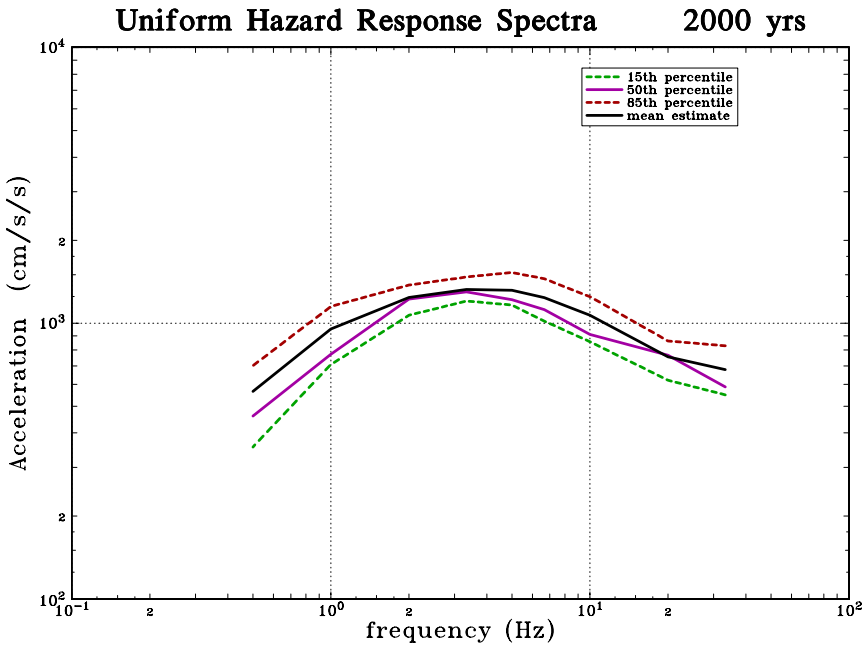

Figure 7.21: 15-th. 50-th and 85-th Percentile Uniform Hazard Response Spectra for Santa Monica (5% Damping) for 1000 year Return Period

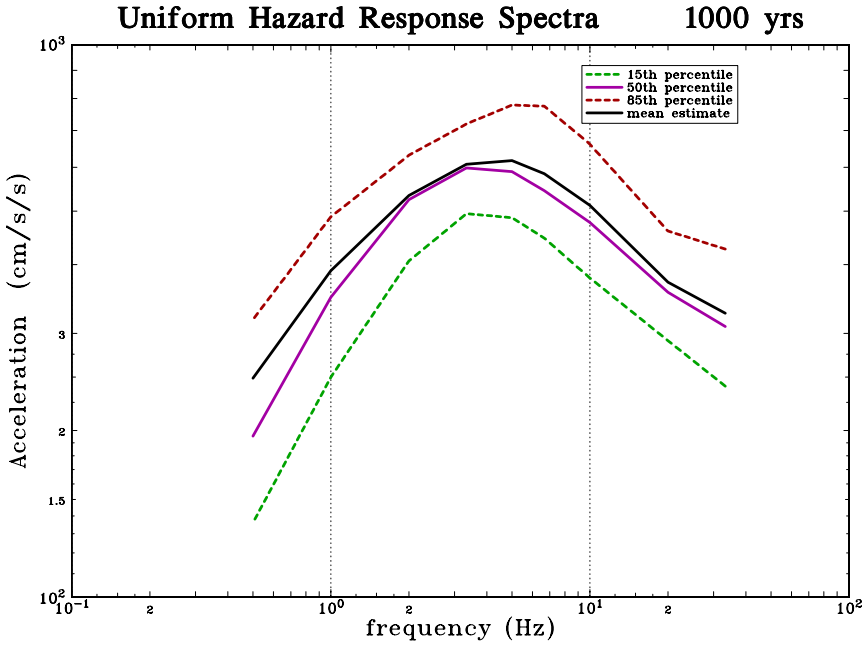

Figure 7.22: 15-th. 50-th and 85-th Percentile Uniform Hazard Response Spectra for Port of Los Angeles (5% Damping) for 2000 year Return Period

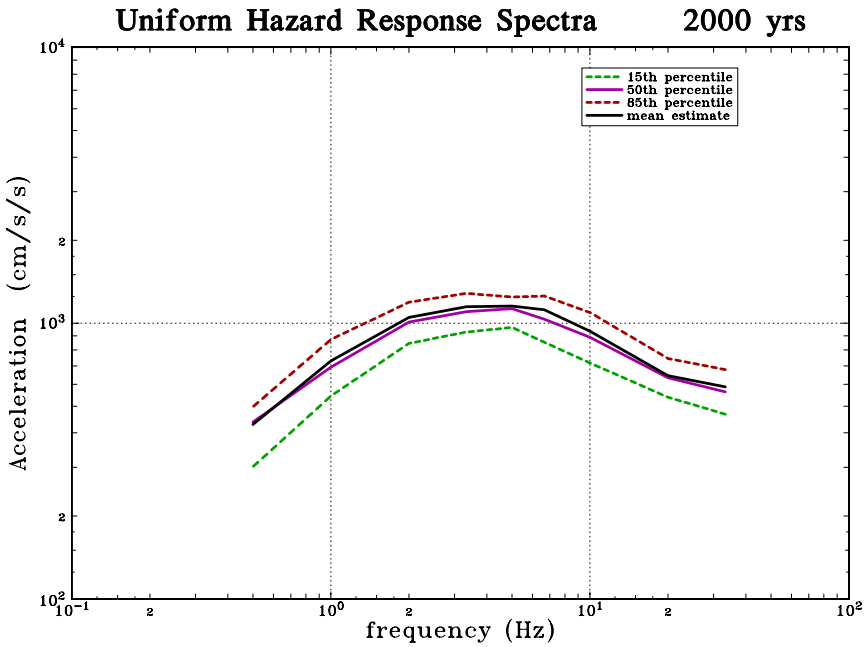

Figure 7.23: 15-th. 50-th and 85-th Percentile Uniform Hazard Response Spectra for Port of Long Beach (5% Damping) for 2000 year Return Period

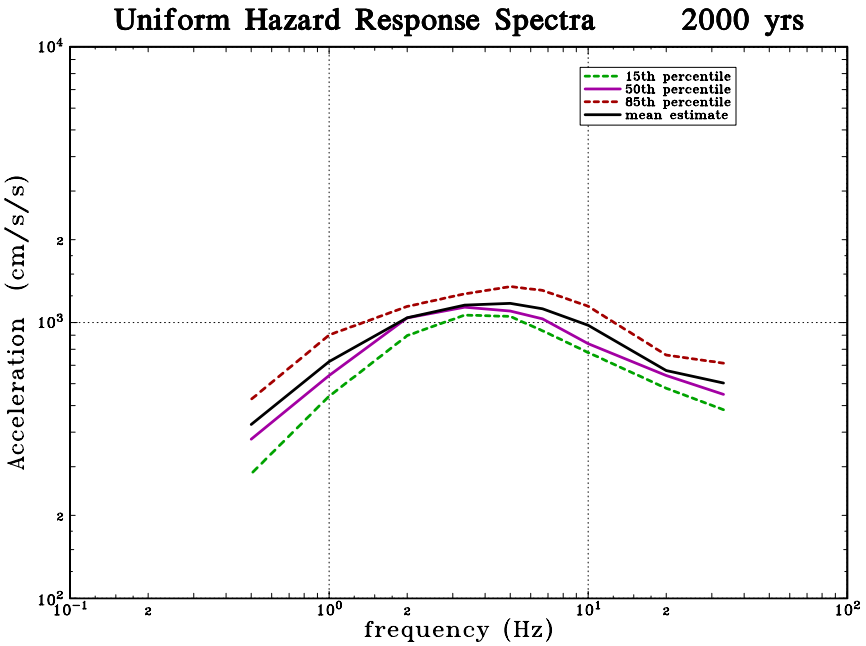

Figure 7.24: 15-th. 50-th and 85-th Percentile Uniform Hazard Response Spectra for Port Hueneme (5% Damping) for 2000 year Return Period

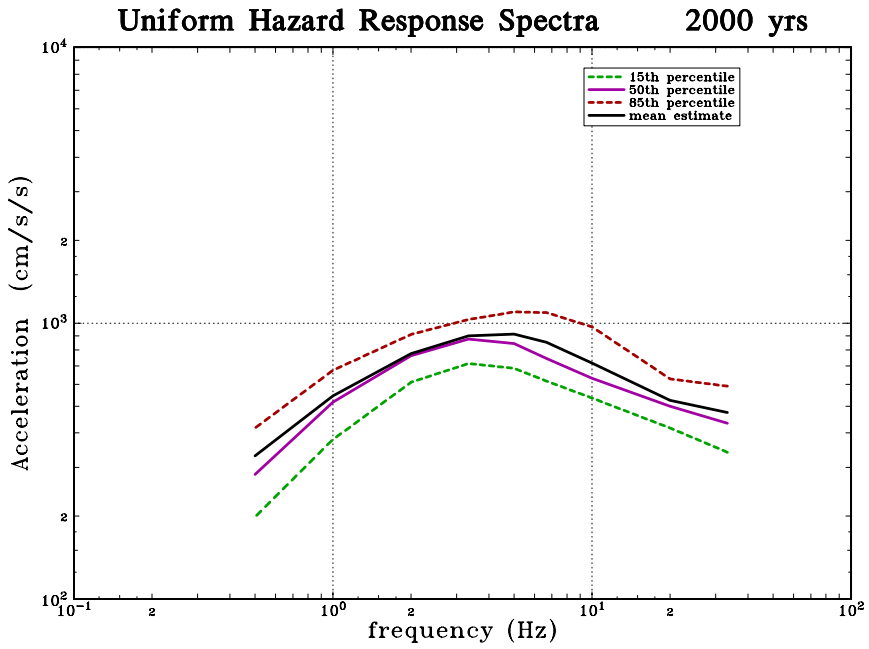

Figure 7.25: 15-th. 50-th and 85-th Percentile Uniform Hazard Response Spectra for Santa Monica (5% Damping) for 2000 year Return Period

7.2 De-aggregation Results

The hazard results were deaggregated to show the relative contribution to the total hazard from each individual seismic source, and from each discreet small range of magnitude and distance values (referred to as M-D “bins”. This latter operation is necessary to calculate the M-dom and D- that are used to define the dominant Magnitude and distance for a particular return period. This, in turn is used to determine the shape of the deterministic response spectrum that should be used as a design parameter.

There is no unique way for expressing quantitatively the relative contribution of each of the seismic sources, and to this date, there is no consensus in the community of PSHA practitioners to achieve that purpose. In this study, we calculate the hazard generated by each seismic source (or fault system) separately, and calculate the ratio of that to the total hazard, where all the sources contribute. This contribution, which is displayed in Figures 7.26 to 7.38 for contribution to the PGA hazard, in terms of a percentage, can be calculated for any representative statistic of the distribution of the hazard. Sensitivity analyses have shown us that in general the median hazard estimates lead to more stable and realistic representations of the relative importance of each of the seismic sources, and consequently the Figures show the relative contribution of the main faults, to the total median hazard. The results for PGA are representative of high frequencies. To show the influence of distant sources, the contributions at low frequency (0.5 Hz) are shown for 3 sites, in Figures 7.39 to 7.41 for the 1000 year Return Period

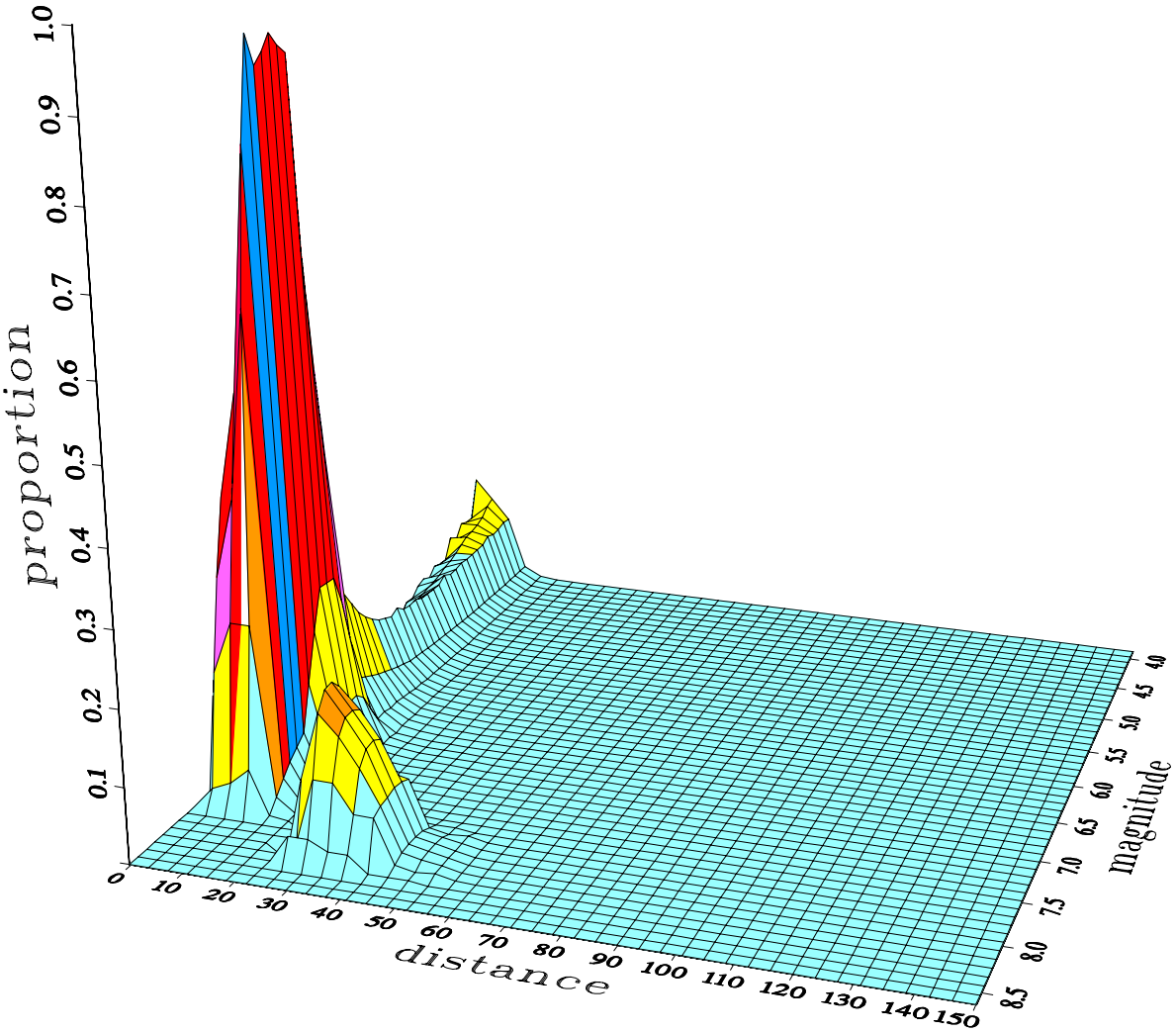

Figure 7.26: Magnitude-and-Distance Bins Contributions to the total Median PGA Hazard of 1000 year Return Period for Port of Los Angeles

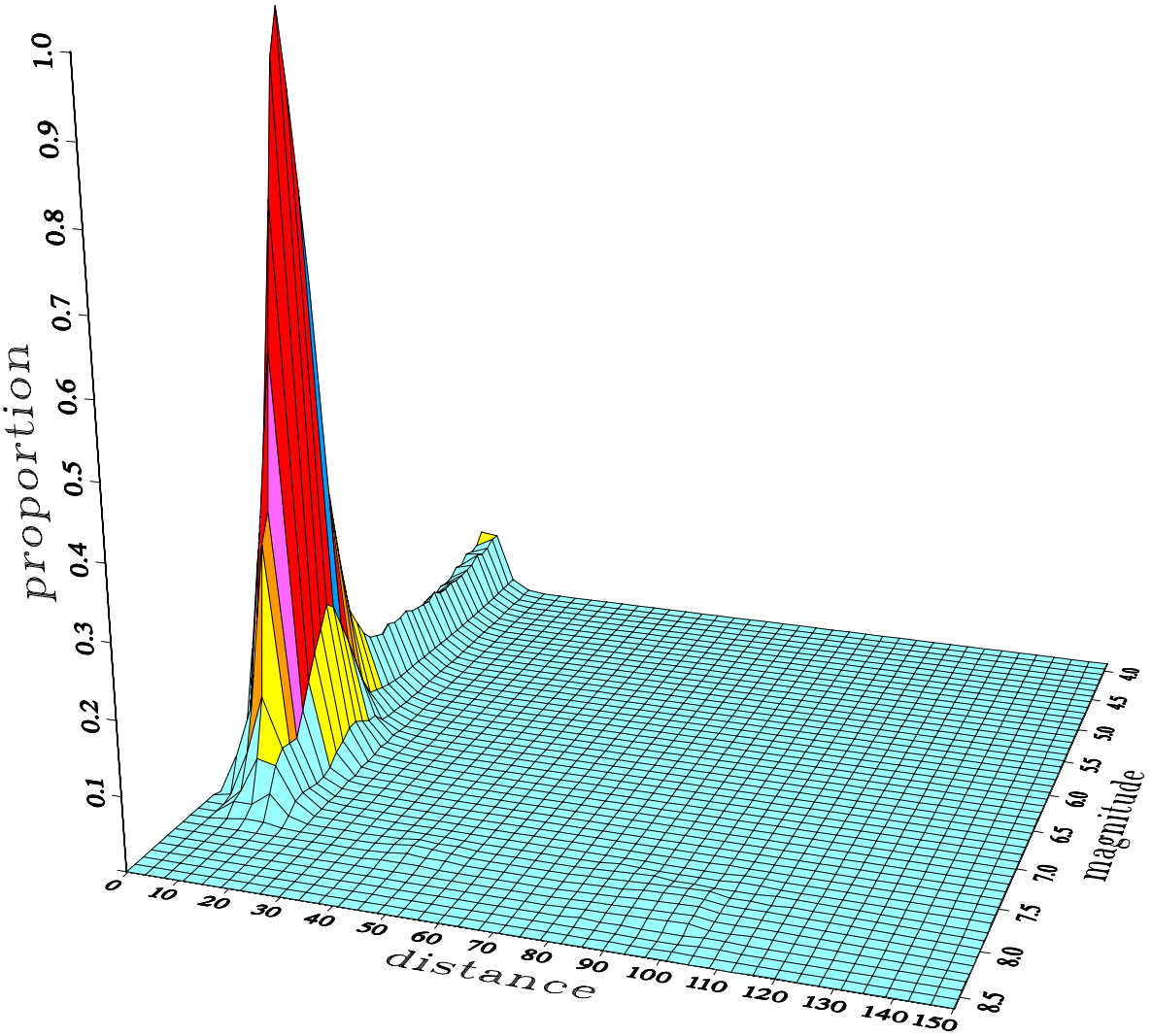

Figure 7.27: Magnitude-and-Distance Bins Contributions to the total Median PGA Hazard of 1000 year Return Period for Port of Long Beach

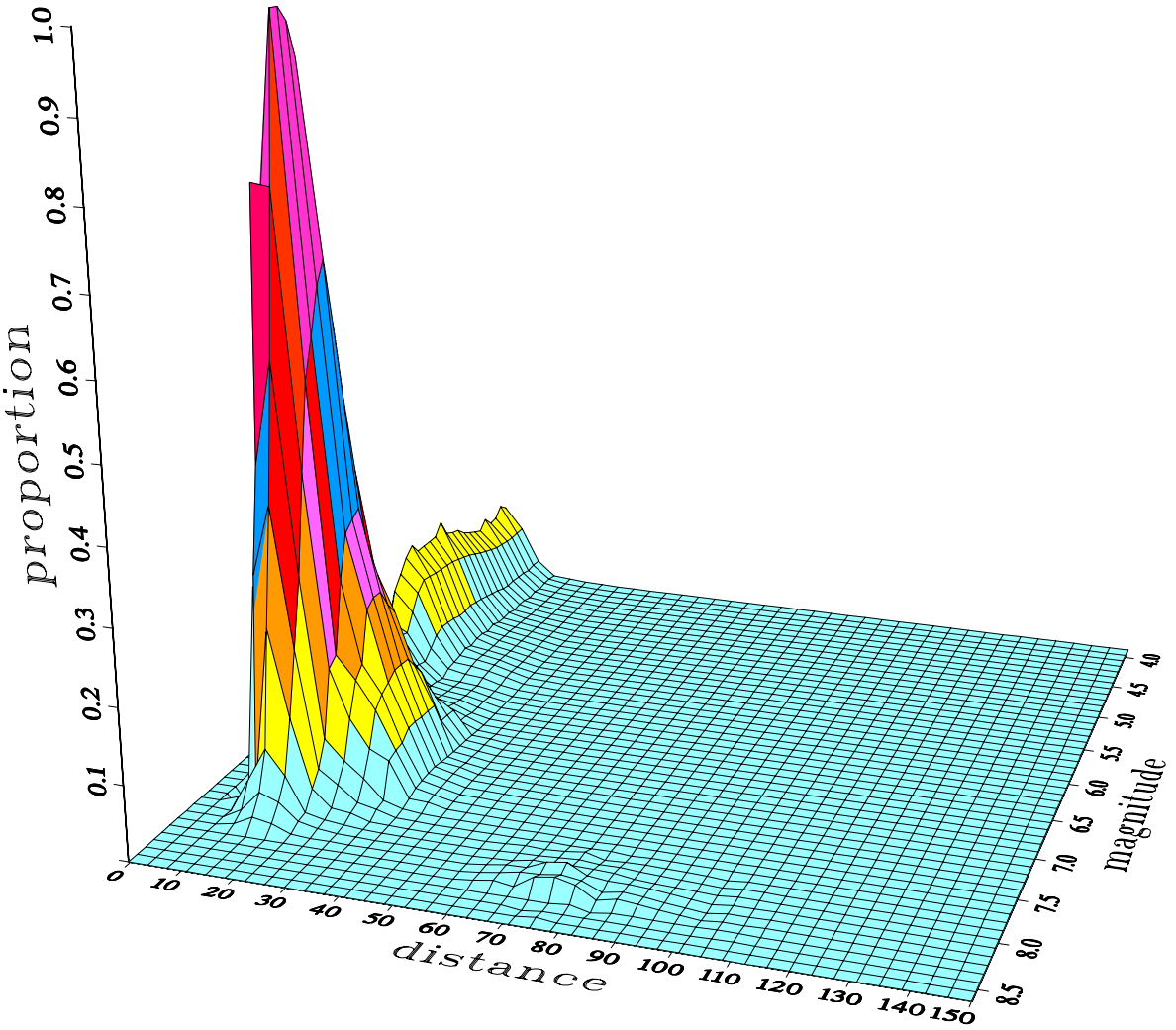

Figure 7.28: Magnitude-and-Distance Bins Contributions to the total Median PGA Hazard of 1000 year Return Period for Port Hueneme

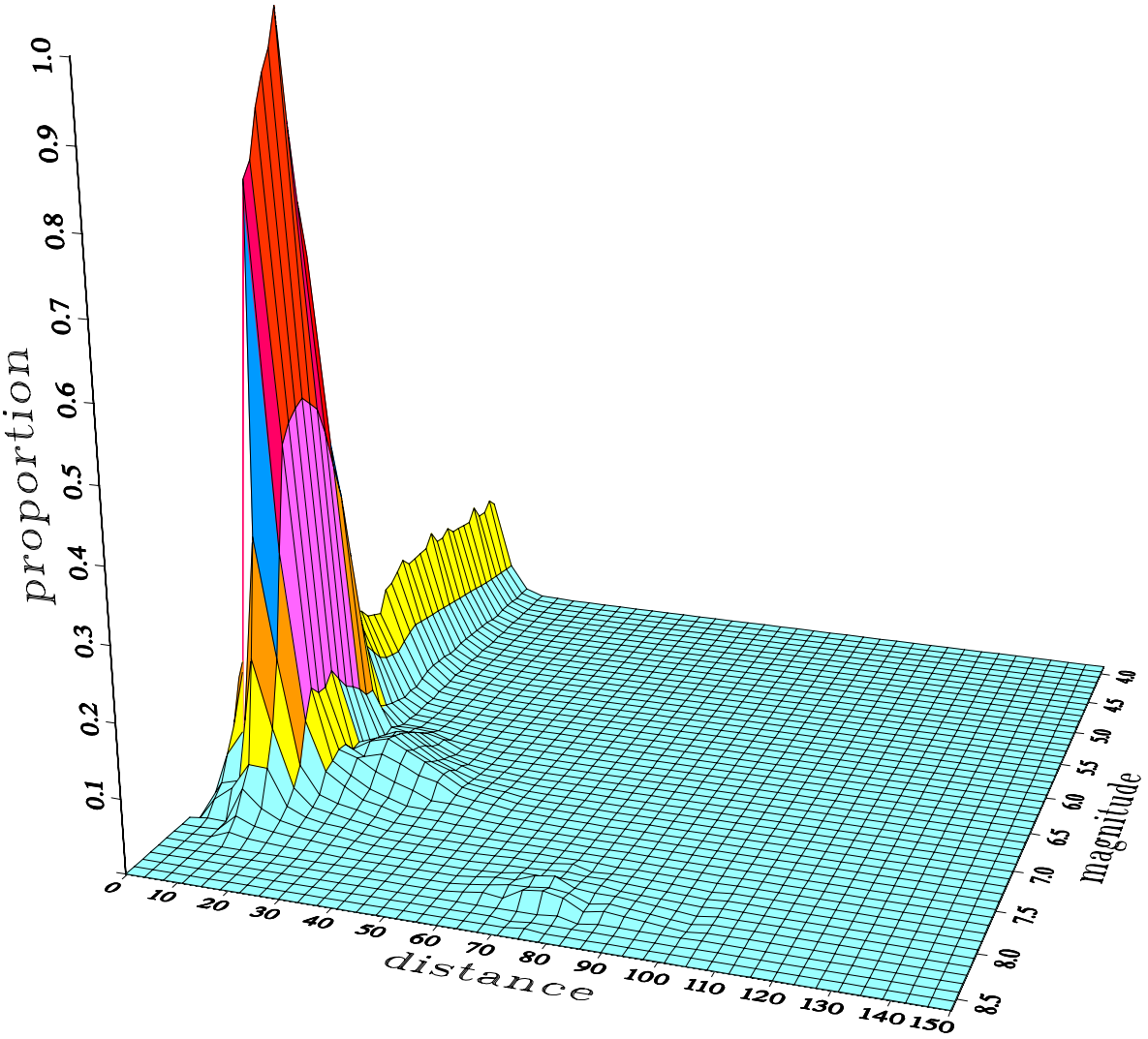

Figure 7.29: Magnitude-and-Distance Bins Contributions to the total Median PGA Hazard of 1000 year Return Period for Santa Monica

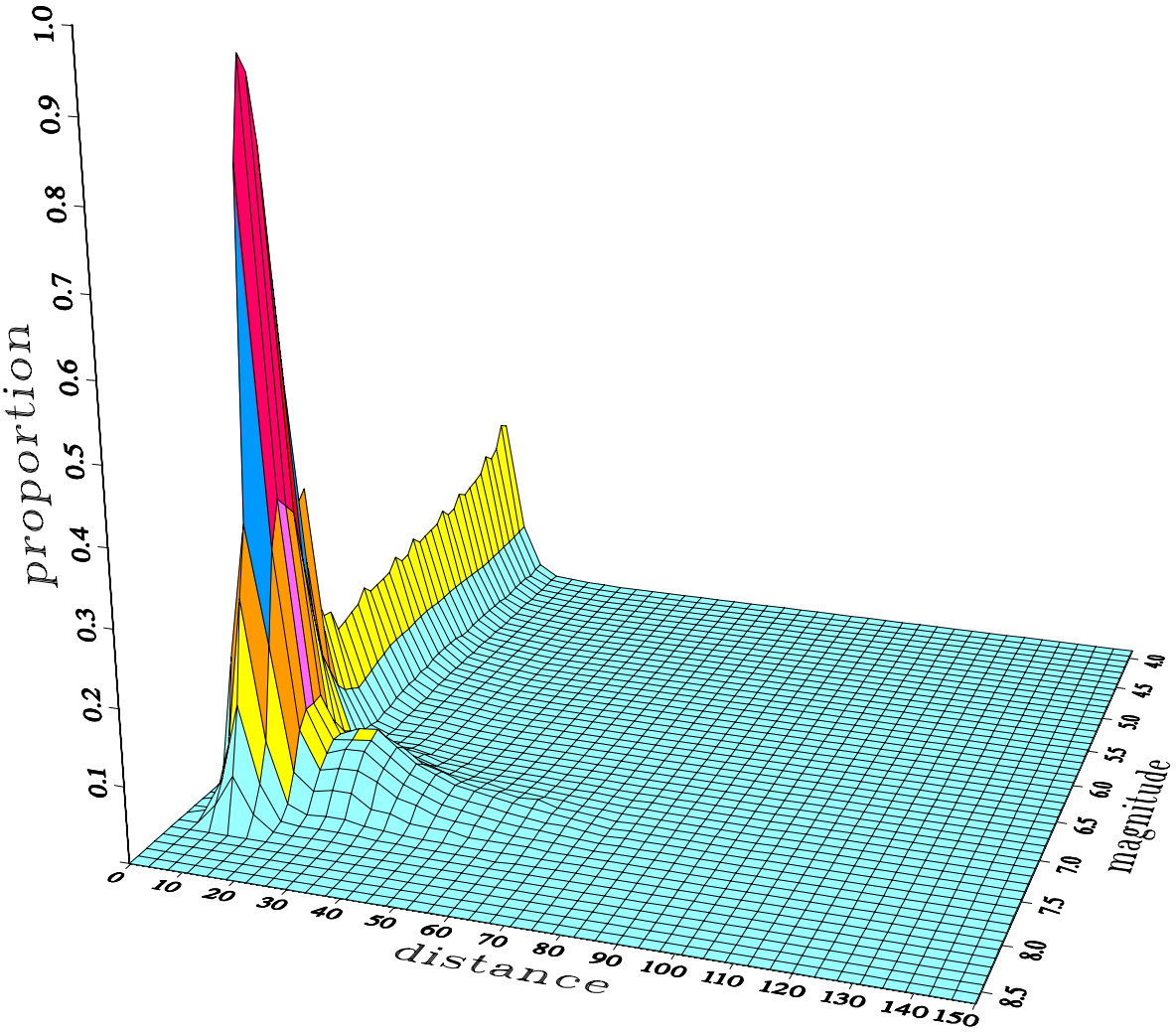

Figure 7.30: Magnitude-and-Distance Bins Contributions to the total Median PGA Hazard of 1000 year Return Period for Offshore San Clemente

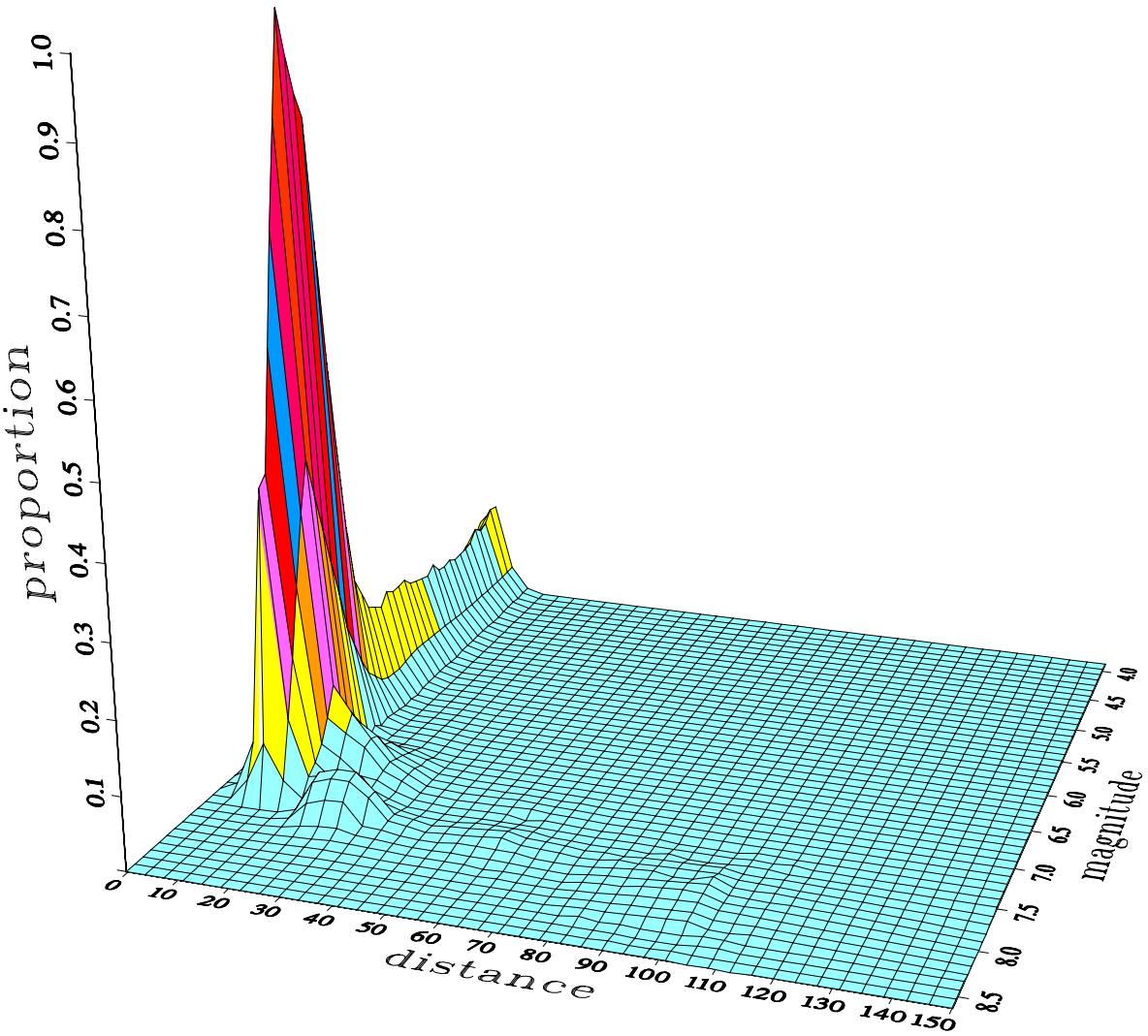

Figure 7.31: Magnitude-and-Distance Bins Contributions to the total Median PGA Hazard of 1000 year Return Period for Redondo Canyon

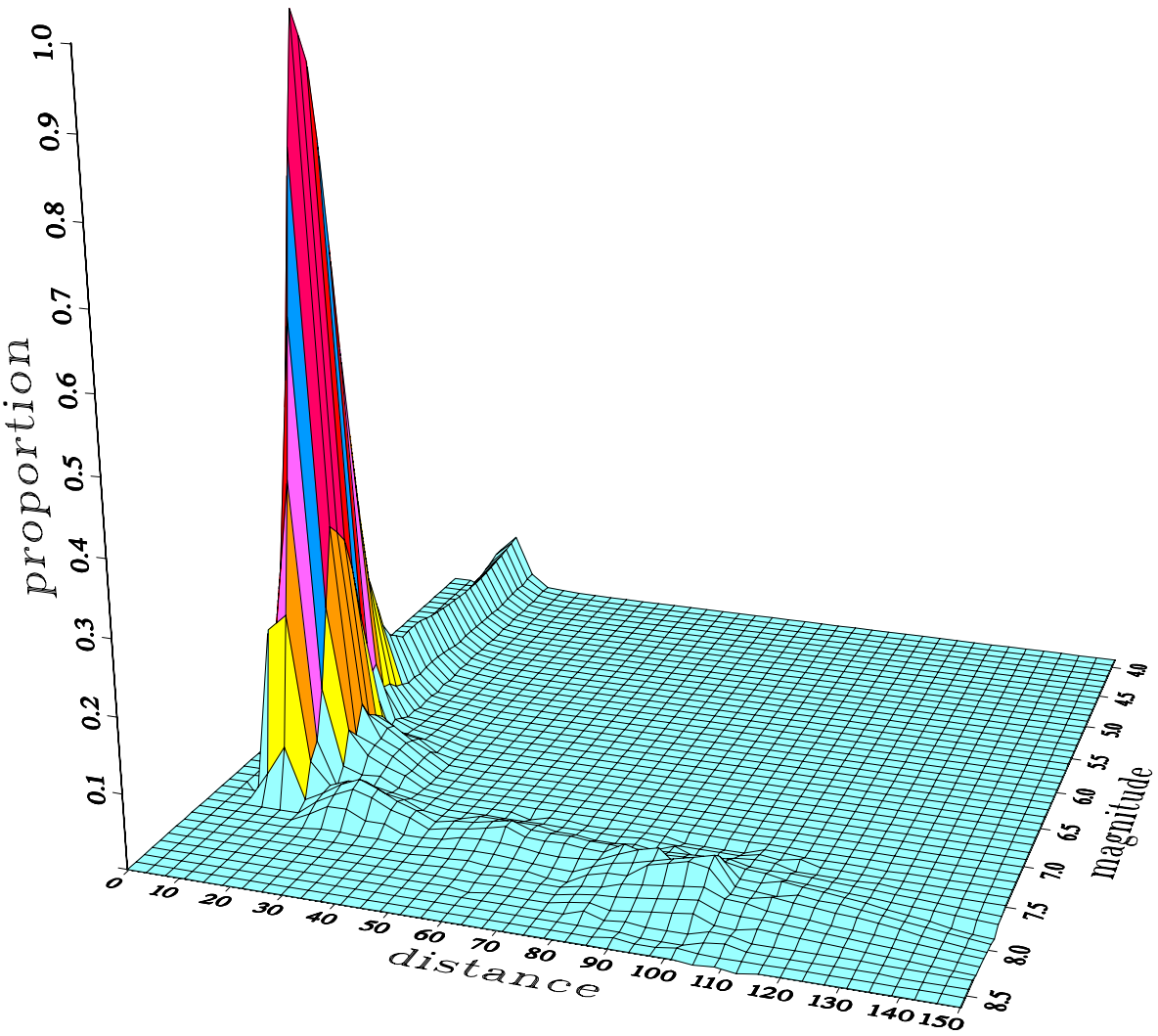

Figure 7.32: Magnitude-and-Distance Bins Contributions to the total Median PGA Hazard of 1000 year Return Period for Palos Verde Point 1

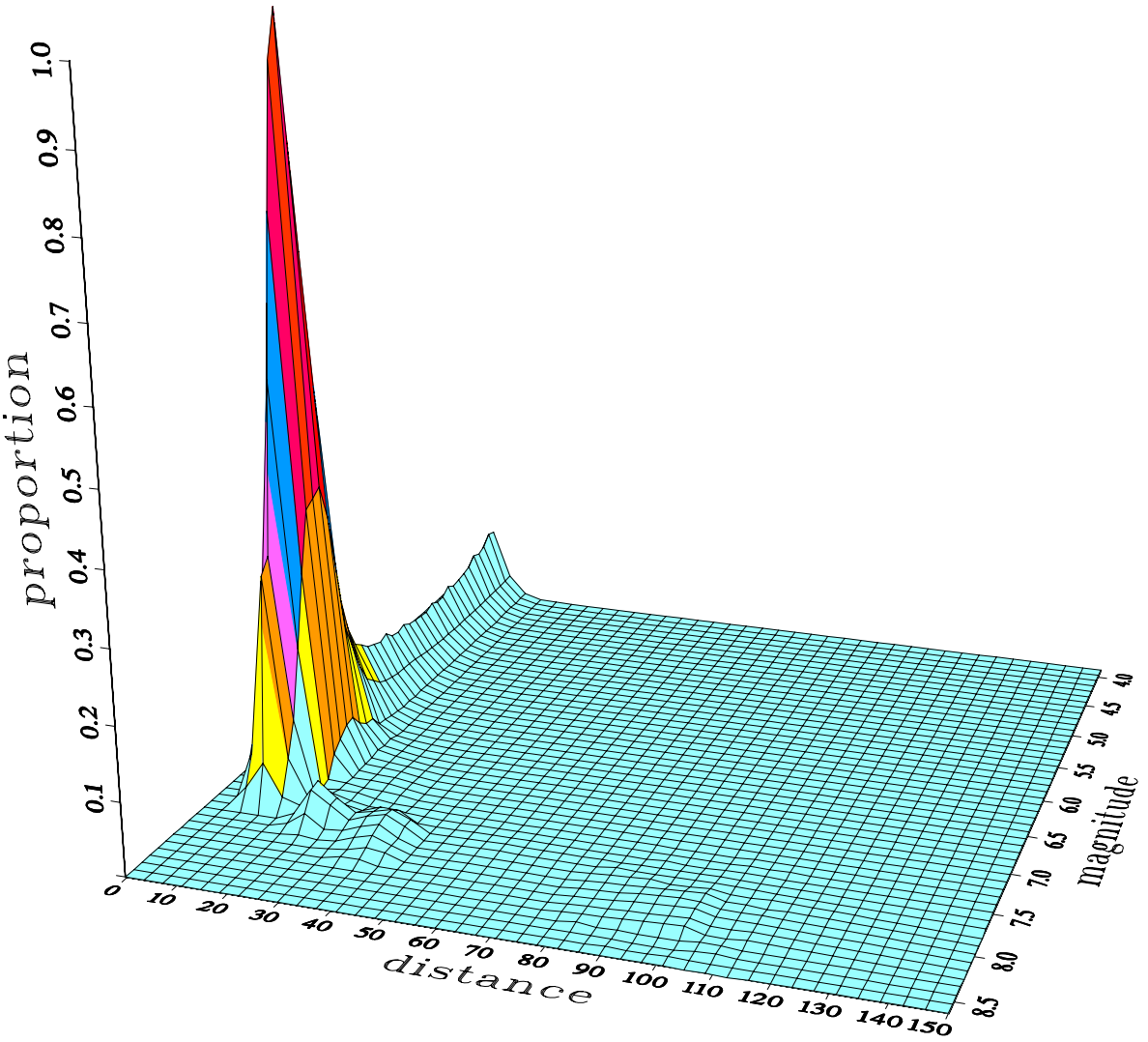

Figure 7.33: Magnitude-and-Distance Bins Contributions to the total Median PGA Hazard of 1000 year Return Period for Palos Verde Point 2

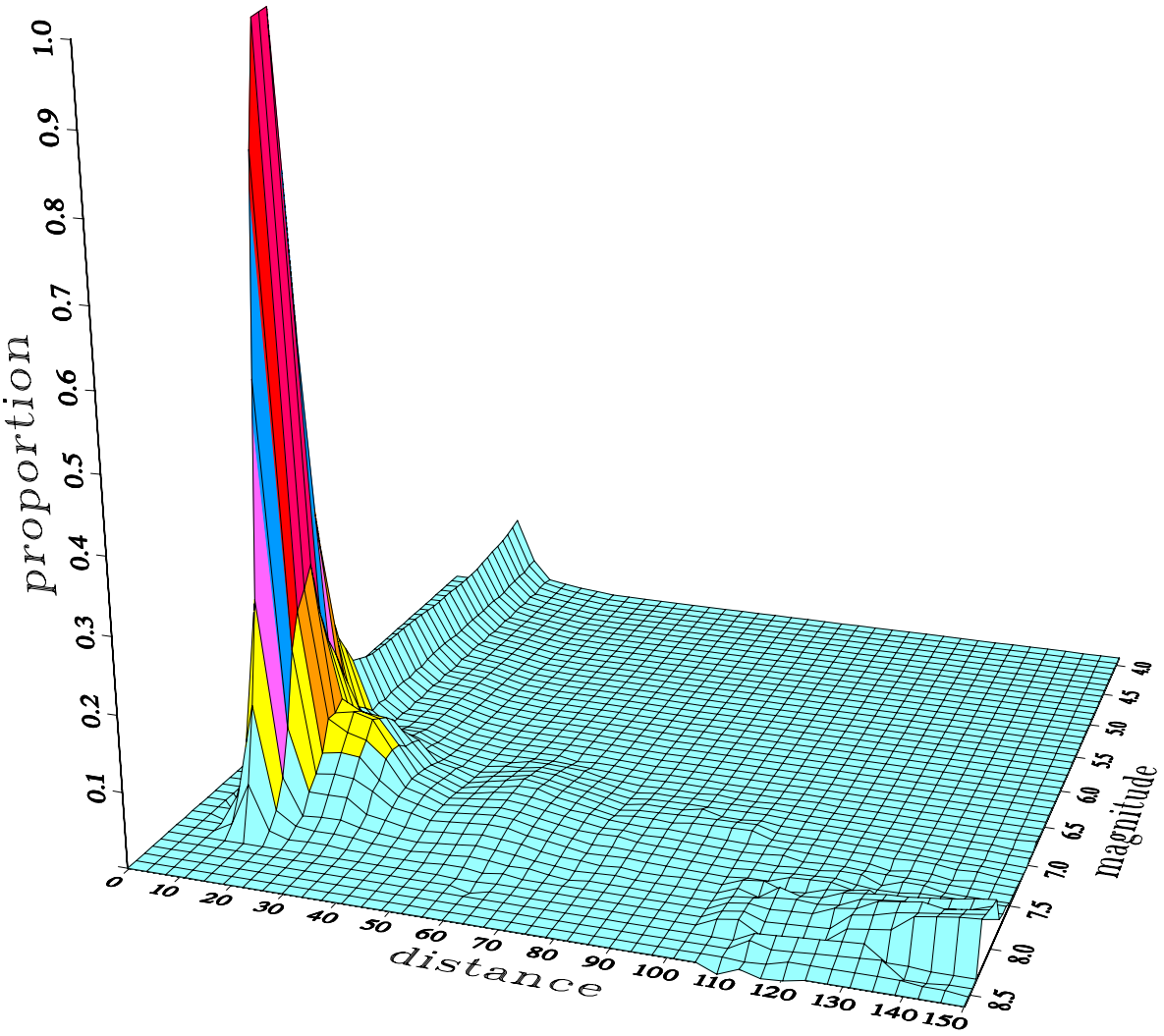

Figure 7.34: Magnitude-and-Distance Bins Contributions to the total Median PGA Hazard of 1000 year Return Period for Catalina Point 1

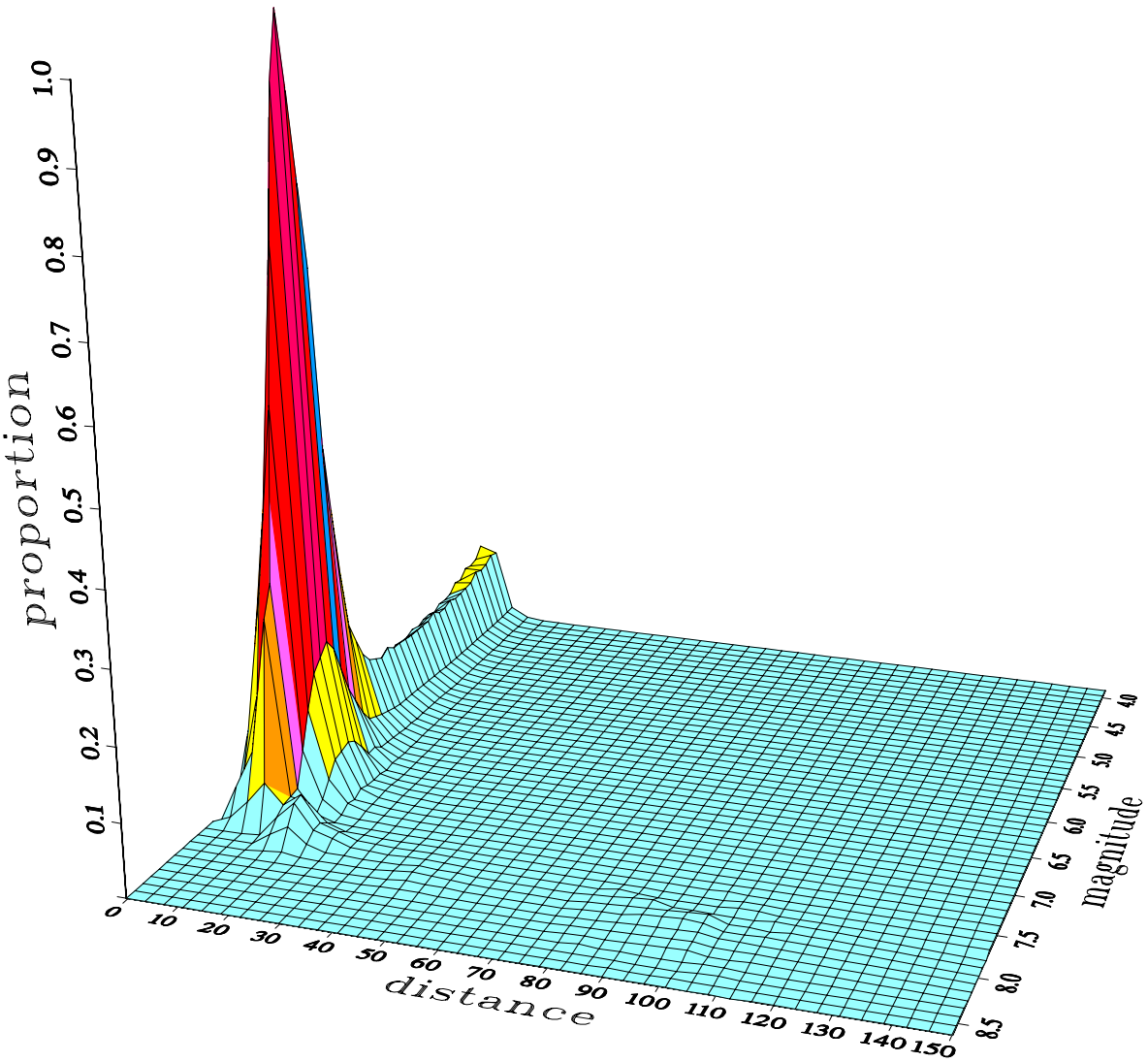

Figure 7.35: Magnitude-and-Distance Bins Contributions to the total Median PGA Hazard of 1000 year Return Period for Catalina Point 2

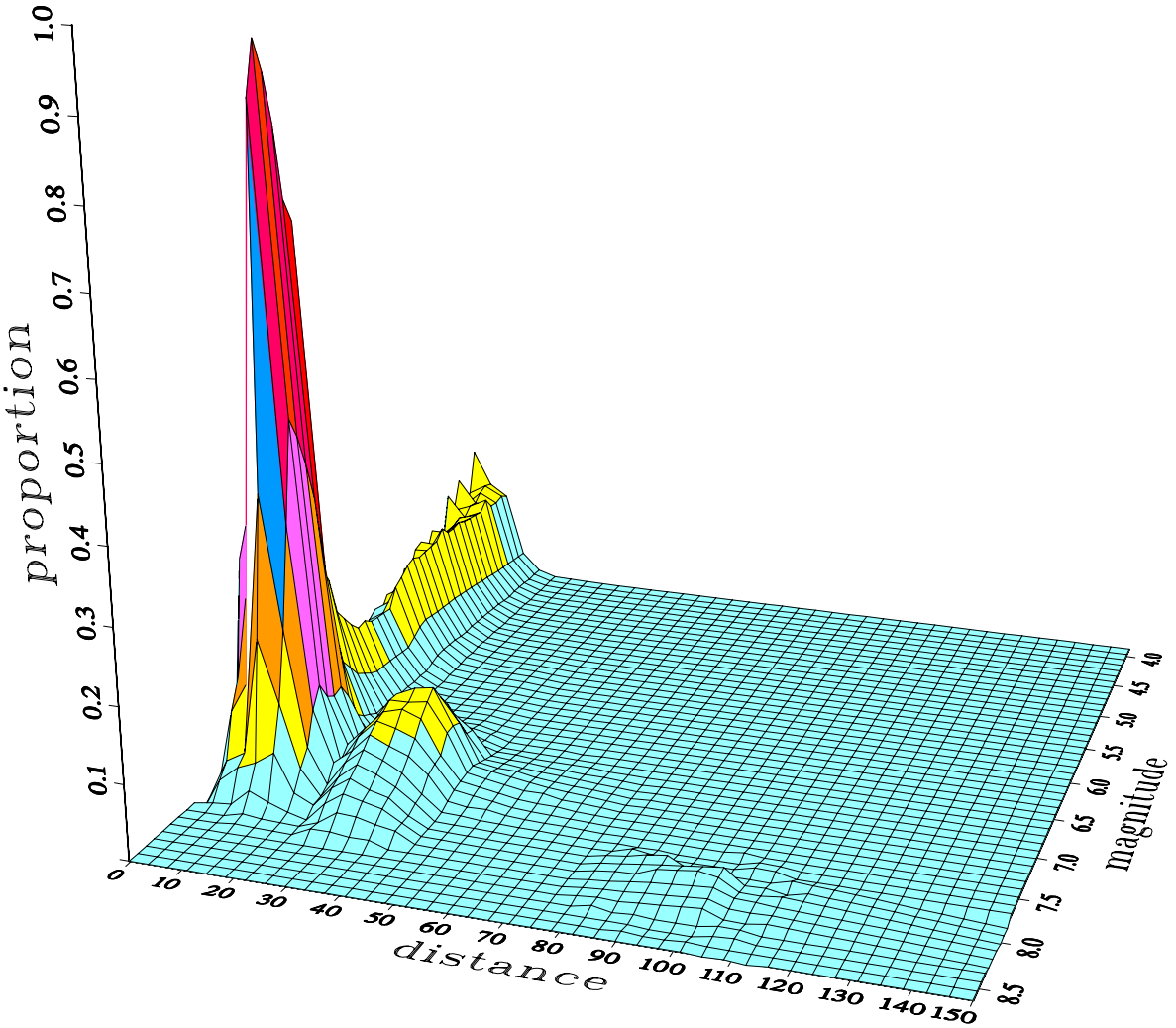

Figure 7.36: Magnitude-and-Distance Bins Contributions to the total Median PGA Hazard of 1000 year Return Period for Point Dume

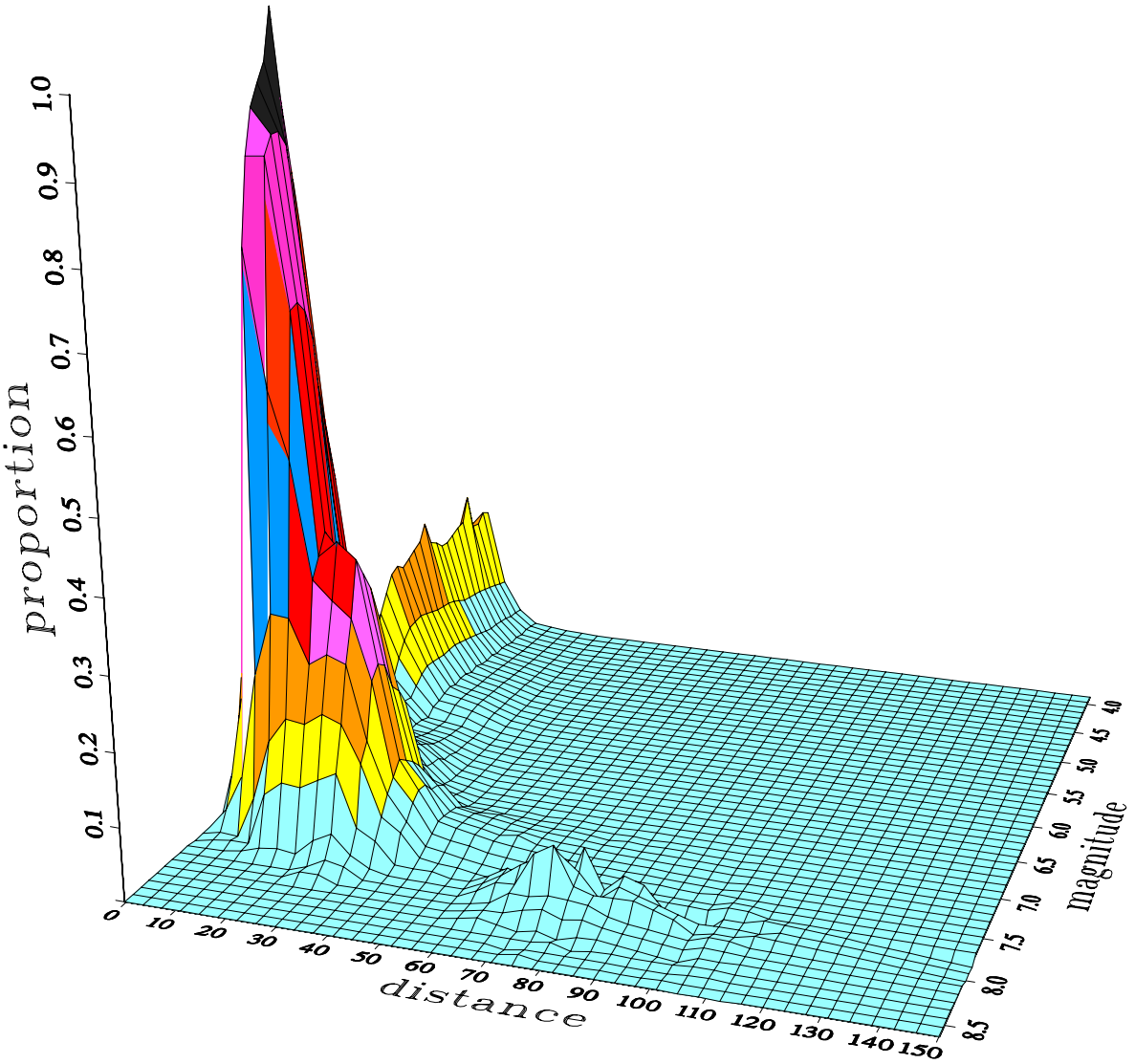

Figure 7.37: Magnitude-and-Distance Bins Contributions to the total Median PGA Hazard of 1000 year Return Period for Goleta

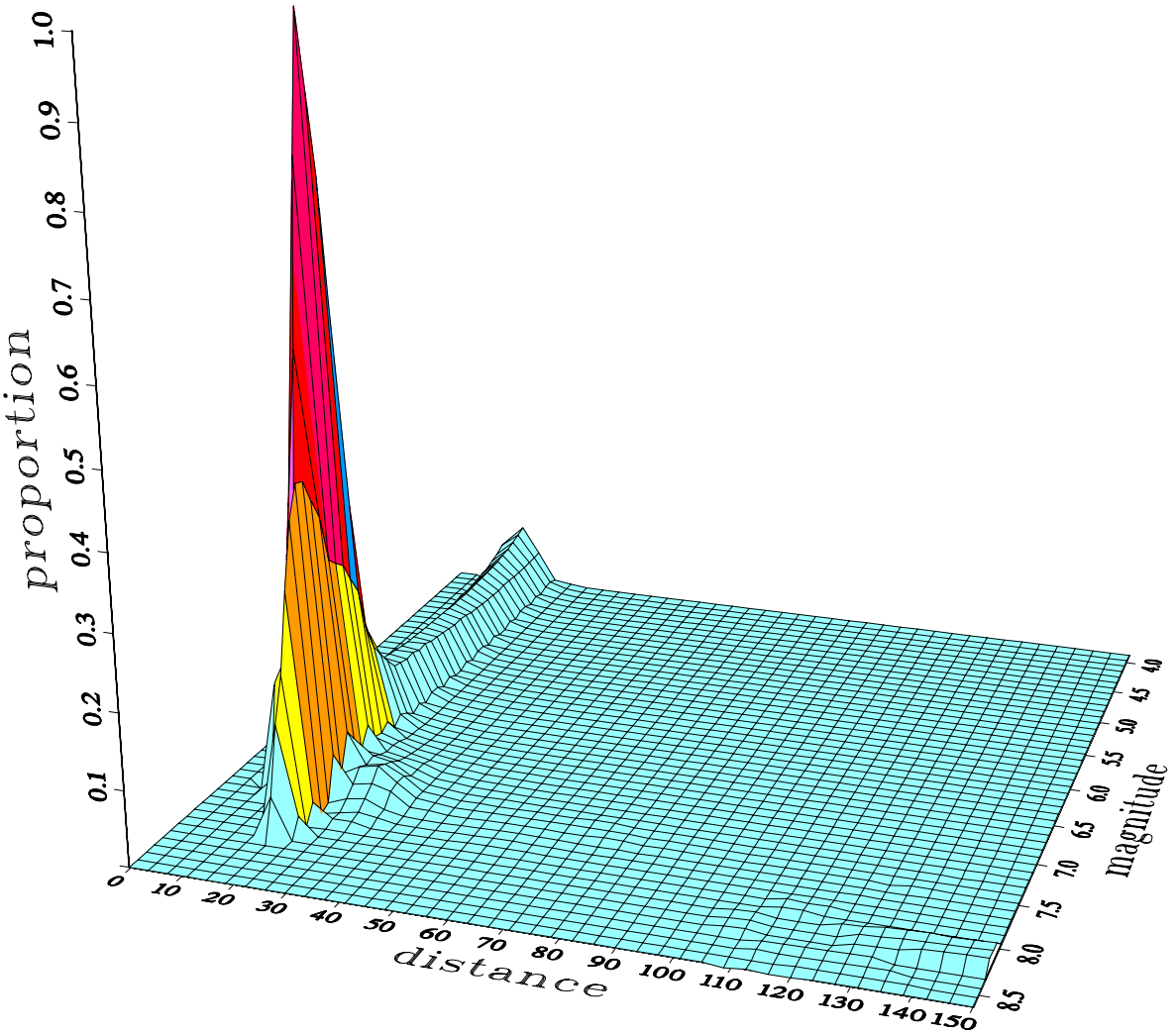

Figure 7.38: Magnitude-and-Distance Bins Contributions to the total Median PGA Hazard of 1000 year Return Period for San Pedro Escarpment

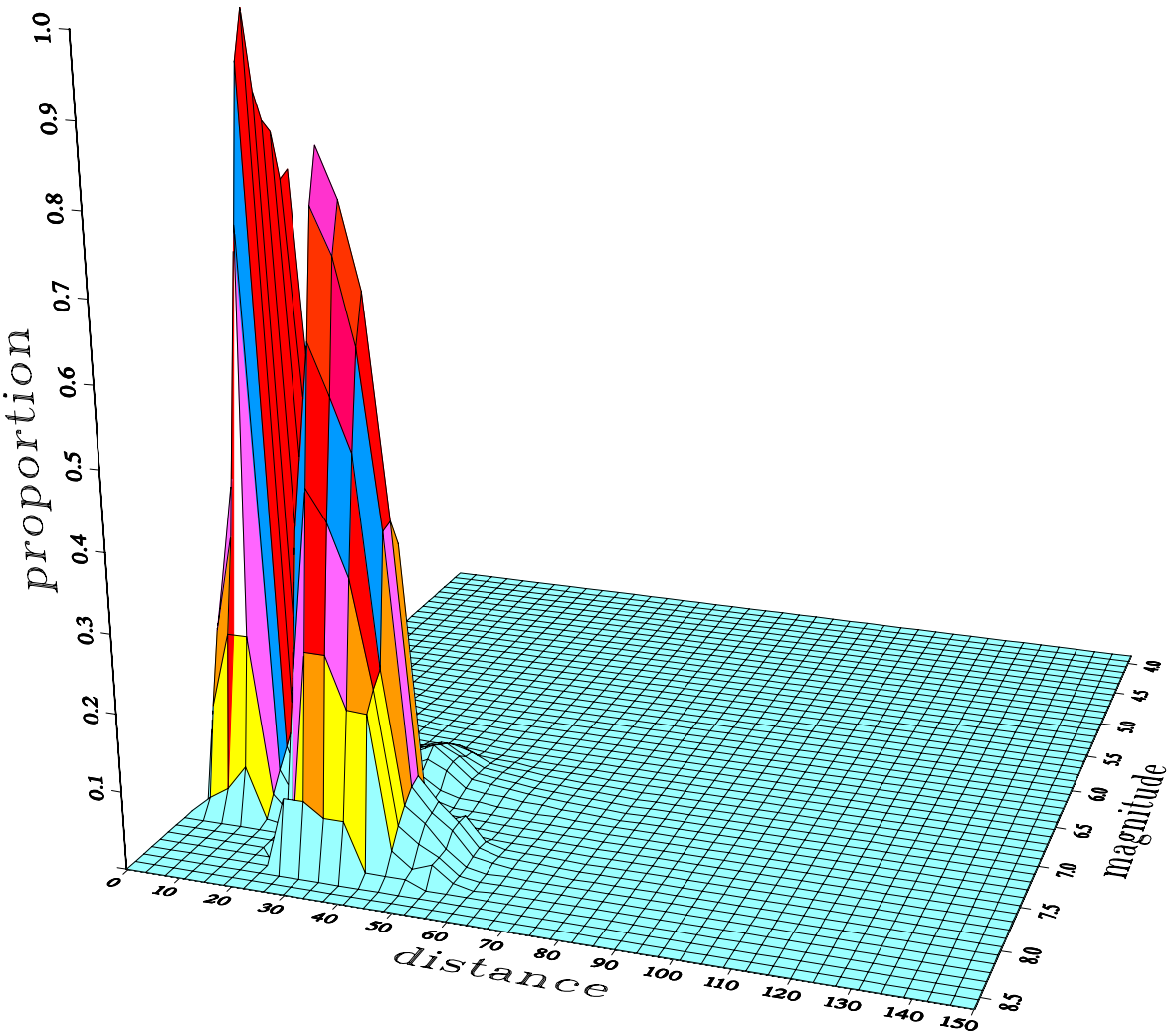

Figure 7.39: Magnitude-and-Distance Bins Contributions to the total Median, 0.5 Hz Response Spectral Acceleration Hazard of 1000 year Return Period for Port of Los Angeles

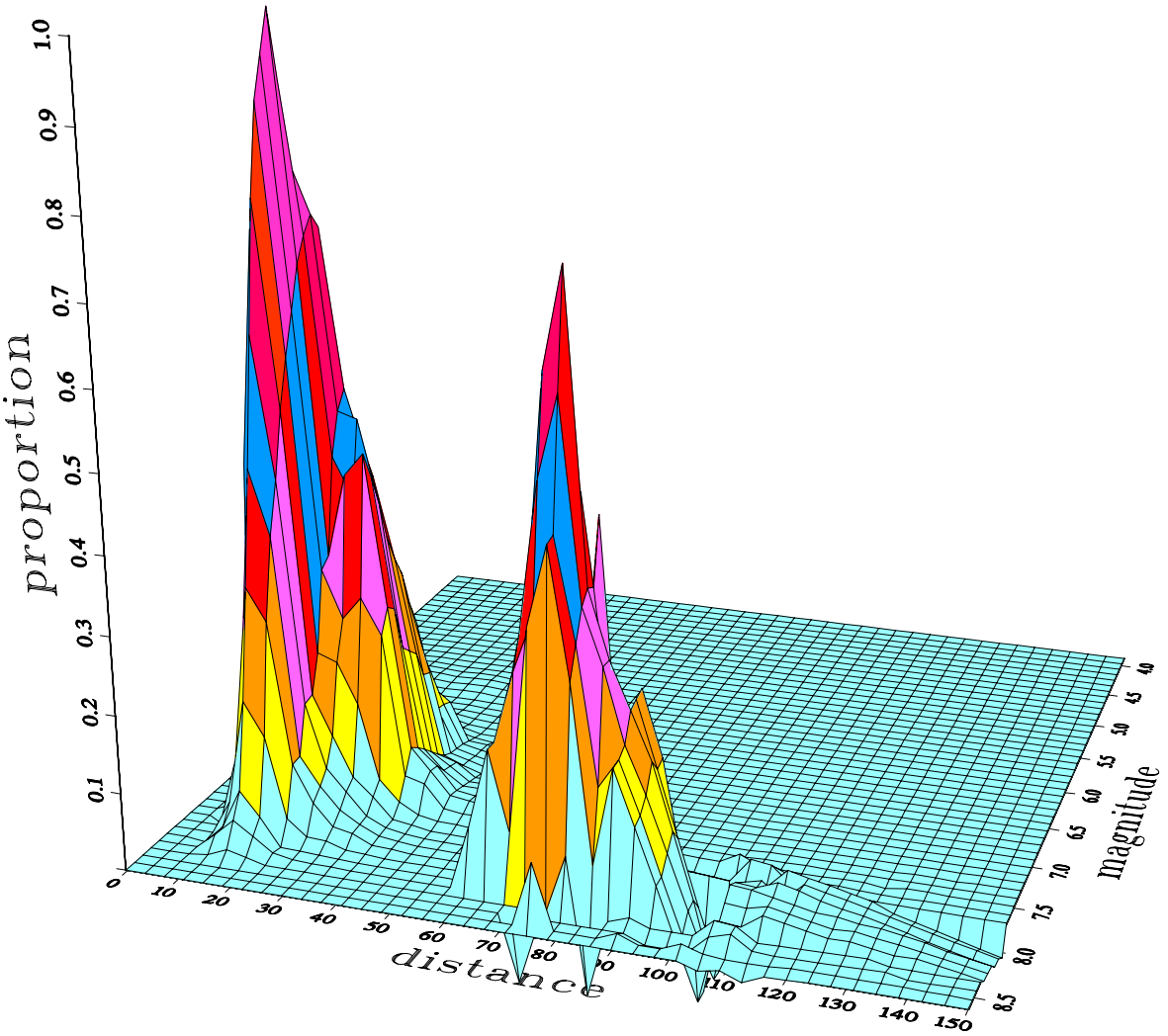

Figure 7.40: Magnitude-and-Distance Bins Contributions to the total Median, 0.5 Hz Response Spectral Acceleration Hazard of 1000 year Return Period for Port Hueneme

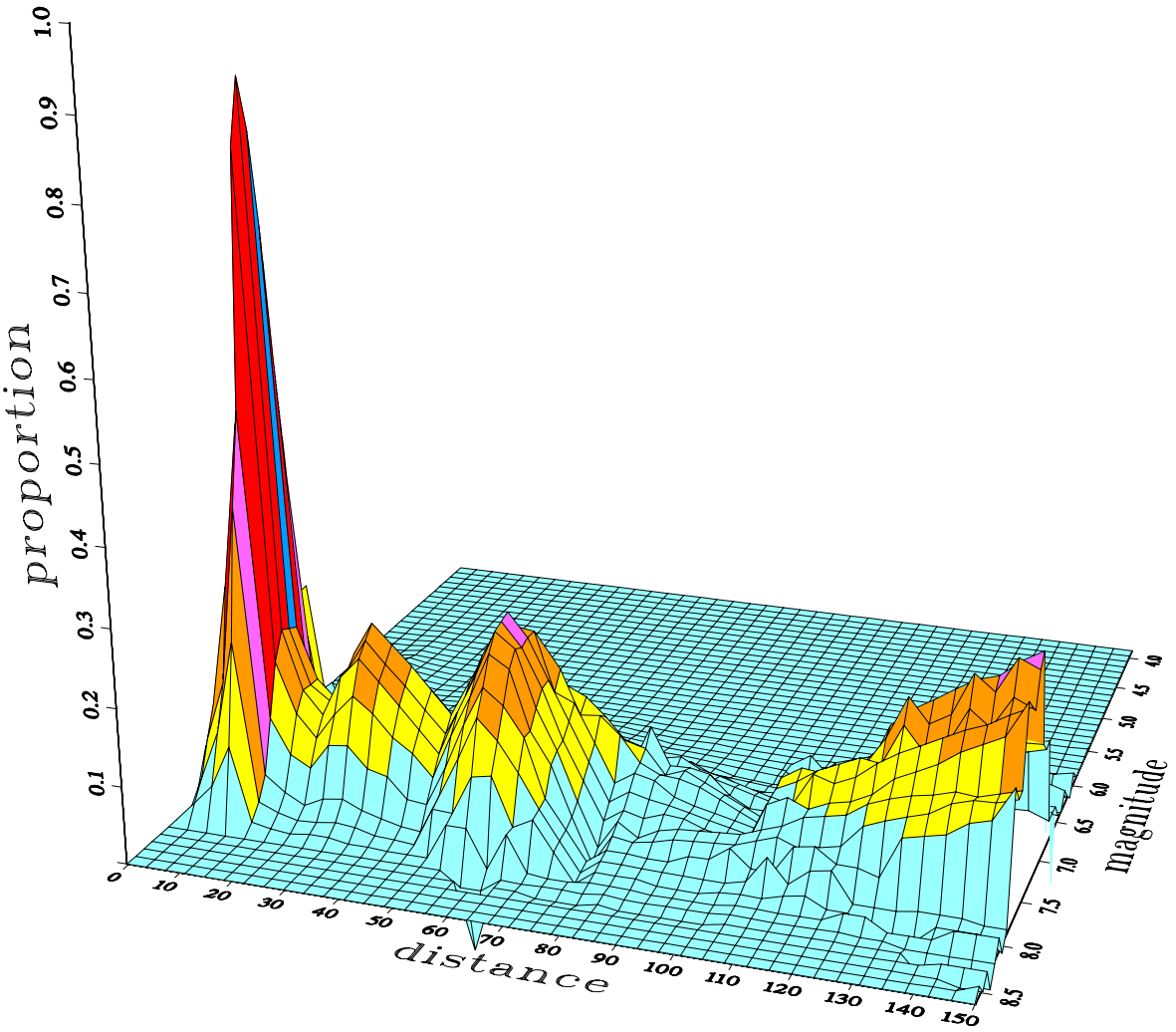

Figure 7.41: Magnitude-and-Distance Bins Contributions to the total Median, 0.5 Hz Response Spectral Acceleration Hazard of 1000 year Return Period for Santa Monica

9. References Cited

Abrahamson, N.A. and W.J. Silva, (1997). Empirical Response Spectral Accelerations for Shallow Crustal Earthquakes, Seism. Res. Let., 68, No. 1, 94-127.

Bohannon, R.G., and E. Geist, Upper crustal structure and Neogene tectonic development of the California continental borderland, Geol. Soc. Am. Bull., 110, 779-800, 1998.

Boore, D.M,W.B. Joyner and T.E. Fumal, (1997). Equations for Estimating Horizontal Response Spectra and Peak Acceleration from Western North American Earthquakes: A Summary of Recent Work, Seism. Res. Let., 68, No. 1, 128-153.

Budnitz, R.J., G. Apostolakis, D.M. Boore, L.S. Cluff, K.J. Coppersmith, C.A. Cornell, and P.A.Morris, Recommendations for Probabilistic Seismic Hazard Analysis: Guidance on Uncertaintyand Use of Experts, Vol. 1, NUREG/CR-6372, U.S. Nuclear Regulatory Commission, Washington, DC, 256 p.

Campbell, D. W. (1989), Empirical Prediction of Near-Source Ground Motion for the Diablo Canyon Power Plant Site, San Luis Obispo County, CA, U.S. Geol. Surv. Open-File Rep. 89-484, 115 p.

Campbell, K.W. (1997). Empirical Near-Source Attenuation Relationships for Horizontal and Vertical Components of peak Ground Acceleration, Peak Ground Velocity, and Pseudo-Absolute Acceleration Spectra., Seism. Res. Let., 68, No. 1, 154-179.

Cornell, C.A. (1968), Engineering Seismic Risk Analysis, Bull. Seismol. Soc. Am., 58, 1583-1606.

Crouch, J.K., and J. Suppe, Late Cenozoic evolution of the Los Angeles basin and inner California borderland: A model for core complex-like crustal extension, Geol. Soc. Am. Bull., 105, 1415-1434, 1993.

Davis, T.L., and J.S. Namson, A balanced cross-section of the 1994 Northridge earthquake, southern California, Nature, 372, 167-169, 1994.

Dolan, J.F., E. M. Gath, L. B. Grant, M. Legg, S. Lindvall, K. Mueller, M. Oskin, D.F. Ponti, C. M. Rubin, T. K. Rockwell, J. H, Shaw, J. A. Treiman, C. Walls, and R. S. Yeats (compiler), Active faults in the Los Angeles Metropolitan region, SCEC Special Pub. Series, No. 001, Southern California Earthquake Center, **http://www.scec.org/research/special/**, 2001.

Dolan, J.F., K. Sieh, and T.K. Rockwell, Late Quaternary activity and seismic potential of the Santa Monica fault system, Los Angeles, California, Geol. Soc. Am. Bull., 112, 1559-1581, 2000.

Fischer, P.J., and G.I. Mills, The offshore Newport-Inglewood-Rose Canyon fault zone, California: Structure, segmentation and tectonics, in Environmental Perils, San Diego Region, P.L. Abbot and W.J. Elliot, eds., 17-36, San Diego Assoc. Geol., 1991.

Fuis, G. S., T. Ryberg, N.J. Godfrey, D.A. Okaya, and J.M. Murphy, Crustal structure and tectonics from the Los Angeles Basin to the Mojave Desert, Southern California, Geology, 29, 15-18, 2001.

Grant, L.B., K.J. Mueller, E.M. Gath, H. Cheng, R.L. Edwards, R. Munro, and G.L. Kennedy, Late Quaternary uplift and earthquake potential of the San Joaquin Hills, southern Los Angeles basin, California, Geology, 27, 1031-1034, 1999.

Jackson, D.D., et al., Seismic hazards in Southern California; probable earthquakes, 1994 to 2024, Bull. Seismol. Soc. Am., 85, 379-439, 1995.

Joyner, W. B., and D. M. Boore (1982), Prediction of Earthquake Response Spectra, U.S. Geol. Surv. Open-File Rep. 82-997, 16 p.

Kier, G., and K. Mueller, Evidence for active shortening in the offshore Borderlands and its implications for blind thrust hazards in the coastal Orange and San Diego counties, Proc. 1999 SCEC Annual Meeting, 71, Southern California Earthquake Center, 1999.

Kier, G., K. Mueller, and T.K. Rockwell, Origin of regional uplift across southern California and northern Baja California, submitted to Tectonics, 2002.

Lettis, W.R., and K.L. Hanson, Crustal strain partitioning implications for seismic hazard assessment in western California, Geology, 19, 559-562, 1991.

Magistrale, H., and H-w Zhou, Lithologic control of the depth of earthquakes in southern California, Science, 273, 639-642, 1996.

Meigs, A., N. Brozovic, and M.L. Johnson, Steady, balanced rates of uplift and erosion of the Santa Monica Mountains, California, Basin Research, 11, 59-73, 1999.

Mueller, K., J. Shaw, and C. Rivera, Determining the geometry of the San Joaquin Hills blind thrust: Implications for earthquake source characterization, Progress report submitted to SCEC, 4 p., 1998.

Mueller, K.J., Recency of folding along the Compton-Los Alamitos trend: Implications for seismic risk in the Los Angeles basin, EOS Trans. AGU, 78(46) Suppl., 702, 1997.

Oskin, M., K. Sieh, T. Rockwell, G. Miller, P. Guptill, M. Curtis, S. McArdle, and P. Elliot, Active parasitic folds on the Elysian Park anticline; implications for seismic hazard in central Los Angeles, California, Geol. Soc. Am. Bull., 112, 693-707, 2000.

Rivero, C., J.H. Shaw, and K. Mueller, Oceanside and Thirtymile Bank blind thrusts: Implications for earthquake hazards in coastal southern California, Geology, 28, 891-894, 2000.

Sadigh, K., C.-Y. Chang, J.A. Egan, F. Makdisi, and R.R. Youngs, (1997). Attenuation Relationships for Shallow Crustal Earthquakes Based on California Strong Motion Data. Seism. Res. Let., 68, No. 1, 180-189.
Schwartz, D. P., and K.L. Coppersmith (1984), Fault Behavior and Characteristic Earthquakes from the Wasatch and San Andreas Faults, J. Geophys. Res. 89,5681-5698.

Senior Seismic Hazards Analysis Committee, Recommendations for probabilistic seismic hazard analysis: Guidance on uncertainty and the use of experts, NUREG/CR-6372, US Nuclear Regulatory Commission, Washington, DC, 256 p., 1997.

Shaw, J.H. and J. Suppe, Earthquake hazards of active blind-thrust faults under the central Los Angeles basin, California, Jo. Geophys. Res., 101, 8623-8642, 1996.

Smith, T.C. (1981), Fault Evaluation Rep. FER-112, Calif. Div. Mines. Geol., 18 p.

Sorlien, C.C., M.J. Kamerling, and L. Seeber, The Dume fault, northern Santa Monica Bay, California, EOS Trans. AGU, 82(47), Abstract S11A-0532, 2001.

Tsutsumi, H., R.S. Yeats, and G.J. Huftile, Late Cenozoic tectonics of the northern Los Angeles fault system, California, Geol. Soc. Am. Bull., 113, 454-468, 2001.

Ward, S.N., and G. Valensise, The Palos Verdes terraces, California: Bathtub rings from a buried reverse fault, Jo. Geophys. Res., 99, 4485-4494, 1994.

Weaver, K.D., and J.F. Dolan, Paleoseismology and geomorphology of the Raymond fault, Los Angeles county, California, Bull. Seismol. Soc. Am., 90, 1409-1429, 2000.
Wells, D.L., and K.J. Coppersmith, Analysis of fault dip and sense of slip for historical earthquakes, Seismol. Res. Lets., 62, 38, 1991.

Working group on California Earthquake Probabilities (2002), Earthquake Probabilities in the San Francisco Bay Region: 2002-2031, U.S. Geol. Surv., Menlo Park, CA, in preparation.

Appendix A: Workshops

Table A.1: List of Participants to the January 29-30, 2001 Workshop 1

Name	Organization	Email address
Duncan Agnew	Scripps/UCSD	dagnew@ucsd.edu
Yehuda Bock	UCSD/SIO	ybock@igpp.ucsd.edu
Bob Bohannon	USGS, Menlo Park	rbohannon@usgs.gov
Jose Borrero	USC, Tsunami Research	jborrero@usc.edu
James Dolan*		dolan@earth.usc.edu
Martin Eskijian	State Land Commission / MFD	eskijim@slc.ca.gov
Ned Field		field@gps.caltech.edu
Hank Fong	Port of Long Beach	fong@polb.com
Bill Foxall	LLNL	Foxall1@llnl.gov
John Freckman	State Land Commission	freckmj@slc.ca.gov
Chris Goldfinger	Oregon State U.	gold@oce.orst.edu
Lisa Grant*		lgrant@uci.edu
Jeanne Hardebeck	UCSD	jeanne@mahi.ucsd.edu
Alistair Harding	SIO/UCSD	aharding@ucsd.edu
Tom Henyey	USC/SCEC	henyey@usc.edu
Dave Jackson	UCLA	djackson@ucla.edu
Tom Jordan	USC/SCEC	tjordan@usc.edu
Marc Kamerling	UCSB	marc@crustal.ucsb.edu

Graham Kent*		gkent@ucsd.edu
Grant Kier*		(Karl Mueller student)
Cheng Lai	Port of Long Beach	lai@polb.com
Mark Legg	Legg Geophysical	mrlegg@attglobal.net
John McRaney	USC/SCEC	mcraney@terra.usc.edu
Bernard Minster	UCSD/SCEC	jbminster@ucsd.edu
Karl Mueller	U. of Colorado	karl.mueller@colorado.edu
Craig Nicholson	UCSB/ICS	craig@crustal.ucsb.edu
Dave Okaya	USC	okaya@earth.usc.edu
Salim Pamukos	USC	pamukos@usc.edu
Tom Rockwell	SDSU/SCEC	trockwel@geology.sdsu.edu
Christophe Rusher	USC	rusher@usc.edu
Sean Sanderman	U. of Colorado	Sean.sanderman@colorado.edu
Jean Savy	LLNL	Savy1@llnl.gov
John Shaw	Harvard U.	shaw@eps.harvard.edu
Peter Shearer	SIO.UCSD	pshearer@ucsd.edu
Matt Swensson	USC, Tsunami Research	swensson@usc.edu
Costas Synolakis	USC	costas@usc.edu
Max Weismair	Port of Los Angeles	mweismair@portla.org
Peter Yin	Port of Los Angeles	pyin@portla.org
* Note: Persons invited who did not attend		

Table A.2 Agenda for January 29-30,2001 Workshop 1

Active Faulting and Uncertainty in Earthquake Source Characterization in the California Continental Borderland

University of Southern California

Davidson Conference Center

January 30 -31, 2001

Tuesday, Jan. 30

9:00	Welcome and introduction.	B. Foxall
	Overview of California State Lands Commission MOTERP project.	G. Gregory
	SCEC RELM project objectives.	N. Field
	Characterization of tsunami sources.	C. Synolakis
	The Borderland and SCEC II.	T. Jordan
9:45	Workshop goals: Uncertainty and expert opinion in probabilistic seismic/tsunami hazard analysis	J. Savy
10:10	Issues in seismic source characterization for the Borderland.	B. Foxall
10:35	Break.	
10:50	Holocene and Pliocene tectonic evolution and hazard potential offshore the Los Angeles urban corridor.	B. Bohannon
11:30	The UnDead Miocene transform: San Clemente and other major right-slip faults in the California Borderland.	M. Legg
12:15	Lunch	
1:15	Net slip, slip rates and submersible observations of Recent activity on the San Clemente and San Diego Trough faults.	C. Goldfinger
1:55	Thrust faulting in the Inner California Borderland.	J. Shaw
2:35	Summary of Ward and Valensise San Clemente blind fault model.	B. Foxall
2:45	Fault slip rates and kinematic constraints on- and offshore	T. Rockwell

	Northern Baja California.	
3:20	Break	
3:35	Geodetic constraints on Borderland crustal deformation.	Y. Bock
4:15	Fault geometry and slip based on improved earthquake locations and focal mechanisms in the Inner Borderland	P. Shearer
4:45	Discussion: Building blocks for alternative source characterizations	
5:30	Adjourn	

Wednesday, Jan. 31

8:45	LARSE imaging of the Borderland and coastal region.	D. Okaya
9:15	Models of uplift along the southern California coast and San Joaquin Hills.	K. Mueller, T. Rockwell
10:00	Break	
10:20	Measurements and age constraints of Holocene uplift along the San Joaquin Hills coast	L. Grant
10:50	Large-scale basement-involved slides and associated tsunami hazard, California Continental Borderland.	M. Kamerling
11:25	Examination and discussion of seismic, well data, etc.	
12:00	Discussion	
12:30	Lunch	
1:30	"Strawmen" alternative source characterization models	B. Foxall
2:00	Breakout groups pro and con alternative source models	
3:00	Break	
3:15	Discussion of relative merits of alternative models; modifications	
4:15	Summary, general discussion and action items	
5:00	Adjourn	

Table A.3: List of attendants at Workshop 2, October 19, 2001, at USC

Name	Organization	Email address
Norm Abrahamson*	Consultant	naa2@pge.com
Jose Borrero	USC, Tsunami Research	jborrero@usc.edu
James Dolan	USC	dolan@earth.usc.edu
Martinb Eskijian	State Land Commission	eskijim@slc.c.gov
Bill Foxall	LLNL	Foxall1@llnl.gov
John Freckman	State Land Commission	freckmj@slc.ca.gov
Po Lam	Earth Mechanics	plam@earthmechcom
Homma Lee	USGS, Menlo Park	hjlee@usgs.gov
Christophe Rusher	USC	rusher@usc.edu
Sean Sanderman	U. of Colorado	Sean.sanderman@colorado.edu
Jean Savy	LLNL	Savy1@llnl.gov
Bruce Shell	EMI	shellbw@aol.com
Matt Swensson	USC, Tsunami Research	swensson@usc.edu
Costas Synolakis	USC	costas@usc.edu
* Note: Persons invited who did not attend		

Table A.4: Agenda for Workshop 2, October 19, 2001 at USC

PSHA for the coastal and offshore areas of Orange,
Los Angeles and Ventura Counties
University of Southern California

8:00 to 8:15	Introduction, Purpose and Goals	Jean Savy
8:15 to 9:30	Tectonic model for the PSHA	Bill Foxall
9:30 to 10:00	Seismicity parameters	Bill Foxall
10:00 to 10:15	Break	
10:15 to 11:00	Ground Motion Modeling	
	Existing modeling and recent work with emphasis on the LA basin and offshore region	Norm Abrahamson
11:00 to 12:00	Calculation Model and Preliminary Results	Jean Savy
12:00 to 13:30	Lunch Break	
13:30 to 14:30	Other Regional Studies	
	Geological Information	Bruce Schell
	Hazards Analysis for the port of LA	Po Lam
14:30 to 15:30	Models of Tsunami Generation from Landslides	Homa Lee
15:30 to 16:00	Break	
16:00 to 17:30	Quantification of the Uncertainty in the Models	
	Zonation Models	
	Ground Motion Models	
17:30 to 18:00	Summary plans for completing the study and wrap-up	USC/SLC/LLNL